THE KINETICS OF THE FERROUS-FERRIC REDOX REACTION IN AQUEOUS PERCHLORIC ACID

JOHN TERRENCE WADDEN

THE KINETICS OF THE FERROUS-FERRIC REDOX REACTION IN AQUEOUS PERCHLORIC ACID

by

John Terrence Wadden, B.Sc.

Submitted in partial fulfillment of
the requirements for the degree of
Master of Science

Memorial University of Newfoundland,
St. John's, Newfoundland, Canada

June, 1978

CONTENTS

CONTENTS (continued)

ABSTRACT

The rotating disc electrode (RDE) has been used to investigate the kinetics of the ferrous-ferric redox reaction on platinum, palladium, and gold in aqueous perchloric acid. The electrode shape was optimized, precise speed control was used for the rotating disc and possible noble metal dissolution was minimized during cyclic activation of the test electrode. Each system was studied using counter and reference electrodes constructed from the same metal as the RDE.

Mass transport effects were eliminated by making a long extrapolation to infinite rotation speed (i_o^{-1} versus $\omega^{-1/2}$). The data were analyzed in several ways including the slope - intercept method of Jahn and Vielstich and the constant mass transport method of Randles. In this regard, diffusion coefficients of the ferrous and ferric species were determined as well as their temperature dependencies.

Observed rates were corrected for real surface areas as measured by oxygen desorption or by hydrogen adsorption techniques. Heterogeneous rate constants at 298 K were measured on platinum, gold, and palladium and were found to be 5.41×10^{-3} cm.s^{-1}, 2.11×10^{-3} cm.s^{-1}, and 1.77×10^{-3} cm.s^{-1}, respectively. A different trend was observed for the pre-exponential factor, $A^{\ddagger}$, decreasing from gold to platinum to palladium. Experimental activation enthalpies for all three metals were essentially constant within experimental error having a median value of 39 ± 3.5 kJ.mol^{-1}. An attempt was made to correlate kinetic parameters with the thermionic work function of each metal. The possible effect upon the kinetics of chloride impurity, arising from reduction of the

perchlorate ion was also considered. Utilizing radiochemical chloride adsorption data, the rate constants of the reaction on a chloride-free and fully covered platinum electrode were estimated to be 2.62×10^{-5} and 6.76×10^{-3} $cm.s^{-1}$ respectively.

ACKNOWLEDGEMENTS

The author is extremely grateful to his supervisor, Professor Frank R. Smith for guidance, helpful suggestions, stimulating discussions, and continued encouragement throughout the period of this work.

Profound thanks are also extended to the staff of Memorial University's Technical Services department for their help in construction of the apparatus, especially Mr. George Pardy and Mr. Russ Callahan of the electronics section, as well as machinists Mr. Roy MacLellan and Mr. Dave Cranford, and glass blowers Mr. Doug Seymour, Mr. Tom Perks, and Mr. Martin Hatswell.

The author would like to offer his thanks to friends and co-workers Mr. Abbas Rostami and Dr. B. Dandapani for generous cooperation in sharing of laboratory facilities in addition to providing a quorum for lively scientific debates.

As well the author is grateful to Mrs. Cathy Chen for graphical drafting, and Miss Teresa Barker for patiently typing this thesis, and also to Mr. Fred Steele for providing computational assistance.

Finally, the joint financial support of Memorial University and the Government of Newfoundland in the form of a graduate student fellowship is hereby gratefully acknowledged.

LIST OF SYMBOLS

a	radius of reacting ion
A	electrode area
$A^{\ddagger}$	pre-exponential factor of the Arrhenius equation for the rate of the ferrous-ferric electrode reaction
C_O, C_R	concentrations of the oxidized and reduced electroactive species, respectively
$C_O^{\sigma}, C_R^{\sigma}$	electrode surface concentrations of the oxidized and reduced species, respectively
$C_O^{\infty}, C_R^{\infty}$	solution bulk concentrations of the oxidized and reduced species, respectively
$C_{Cl^-}^{\infty}$	bulk concentration of chloride ions
D_i	diffusion coefficient of species "i"
$D_{Fe^{2+}}, D_{Fe^{3+}}$	diffusion coefficients of the ferrous and ferric ions respectively
D_R, D_O	diffusion coefficients of the reduced and oxidized electroactive species respectively
D_o	pre-exponential factors of Arrhenius equation for diffusion coefficients $D_{Fe^{n+}} = D_o \exp(-E_D/RT)$
D_{opt}	square of the refractive index of the solvent
D_{stat}	static dielectric constant of the solvent
E_D	activation energy for variation of diffusion coefficient with temperature
$E_{1/2}$	half-wave potential as determined from a RDE polarogram
F	Faraday's constant
$\Delta G_a^{\ddagger}, \Delta G_c^{\ddagger}$	activation free energy barriers for the anodic and cathodic reactions, respectively
$\Delta G_{electrode}^{\ddagger}$	free energy of activation for an electrodic process

$\Delta\bar{G}^{o\ddagger}$	standard electrochemical free energy of activation
$\Delta G^{o\ddagger}$	standard (chemical) free energy of activation
ΔG^{o}_{f}	standard Gibbs free energy of formation
h	Planck's constant
$\Delta H^{\ddagger}$	enthalpy of activation of the ferrous-ferric electrode reaction at infinite rotation speed
$\Delta H^{\ddagger}_{\omega}$	enthalpy of activation obtained at rotation speed ω
i	net current density
$\vec{i}$	anodic current density, forward reaction
$\overleftarrow{i}$	cathodic current density, reverse reaction
i_o	exchange current density, the current density in either direction at equilibrium
$(i_o)_\infty$	exchange current density at infinite rotation speed
$(i_{oR}^{-1})_\omega$	reciprocal of the exchange current density at rotation speed ω, according to Randles' method
i_{LIM}	mass transport limited current density at high values of the overpotential
$i_{LIM,a}, i_{LIM,c}$	mass transport limited current densities for the anodic and cathodic electrode processes, respectively
J_i	flux of reacting material "i", through a unit area per unit time
k	Boltzmann constant
$\vec{k}, \overleftarrow{k}$	forward and reverse heterogeneous rate constants under non-equilibrium conditions
$\vec{k}_o, \overleftarrow{k}_o$	forward and reverse heterogeneous rate constants at zero overpotential
k_o	heterogeneous rate constant for both forward and reverse reactions for equal concentrations of reactant and product

$k_{o'app}$	apparent heterogeneous rate constants at zero overpotential in the notation of Johnson and Resnick
k_1	heterogeneous rate constant for maximum coverage by chloride ions
k_2	heterogeneous rate constant for zero coverage by chloride ions
$k_{solution}$	homogeneous rate constant
$k_{electrode}$	heterogeneous rate constant
pzc	point of zero charge of a metal electrode
r	one-half the distance between the centres of reacting ions
R	gas constant
t	time
T	absolute temperature (K)
V_z	velocity of solution being transported up to the disc
W_1, W_2	energies of transport of reactant and product between electrode and solution bulk
Y	the right hand side of either equation (49) or (50)
Y_L	laminar boundary layer
Y_T	transport boundary layer
α	transfer coefficient
α_R	the apparent transfer coefficient as obtained by Randles' method
Γ_{max}	maximum surface coverage by adsorbed chloride ions
δ	diffusion layer thickness
δ_{GR}	diffusion layer thickness as calculated by Gregory and Riddiford (for any electroactive species)

δ_N	diffusion layer thickness as determined by Newman (for any electroactive species)
$\delta_{N,O}, \delta_{N,R}$	Newman's diffusion layer thicknesses for the oxidized and reduced species, respectively
η	overpotential = electrode potential, E, with current flowing, minus the reversible potential E_{rev}, without net current
θ_{Cl^-}	fractional coverage of the electrode by chloride ions
λ	solvent reorganization energy
ν	kinematic viscosity of the solution
Πc_i	product of the concentrations of species "i" in its various oxidation states
$\Delta\phi$	absolute metal-solution potential difference with current flowing
$\Delta\phi_{rev}$	absolute metal-solution potential difference at equilibrium
Φ_M	work function of a metal
ω	rotation speed of the electrode, radians $second^{-1}$

INTRODUCTION

The ferrous-ferric electrode reaction is generally considered to be a first order [1-4] single electron transfer and is an example of the simplest type of process that can occur at an electrode-solution interface.

Most experimental studies of the heterogeneous kinetics of this system have been with platinum in chloride [5-8] and sulphate [2,4-7,9-14] media. Very little research has utilized other noble metals. [5-7,13]

This work is concerned with perchlorate medium, in which the electroactive hydrated ferrous and ferric ions are thought to exist uncomplexed by perchlorate anions [67]. Research using this medium has been confined to platinum electrodes, [11,13,15-18] the kinetics of electron transfer between ferrous and ferric ions at palladium and gold having previously been studied only in sulphate and chloride media.

The main purpose of this research was to reinvestigate the rates of the ferrous-ferric reaction on platinum, as well as extending knowledge of the kinetics to palladium and gold. In this work rates on all three metals were measured under special experimental conditions, which it was hoped would produce unambigious results. This was achieved primarily by use of a rotating disc electrode (RDE) and an extrapolation method which yielded rates of electron transfer completely isolated from mass transport effects. In addition, special consideration was given to the choice of the correct electrochemical pre-activation procedure for each metal, so as to avoid

possible electrode dissolution during cycling of the potential. In this regard, the noble metal dissolution studies of Rand and Woods[19] were found to be most pertinent, and their findings were applied to our experimental approach. As a further precaution, real surface areas were measured by either hydrogen adsorption or oxygen desorption, and the observed rates corrected accordingly. A brief study was also undertaken to ascertain the effects of precision speed and temperature control upon the ability of the RDE to perform as an accurate rate measuring device.

Having satisfied these criteria, the corrected rates were analysed for clues as to the mechanism of electron transfer. The theories of Marcus[20], Hush[21], Levich[22], Dogonadze[22] and others[23-26] conclude that interfacial electron transfers in simple systems proceed through a process in which bonds are neither broken nor formed from metal-electroactive species interactions. The heterogeneous rate constants for electron transfer were measured as a function of temperature from 273 K to 298 K and the enthalpies of activation and the pre-exponential factors determined from Arrhenius plots. Knowledge of such quantities may be helpful in support of a particular mechanism of electron transfer. The electrocatalytic effect of adsorbed chloride ions (a probable impurity) on the electron transfer process at platinum was estimated by consideration of radioactive tracer studies of chloride adsorption by Balashova et al.[27], and Horanyi et al.[64] and the electrocatalysis research of Johnson and Resnick[28].

THEORETICAL BACKGROUND

Electron Transfer Theory

Simple one electron transfer reactions occurring in solution (homogeneous) or on an electrode surface (heterogeneous) may take place by two distinguishable mechanisms known as outer sphere and inner sphere electron transfers. Outer sphere charge transfers take place without bond rupture or formation occurring during the rate-determining step. The cluster of solvent or ligand molecules surrounding the electroactive species remains intact during electron transfer. Structural changes in this cluster may occur, however, either before or after the electron jump. Inner sphere charge transfers, on the other hand, imply distinct bond character modifications. An electron is transferred at the same instant that some metal-ligand bond is altered. The process must therefore entail the passage of an electron between reactants which share a mutual solvent or ligand molecule. Due to the difficult task of theoretically describing a process involving a simultaneous chemical reaction and electron transfer step, no detailed theories exist for the inner sphere mechanism. However, the other non-bonding mode of electron transfer has been well treated theoretically.

Since the early part of this century, electron transfer reactions have received many theoretical treatments. Several excellent reviews[29-32] of the subject exist, as well as a historical account[33] of the quantum mechanical aspects of the theory. For the purpose of the heterogeneous studies, the most notable contributions are those

of Marcus[20], Hush[21], and Levich and Dogonadze[22], all of whom converted their theories for the homogeneous case so that they were useful for heterogeneous kinetics. In order to fully appreciate the implications of this extended theory, the physical differences between homogeneous and heterogeneous processes must be understood. According to the non-bonding theory, the homogeneous exchange reaction involves a diffusion step in which the reactants come together, coupled by a weak electrostatic interaction. For the case of ferrous and ferric ions, electron transfer cannot occur until each species has rearranged its solvation shell. This rearrangement implies two possible activated complexes for this system, one with the electronic description of the ferrous ion and the other with the electronic description of the ferric ion. The Franck-Condon principle forms the basis for both the Marcus and Levich theories, imposing the restriction that the relative positions of the nuclei remain unchanged during electronic transitions. Hence, when the electron is transferred there is no change in energy. For homonuclear electron exchange reactions such as the ferrous-ferric reaction, this principle requires that the total energies of the ferrous and ferric activated complexes must be identical. The activated complexes of the ferrous and ferric ions are formed by a compression of the ligands about the ferrous ion and an expansion of the ligands about the ferric ion, respectively. When the metal-ligand bond distance is the same in each, an electron exchange takes place. This distortion of ligands or solvent to form symmetrical activated complexes may still keep within the confines of the outer sphere

theory, satisfying the Franck-Condon principle as long as any distortion of inner spheres and rearrangement of outer spheres does not require energies larger than those of ground state vibrations of the reactants. Following the electron transfer, the process is reversed, the activated complexes returning to normal size and diffusing into the bulk of the solution. The Marcus theory, embodying a statistical mechanical treatment of solvent polarization, uses a quadratic approximation for the energy of this ligand compression and expansion, so that a homogeneous rate constant may be predicted.

The theory is extended to predict the rate constants of heterogeneous electron transfers. The nature of this prediction will shortly be made clear. Unlike the homogeneous reaction involving a homonuclear electron exchange, the analogous heterogeneous transfer now has the metal electrode as one of its reactants. The reaction at the metal surface can now only involve one activated complex, consisting of just one molecular reactant species, which resides in the double layer. Its properties are now dependent upon the double layer, and the double layer will itself be disturbed by it. According to the theories of Marcus and others the role of the metal in heterogeneous transfers is simply to provide or accept an electron. The metal's possible activity as an electrocatalyst to electron transfer has been omitted from consideration. Its power to release or retain electrons is considered to be controlled solely by the overpotential which has been applied to it, this governing the heights and distribution of its energy levels. By forcing the metal to

remain in a non-equilibrium state ($|\eta|>0$), the overvoltage or polarization contributes to the overall standard free energy as well as to the reaction rate (the overvoltage η is the difference between the equilibrium potential E_{rev} and the working electrode potential E).

On the basis of the theory of R.A. Marcus[20] one is able to relate heterogeneous and homogeneous rate constants for non-bonding electron transfers by the following expression:

$$\left(\frac{k\ \text{solution}}{10^{11}}\right)^{1/2} \geq \left(\frac{k\ \text{electrode}}{10^{4}}\right) \qquad (1)$$

The denominators are typical collision numbers for the solution and electrode reactions having units of $\ell.mol^{-1}s^{-1}$ and $cm.s^{-1}$ respectively. By considering heterogeneous reactions in this way, the intrinsic nature of the metal has been excluded. Thus, the Marcus theory predicts that the rate of an electrodic process is independent of the metal. This prediction is also implied in the calculation of the free energy of activation for a one electron transfer, $\Delta G^{\ddagger}_{electrode}$, i.e.

$$\Delta G^{\ddagger}_{electrode} = \frac{W_1 + W_2}{2} + \frac{\lambda}{8} - \frac{\eta e}{2} + \frac{1}{2\lambda}(\eta e + W_1 - W_2)^2 \qquad (2)$$

where W_1 and W_2 respresent the energies involved in transporting reactant and product between the electrode and bulk of solution, e is the electronic charge, η is the overpotential ($E - E_{rev}$), and

λ is given by the Landau[48] expression

$$\lambda = e^2\{\frac{1}{a} - \frac{1}{r}\}\{\frac{1}{D_{opt}} - \frac{1}{D_{stat}}\} \qquad (3)$$

to be the energy involved in transferring an electron from an ion of radius "a" to an ion whose centre is at a distance 2r via a hemispherical transition state, that is, the work required to reorganize the environment about the reactant. D_{opt} is the optical dielectric constant, equal to the square of the refractive index of the solvent and D_{stat} is the static dielectric constant of the solvent. This derivation involves the assumption that the free energy of activation for the homogeneous reaction is double the free energy of activation for the electrode reaction. Proofs of this are elementary, e.g. Bockris[33]. Again, the role of the electrode is evident from such a relationship, i.e. having no effect upon the free energy of activation, due to the absence of any electrode-related terms. Alternatively the theory of N.S. Hush contains slight modifications. Here the probability density of electrons in each reaction path state is used to derive expressions for activation free energy and entropy. Hush's approach is consistent with respect to independence of the metal, but expressions for activation free energies for both heterogeneous and homogeneous electron transfers yield similar results since the reorganizational energy of the reactant's ligands is considerered to be minimal. Then, a complete perspective of the non-bonding theories would imply

the absence of any dependence of both rate constant and free energy of activation upon the metal used. In order to adequately test the applicability of the non-bonding theory to the ferrous-ferric electrode process, it is desirable that the rate constant and activation free energy be measured as accurately as possible.

Electrode Kinetics

From the general theory of electrode processes, the transfer of an electron occurs when the potential energy surfaces of ion and electrode overlap. From the general relationships for rate processes given by the transition state theory, we can visualize the forward (anodic) and reverse (cathodic) current densities as the rates of transfer of ions over the free energy barrier at the surface of the electrode. Away from equilibrium, the Gibbs free energy barriers $\Delta G_a^{\ddagger}$ and $\Delta G_c^{\ddagger}$ for the anodic and cathodic reactions, respectively, are unequal. At equilibrium, these energy barriers are symmetrical and we may calculate the free energy of activation from the temperature dependence of the rate constant at the potential of the electrode where this symmetrical barrier occurs. The standard electrochemical free energies of activation ($\Delta\bar{G}^{o\ddagger}$) are related in general to the standard chemical free energies of activation ($\Delta G^{o\ddagger}$) by:

$$\Delta\bar{G}_a^{o\ddagger} = \Delta G_a^{o\ddagger} - \alpha F\Delta\phi \qquad (4)$$

$$\Delta\bar{G}_c^{o\ddagger} = \Delta G_c^{o\ddagger} + (1-\alpha)F\Delta\phi \qquad (5)$$

where $\Delta\phi = \Delta\phi_{rev} + \eta$, the sum of the absolute metal-solution potential

difference, $\Delta\phi_{rev}$, at equilibrium and the overpotential, η. Note that $\Delta\phi$ and $\Delta\phi_{rev}$ are not measurable, only their difference, η. The transfer coefficient, α, is that fraction of the overpotential which diminishes the activation free energy of the anodic (forward) reaction.

Then for a single electron transfer, the respective anodic and cathodic current densities will be:

$$\vec{i} = F \frac{kT}{h} \prod_i c_i \, e^{-\Delta G_a^{o\ddagger}/RT} \, e^{\alpha F \Delta\phi/RT} \tag{6}$$

$$\overleftarrow{i} = F \frac{kT}{h} \prod_j c_j \, e^{-\Delta G_c^{o\ddagger}/RT} \, e^{-(1-\alpha)\Delta\phi/RT} \tag{7}$$

where $\prod_i c_i$ and $\prod_j c_j$ are the products of the concentrations of the reactants and products, respectively. F is the Faraday constant, k, the Boltzmann constant, T, the Kelvin temperature, h, Planck's constant and R is the gas constant. At equilibrium, $\Delta G_a^{o\ddagger} = \Delta G_c^{o\ddagger}$, $\Delta\phi = \Delta\phi_{rev}$ and forward and reverse current densities are equal:

$$\vec{i} = F \frac{kT}{h} \prod_i c_i \, e^{-\Delta G_c^{o\ddagger}/RT} \, e^{\alpha F \Delta\phi_{rev}/RT} = \vec{k}_o \prod_i c_i F = i_o \tag{8}$$

$$\overleftarrow{i} = F \frac{kT}{h} \prod_j c_j \, e^{\Delta G_a^{o\ddagger}/RT} \, e^{-(1-\alpha)F\Delta\phi_{rev}/RT} = \overleftarrow{k}_o \prod_j c_j F = i_o \tag{9}$$

Here, $\vec{k}_o$ and $\overleftarrow{k}_o$ represent the forward and reverse heterogeneous rate constants at zero overpotential. For the special case of equal concentrations, considered here, $\vec{k}_o = \overleftarrow{k}_o = k_o$. The net current density measured is the difference between the current densities

in the anodic and cathodic directions, obtained by substituting $\Delta\phi = \Delta\phi_{rev} + \eta$ into equations (6) and (7) respectively to obtain

$$i = \vec{i} - \overleftarrow{i} = i_o \{e^{\alpha\eta F/RT} - e^{-(1-\alpha)\eta F/RT}\} \quad (10)$$

where i_o, the exchange current density, is the magnitude of current density flowing in each direction at equilibrium and given by equations (8) or (9). The partial currents may also be expressed in terms of rate constants, i.e.

$$\vec{i} = F \vec{k} C_O \quad (11)$$

$$\overleftarrow{i} = F \overleftarrow{k} C_R \quad (12)$$

where C_O and C_R are the concentrations of the oxidized and reduced species, respectively, and the forward and reverse rate constants are related to the rate constant at the equilibrium potential similarly to equation (10):

$$\vec{k} = k_o e^{\alpha\eta F/RT} \quad (13)$$

$$\overleftarrow{k} = k_o e^{-(1-\alpha)\eta F/RT} \quad (14)$$

A more explicit form of the exchange current density may be obtained by inclusion of the Nernst equation expression for $\Delta\phi_{rev}$ in equations (8) or (9) (see for example Delahay[49]) to obtain:

$$i_o = F k_o C_O^{1-\alpha} C_R^{\alpha} \qquad (15)$$

but if $C_O = C_R$, the heterogeneous rate constant is obtainable from the exchange current density without knowledge of α; thus

$$k_o = i_o/FC_i \qquad (16)$$

For the purposes of the present work, the exponential coefficients of i_o in (10) are linearized by making the simplifying approximation $e^x \simeq 1 + x$, for low values of x. Thus, at low overpotential the current varies linearly with overpotential:

$$i = i_o\left(\frac{\eta F}{RT}\right) \qquad (17)$$

The exchange current density may be obtained by use of the relationship:

$$i_o = \left(\frac{\partial i}{\partial \eta}\right) \frac{RT}{F} \qquad (18)$$

For typical transfer coefficients of about 0.5, this introduces a maximum error of 0.7% at $|\eta| = 10$ mV.

RDE Theory

The general aspects of electron transfer theory and the possible role of the metal in electrocatalysis have been introduced in the preceding section. In doing so, the integral role of mass transport

in the observed charge transfer process has been entirely neglected. By restricting the study to non-complexing perchlorate media and millimolar redox ion concentrations, the following simple one step charge transfer was assumed to take place at the electrode surface.

$$[Fe(H_2O)_6]^{3+} + e^-_{metal} \rightleftharpoons [Fe(H_2O)_6]^{2+}$$

However, under normal solution conditions, one cannot observe this process alone but must witness a more complete mechanism entailing mass transport, i.e.,

$$O^{\infty} \underset{\text{mass transport}}{\rightleftharpoons} O^{\sigma} \underset{\text{charge transfer}}{\rightleftharpoons} R^{\sigma} \underset{\text{mass transport}}{\rightleftharpoons} R^{\infty}$$

In this case, O and R refer to the oxidized and reduced electroactive species, ferric and ferrous ions, respectively. The superscripts pertain to either the bulk (∞) of the solution or the electrode surface (σ). The transport step comprises the process by which either reacting or product species is conveyed towards or away from the electrode reaction surface. Previously, in our discussion of basic electrode kinetics, surface and bulk designations were unnecessary because the electron transfer step itself was considered to be rate-determining. For a practical measurement of the rate of charge transfer, the role of mass transport must be characterized and separated from the total reaction. For many heterogeneous kinetic studies the mass transport step is usually rate-determining. The ferrous-ferric system is an example, and the true rate of electron

transfer can only be discovered by eliminating mass transport hindrance. In this fashion, the system can be observed under complete kinetic control.

Mass transport occurs by three modes of motion: (1) migration, (2) diffusion, and (3) convection. Migration is the movement of charged species through a medium due to the effect of an applied electric field. Migratory effects for the ferrous-ferric system are suppressed by using an excess of unreactive background electrolyte. Diffusion is the movement of species through a solution in the direction opposite to a positive concentration gradient. Such diffusion is quantitatively described by Fick's first law, i.e.,

$$J_i = -D_i \left(\frac{\partial C_i}{\partial z}\right) \qquad (19)$$

according to which, the movement of reactant material through a unit area per unit time is the flux (J_i) of that species in $mol.cm^{-2}s^{-1}$, with D_i the diffusion coefficient of the reactant species in $cm.^2s^{-1}$. D_i is a solution property, being dependent upon the size, charge, and hydration number of the diffusing reactant. It is independent of any electrocatalytic effects arising from the condition of the electrode's surface. The concentration gradient of equation (19) may be extended into three dimensions if necessary but, for the case of the RDE, all gradients in the plane of the electrode are zero, due to the hydrodynamic flow pattern. For the RDE only $\partial/\partial z$ terms need be considered, where z refers to the vertical direction, perpendicular

to the horizontal RDE surface. Mass transport by convection is forced to occur if the medium is operated upon by some external mechanical force. The spinning of a RDE provides the necessary convective force to transport electroactive species from the bulk of the solution towards the electrode surface.

With migration eliminated, the two remaining modes of transport are successfully manipulated by a RDE. Transport to the electrode surface occurs in two stages. The primary stage is movement by convection from the bulk of the solution to the outer boundary of the diffusion layer. This layer is a very thin lamina of more or less stagnant solution adjacent to the electrode surface. Constant stirring of the bulk solution does not disturb it, but its thickness, δ, is dependent upon the magnitude of the rotation speed and the hydrodynamic properties of the solution, which are inherently temperature-dependent. (These include the diffusivity of the electroactive species and the kinematic viscosity of the solution.) Final transport of reactant across this quiescent layer is entirely by diffusion. At the electrode's surface the concentration of the reacting species, C_i^{σ}, may be considerably different from its bulk concentration, C_i^{∞}, due to polarization of the electrode and the resultant reduction or oxidation. A concentration gradient therefore exists across the diffusion layer. According to equation (19) the total flux to the surface of the electrode will be

$$J_i = -D_i\left(\frac{C_i^{\infty} - C_i^{\sigma}}{\delta}\right) \qquad (20)$$

The thickness of the diffusion layer is determined by considering the time-dependent aspects of convective-diffusion at a RDE. Quantitatively, we do this by utilizing Fick's second law of diffusion, i.e.,

$$\frac{\partial C_i}{\partial t} = D_i \left(\frac{\partial^2 C_i}{\partial z^2}\right) \tag{21}$$

and the time derivative of transport by convection, i.e.,

$$\frac{\partial C_i}{\partial t} = V_z \left(\frac{\partial C_i}{\partial z}\right) \tag{22}$$

where V_z is the velocity of the solution being transported up to the disc. Under steady state conditions, where reacting material is being supplied to the disc at a constant rate, i.e.,

$$\frac{\partial C_i}{\partial t} = 0, \text{ then, } D_i \left(\frac{\partial^2 C_i}{\partial z^2}\right) = V_z \left(\frac{\partial C_i}{\partial z}\right)$$

$$\text{or} \quad D_i \left(\frac{\partial^2 C_i}{\partial z^2}\right) - V_z \left(\frac{\partial C_i}{\partial z}\right) = 0 \tag{23}$$

This equation of transport to the disc was originally solved by V.G. Levich[35]. The value of V_z was approximated by Levich from an infinite series to be $-0.51\ \omega^{3/2}\ \nu^{1/2}\ z^2$ and the equation was solved[35-37] by applying the diffusion layer boundary conditions that as $z \to \infty$, then $C_i \to C_i^{\infty}$ and at $z = o$, $C_i \to C_i^{\sigma}$. The following solution was obtained:

$$\left(\frac{\partial C_i}{\partial z}\right)_{z=0} = \frac{C_i^{\infty} - C_i^{\sigma}}{1.61\ D_i^{1/3}\ \nu^{1/6}\ \omega^{-1/2}} \tag{24}$$

where ν is the kinematic viscosity and ω is the rotation speed. Comparing equations (24) and (19) and (20), Levich obtained $\delta = 1.61\, D_i^{1/3}\, \nu^{1/6}\, \omega^{-1/2}$. Substitution of Levich's δ in equation (20) yields the flux for the material being transported through the diffusion layer. In the steady state the flux of material reacting at the electrode surface must be equal and opposite to the diffusional flux, thus

$$\frac{D_i\,(C_i^{\infty} - C_i^{\sigma})}{\delta} = \vec{k}\, C_i^{\sigma} \qquad (25)$$

where $\vec{k}$ is the potential-dependent heterogeneous rate constant ($cm.s^{-1}$). If equation (25) is rearranged in terms of C_i^{σ},

$$C_i^{\sigma} = \frac{C_i^{\infty}}{1 + \delta\vec{k}/D_i} \qquad (26)$$

and multiplied by $\vec{k}F$, the left hand side becomes the net current ($F\vec{k}\, C_i^{\sigma}$), i.e.,

$$i = \frac{F\vec{k}C_i^{\infty}}{1 + \delta\vec{k}/D_i} \qquad (27)$$

This two-parameter relationship predicts the current as a function of rotation speed (in δ) and overpotential (in $\vec{k}$). For practical measurements, one of these parameters is kept constant while the other is varied. From equation (27) it is apparent that at constant rotation speed and high values of the overpotential, where $\delta\vec{k}/D_i \gg 1$, the net current density becomes the mass transport

limited current density.

$$i_{LIM} = \frac{F C_i^{\infty} D_i}{\delta} \tag{28}$$

As previously stated, Levich approximated δ as $1.61\ D_i^{1/3}\ \nu^{1/6}\ \omega^{-1/2}$ by truncating the series in V_z. Other authors have expanded V_z to obtain more exact expressions for δ. Gregory and Riddiford[38] approximated this expansion by numerical evaluation to obtain

$$\delta_{GR} = \delta\{1 + 0.354\ (D_i/\nu)^{0.36}\} \tag{29}$$

where δ refers to the Levich expression and δ_{GR} to that of Gregory and Riddiford. Newman[39] expanded δ even further to obtain a more exact expression:

$$\delta_N = \delta\{1 + 0.2980\ (D_i/\nu)^{1/3} + 0.1450\ (D_i/\nu)^{2/3}\}$$

$$= 1.61\ D_i^{1/3}\ \nu^{1/6}\ \omega^{-1/2} + 0.4798\ D_i^{2/3}\ \nu^{-1/6}\ \omega^{-1/2}$$

$$+ 0.2335\ D_i\ \nu^{-1/2}\ \omega^{-1/2} \tag{30}$$

The complete expression for the limiting current density according to Newman is rewritten as:

$$i_{LIM} = \frac{0.620\ FD^{2/3}\ \nu^{-1/6}\ C_i^{\infty}\ \omega^{1/2}}{1 + 0.2980(\nu/D)^{-1/3} + 0.14514(\nu/D)^{-2/3}} \tag{31}$$

This expression should be accurate to within 0.1%. According to equation (31) the limiting current varies linearly with $\omega^{1/2}$. By

using the slope of a i_{LIM} versus $\omega^{1/2}$ plot (referred to as a "Levich plot") the diffusion coefficient is determinable provided the other parameters are known. Newman's expression has been cleverly manipulated in quadratic form, by Bruckenstein[40] to yield the following convenient expression for the calculation of D_i:

$$D_i = \nu[(J^{-1} - 0.122939)^{1/2} - 0.1490]^{-3} \quad (32)$$

where

$$J^{-1} = (0.620\ F\nu^{-1/6}\ \omega^{1/2}\ C_i^{\infty})/i_{LIM} \quad (33)$$

J^{-1} being the reciprocal of the observed slope; $\omega^{1/2}/i_{LIM}$, multiplied by various solution constants.

In the derivation of the limiting current expression only the forward reaction has been considered, since the back reaction is negligible at high overpotentials. For rate determinations in the present work, studies are done at low overpotentials, in the region of the equilibrium potential, where both the forward and back reactions are possible, the net observed current density being the difference between that of forward and reverse reactions, i.e. $i = \vec{i} - \overleftarrow{i}$. Here, we use the convention that $\overleftarrow{i}$ is the reduction and $\vec{i}$ is the oxidation. In terms of rate constants and concentrations we have:

$$i = \vec{F}kC_R^{\sigma} - \overleftarrow{F}kC_O^{\sigma} \quad (34)$$

The surface concentrations of oxidant and reductant may be calculated using the Nernst diffusion relations[41,42], which have the general form,

$$C_i^{\sigma} = C_i^{\infty}(1 - i/i_{LIM}) \tag{35}$$

where i_{LIM} (anodic or cathodic) has been shown to be $FD_i C_i^{\infty}/\delta$. If we use Newman's expression for the diffusion layer thickness, δ_N, we obtain

$$C_O^{\sigma} = C_O^{\infty} + \frac{i\delta_{N,O}}{FD_O} \quad \text{and} \quad C_R^{\sigma} = C_R^{\infty} - \frac{i\delta_{N,R}}{FD_R} \tag{36,37}$$

where for sake of convenience we have rewritten the diffusion layer thickness as $\delta_{N,O}$ and $\delta_{N,R}$, where each may be obtained by substituting D_O and D_R, as appropriate, into equation (30) for δ_N. By substituting equations (36) and (37) into equation (34) and rearranging for i, we obtain:

$$i = \frac{F(\vec{k} C_R^{\infty} - \overleftarrow{k} C_O^{\infty})}{1 + \vec{k}\delta_{N,R}/D_R + \overleftarrow{k}\delta_{N,O}/D_O} \tag{38}$$

Taking reciprocals of both sides of equation (38) and substituting the exact expressions for $\delta_{N,O}$ and $\delta_{N,R}$, an expression of the following form results:

$$\frac{1}{i} = \frac{1}{B} + \left(\frac{M}{B}\right)\omega^{-1/2} \tag{39}$$

where

$$B = F\vec{k}\, C_R^{\infty} - F\overleftarrow{k}\, C_O^{\infty} \tag{40}$$

and

$$M = \vec{k}(1.61\nu^{1/6}D_R^{-2/3} + 0.4798\nu^{-1/6}D_R^{-1/3} + 0.2335\nu^{-1/2}) + \overleftarrow{k}(1.61\nu^{1/6}D_O^{-2/3} + 0.4798\nu^{-1/6}D_O^{-1/3} + 0.2335\nu^{-1/2}) \tag{41}$$

As is evident, a plot of i^{-1} versus $\omega^{-1/2}$ should be linear. Kinetic information may be obtained from the slope and intercept. For our particular application the exchange current density (i.e. at $\eta = o$) can be determined at each rotation speed and should vary in the same fashion as the net current under non-equilibrium conditions. Equation (39) is then transformed to the following:

$$\frac{i}{i_o} = \frac{1}{(i_o)_\infty} + \left(\frac{M_o}{(i_o)_\infty}\right)\omega^{-1/2} \tag{42}$$

where $(i_o)_\infty$ is assumed to be the true exchange current density at infinite rotation speed. For this special case ($\vec{k} = \overleftarrow{k} = k_o$), M is rewritten as M_o:

$$M_o = k_o\{1.61\nu^{1/6}(D_R^{-2/3} + D_O^{-2/3}) + 0.4798\nu^{-1/6}(D_R^{-1/3} + D_O^{-1/3}) + 0.4670\nu^{-1/2}\} \tag{43}$$

The heterogeneous rate constant at zero overpotential, k_o, can be determined directly from such a plot, without even knowing the bulk concentration of the electroactive species provided only that $C_R^\infty = C_O^\infty$. Thus both k_o and $(i_o)_\infty$ can be obtained from the magnitudes of slope and intercept. They are related by $(i_o)_\infty = Fk_oC_i^\infty$, an expression identical with equation (16) under these infinite mass transport conditions. Obtaining $(i_o)_\infty$ from the intercept alone will be referred to here as the "intercept" method. Consideration of both the slope and intercept to obtain k_o will be known as the "Jahn - Vielstich"[15] method. Data analysis using either method achieves our intended purpose of isolating mass transport contributions, thus giving true kinetic information. The underlying basis for each method is that the electron transfer is rate-determining at infinite rotation speed. Because of their origin these extrapolation-to-infinity plots will be referred to as "inverse Levich" plots.

Randles' Approach

An alternative approach to extracting electron transfer rate constants was proposed by J.E.B. Randles[43]. This method offers a means for interpreting current-overpotential curves for systems of which the mass transport conditions are constant and reproducible. The RDE fulfills these conditions perfectly.

If we again consider the Nernst diffusion relation, equation (35), and substitute this into equation (34) for C_O and C_R we obtain:

$$i = F\{k_f C_R^\infty\left(1 - \frac{i}{i_{LIM,a}}\right) - k_b C_O^\infty\left(1 + \frac{i}{i_{LIM,c}}\right)\} \qquad (44)$$

The forward and reverse rate constants have already been defined by equations (13) and (14) for non-equilibrium conditions. We may rewrite C_R^∞ and C_O^∞ as C_i^∞ since they have been made equal in this work. It is apparent from equations (13) and (14) that $\vec{k}/\overleftarrow{k} = e^{\eta F/RT}$ or we may rewrite as

$$\vec{k} = \vec{k}\, e^{\eta F/RT} \quad \text{and} \quad \overleftarrow{k} = \vec{k}\, e^{-\eta F/RT} \tag{45,46}$$

By invididually substituting equations (45) and (46) into (44), the following two equations result:

$$i = F\vec{k}C_i^\infty\{e^{\eta F/RT}(1 - \frac{i}{i_{LIM,a}}) - (1 + \frac{i}{i_{LIM;c}})\} \tag{47}$$

$$i = F\vec{k}C_i^\infty\{(1 - \frac{i}{i_{LIM,a}}) - e^{-\eta F/RT}(1 + \frac{i}{i_{LIM,c}})\} \tag{48}$$

By solving equations (47) and (48) for $\overleftarrow{k}$ and $\vec{k}$, respectively, rearranging, and taking logs of both sides we get the final results:

$$-\log_e F\overleftarrow{k}C_i^\infty = \log_e\{(\frac{e^{\eta F/RT} - 1}{i}) - \frac{e^{\eta F/RT}}{i_{LIM,a}} - \frac{1}{i_{LIM,c}}\} \tag{49}$$

$$-\log_e F\vec{k}C_i^\infty = \log_e\{(\frac{1 - e^{-\eta F/RT}}{i}) - \frac{e^{-\eta F/RT}}{i_{LIM,c}} - \frac{1}{i_{LIM,a}}\} \tag{50}$$

By observing current-overpotential curves under reproducible mass transport conditions (i.e. constant rotation speed), use of expressions (49) and (50) will yield both the exchange current density and the

transfer coefficient. This is evident if we break up equation (10) to get the two partial currents

$$\vec{i} = i_o e^{\alpha\eta F/RT} \tag{51}$$

$$\overleftarrow{i} = i_o e^{-(1-\alpha)\eta F/RT} \tag{52}$$

By recalling the relationships between current and rate constant (equations (11) and (12)) and comparing the logarithmic forms of equations (51) and (52), i.e. $\log_e \vec{i} = \log_e i_o + \alpha\eta F/RT$ and $\log_e \overleftarrow{i} = \log_e i_o - (1-\alpha)\eta F/RT$ with (49) and (50) we get

$$-\log_e \vec{FkC}_i^{\infty} = -\log_e i_o - \alpha\eta F/RT \tag{53}$$

$$-\log_e \overleftarrow{FkC}_i^{\infty} = -\log_e i_o + (1-\alpha)\eta F/RT \tag{54}$$

Plots of the right hand side of both equations (49) and (50) (designated as "$\log_e Y$" for convenience) against η should be linear for anodic and cathodic plots. The exchange current density, i_o, is obtained from the intercept at $\eta = 0$ and α may be calculated from either slope.

The important point brought forward here is the absence of any dependency upon rotation speed in the final expressions. According to Randles' theory any rotation speed may be used to obtain the same i_o and α. These predictions were tested by use of the ferrous-ferric system.

EXPERIMENTAL

The conclusions drawn herein were made by use of two different experimental systems. An extensive series of preliminary experiments were undertaken, with an apparatus left by a previous worker, so that any difficulties of either a mechanical or electrochemical nature could be corrected. This equipment was like that of Wojtowicz and Conway[44]. This RDE was the cylindrical type (CEL), differing from the bell shaped design (BEL) favoured by Blurton and Riddiford[45]. Because of the absence of a servo system, speed control was very poor, being maintainable to within only 10% of the desired rotation velocity. Nevertheless, the device was used for obtaining kinetic data by operating at speeds kept constant manually, using a pre-set General Radio Type 1531 stroboscope (±1%). The results obtained by this means are presented to show in a qualitative manner the kinetic behaviour of the system when certain thermal and electrochemical conditions were imposed. The main conclusion obtained from using this old apparatus, was the essential need for the design and construction of a new device, with all of the faults of the former device eliminated.

The Construction of the Improved RDE

In planning the new electrode, the recommendations of Riddiford[50] pertaining to the absolute dimensions of the noble metal disc and the inert cup-shaped sheath surrounding it were considered, and implemented to the greatest extent possible. He concluded that the BEL type electrode best agreed with the limiting current predictions (within 1%) of Gregory and Riddiford's expression (equations (28) and (29)). This

accuracy is further augmented (to within 0.1%) if the Newman equation is substituted instead (equation (31)).

Riddiford suggested that the radius of the noble metal disc, r_o, be at least 100 times greater than Y_T, the transport boundary layer ($Y_T = 3.61(D/\nu)^{1/3}(\nu/\omega)^{1/2}$). He showed this to be an extremely conservative figure, however, illustrating that electrodes with $r_o \sim 10Y_T$ work equally well. It is into this latter category that our electrode belongs, since we were restricted to noble metal rods of 0.1 cm radius. The specification for r_1, the radius of the inert sheath, was easily satisfied. Having a thickness of 1.5 cm, this sheath exceeded the laminar boundary layer, ($Y_L = 2.8\ (\nu/\omega)^{1/2}$) by a hundred fold at rotation speeds from 360 to 3600 rpm.

A separate electrode was constructed for each noble metal studied. The main body of each was manufactured from an 8" length x 1.25" diameter Kel-F cylinder obtained from Commercial Plastics Limited, Montreal. The 0.2 cm diameter noble metal rod (platinum, palladium, or gold) was screw threaded into a 4.0 cm length x 0.2 cm diameter stainless steel shaft with a 1° taper at its upper end (see inset Fig. 1). The interior of the Kel-F cylinder was then bored out to 1.0 cm diameter and threaded on the inside near the top in a clockwise direction. A 0.1 cm diameter opening was centre drilled in the end of the Kel-F tube and the noble metal/stainless steel piece was then inserted into a very tight press fit. The entire electrode was screwed onto the main rotating shaft and the final machining into the characteristic bell shape was done "in situ". Electrical contact

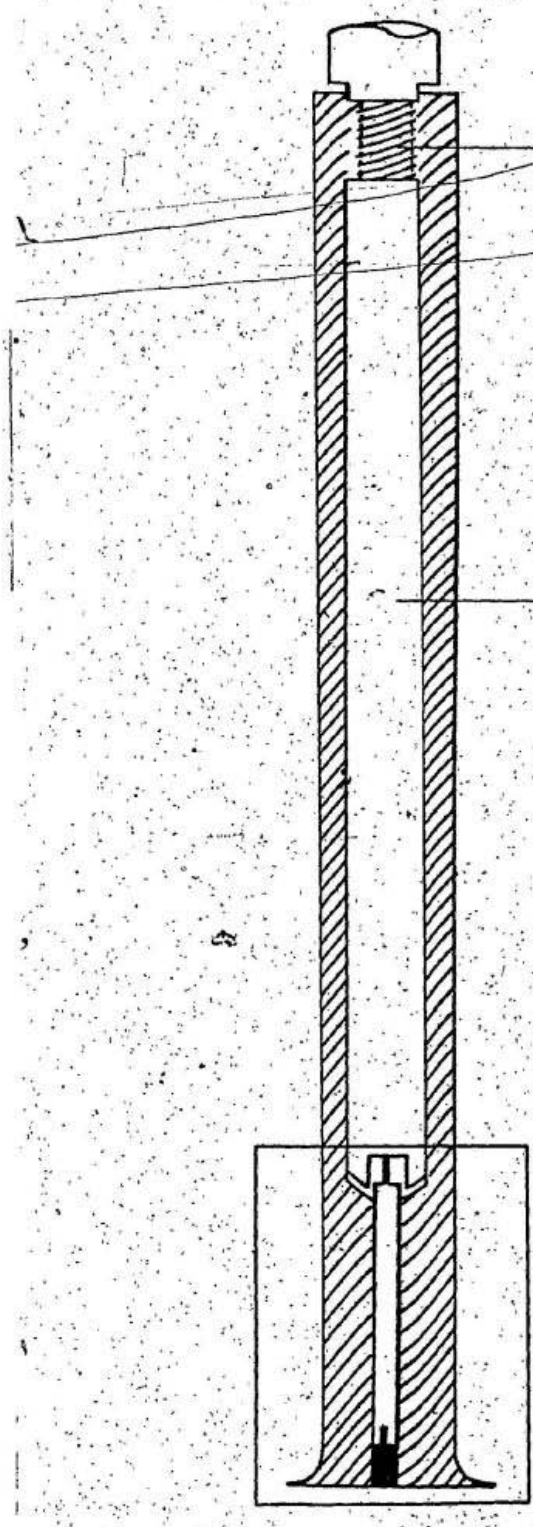

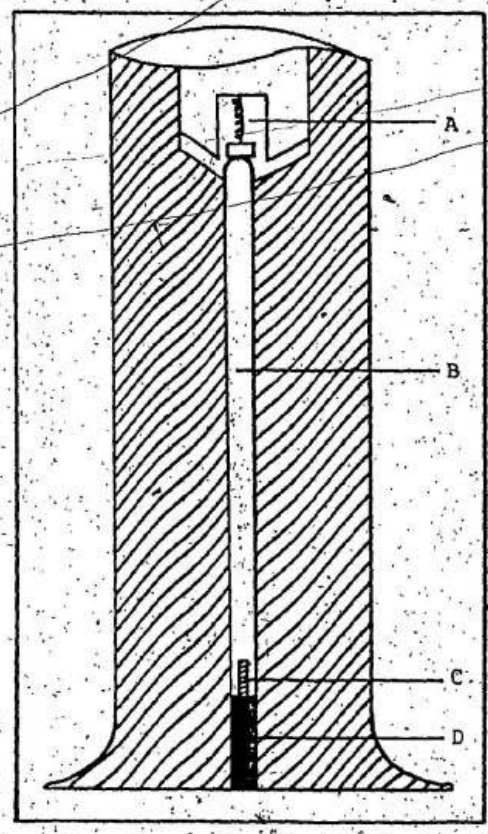

A - spring-loaded stainless steel contact

B - 2 mm stainless steel shaft tapered 1° at upper end

C - stainless steel screw-threaded into noble metal disk

D - Pt, Pd, or Au (2 mm diameter)

E - main shaft threaded opposite to direction of rotation

F - main shaft machined down to 10 mm.

Fig. 1 The BEL type rotating disk electrode (lower portion)

between the rotating shaft and the noble metal insert was achieved with a stainless steel spring positioned in a cavity at the end of the rotating shaft. The shaft operated in a counterclockwise fashion, to prevent slippage during use. The electrode surface was given a mirror finish by machining the Kel-F/noble metal interface with a high speed precision cutting tool. The surface was left in this polished state and was not further abraded with grinding powders for fear of surface contamination. Eccentricities were measured on the experimental set-up and observed to be not greater than 0.002 cm. Reference to Fig. 1 will clarify the details of construction of the electrode itself. It will be observed that the main connecting shaft from the motor was machined down from 1.59 cm (5/8") to 1.0 cm diameter so that the Kel-F tube could have thicker stronger walls.

The RDE Support Assembly

The entire assembly containing the RDE and peripheral accessories was massive. The main vertical support was a 9" thick piece of channel iron, which was electric arc-welded to a 9" x 12" x 1/4" steel base plate. Following secure mounting to the working bench, the assembly was further stabilized by the installation of horizontal metal struts, rigidly connecting it to the concrete wall of the laboratory. The RDE was powered by a 7 amp 1 horsepower Servo-Tek control motor, model STE-232-1F, manufactured by Servo-Tek Products Company, New Jersey. Speed control of this unit was attainable to within 0.25%. This was achieved through the coupling of its precision adjustable-speed drive to a solid state tachometer feedback circuit. Constant, accurately known speeds up to

3600 rpm were possible for extended periods of time, if required. Speeds were obtained by setting the potentiometer type control head to the desired position. Its resolution was within 0.1%.

The Servo-Tek control motor was carefully mounted atop the channel iron assembly and connection to the RDE shaft was made indirectly through a piece of Tufnol, a non-conducting plastic (see Fig. 2) to ensure that the electrode was insulated from the motor. The flexibility of this coupling material minimized possible motor - RDE shaft alignment problems. The coupling bolts were mounted in Teflon for further electrical insulatory protection.

The main RDE shaft was mounted in a stainless steel bearing housing using Teflon encased "Red Seal" high speed SKF bearings. This finalized the isolation of the shaft from the main support assembly. A Teflon seal-housing was mounted beneath the bearing support, which also served as an adaptor to the main joint of the experimental glass cell. A "Silicone Seal" rubber ring was used as a gasket between cell and housing. Inside the housing were positioned two Teflon angle seals (tapered to zero thickness, one angled up, the other down). This minimized contact of corrosive acid vapours with the metal interior components of the RDE drive train. These details are outlined in Fig. 2.

Electrical contact to the rotating shaft was made by a phosphor bronze cylinder key-fitted to the shaft between the Tufnol coupler and the main bearing housing (see Fig. 3). Two brass brushes provided dynamic contact to the bronze. Grooving of the phosphor bronze was observed only after extensive usage.

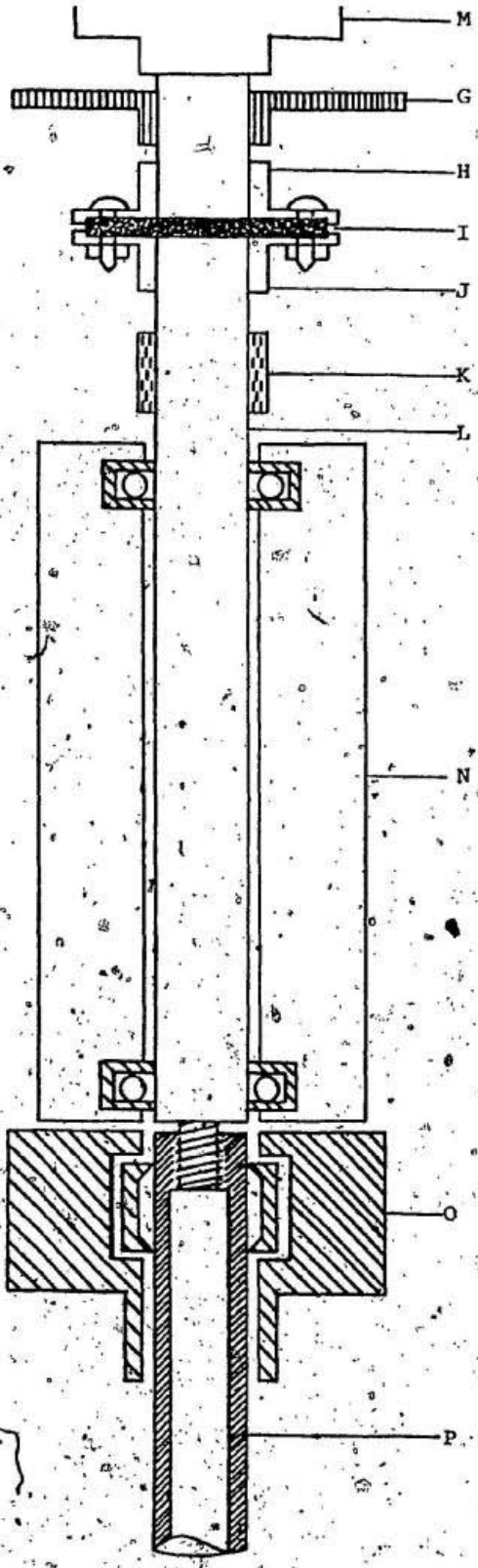

— Aluminum

— Stainless Steel

— Tufnol

— Teflon

— Kel-F

— Phosphor Bronze

M - Servo-Tek 1 h.p. motor

G - slotted aluminum disk

H - upper coupling

I - Tufnol (electrical insulator)

J - Lower coupling

K - Phosphor bronze contact collar

L - stainless steel 5/8" shaft

N - bearing housing with high speed Teflon-insulated "red seal" bearings.

O - Teflon cell adapter and seal housing

P - Kel-F sheath containing noble metal disk (not shown) over machined-down portion of solid stainless steel shaft

Fig. 2 Rotating disk electrode assembly

To facilitate data handling, an automatic plotting device was included in the assembly (see Fig. 3). This included a thin slotted circular disc located between the motor and Tufnol coupler. A C-type jaw piece was mounted over this, containing a phototransistor on one side and a stationary light source on the other. Connection was made to further circuitry (see Fig. 4, X section) to generate a voltage proportional to $\omega^{-1/2}$. The current was fed into the Y section of the same circuit so that i^{-1} could be plotted versus $\omega^{-1/2}$.

The Glass Cell

The experimental cell was a single walled Pyrex multijointed vessel with a large 'button type' support ring pressed out near the top (see Fig. 5 noting that the cell and glass support are fused together into a one piece unit). With this support the cell was able to fit neatly into a thermostatically controlled jacket (see Fig. 6) fitted with a ground glass rim. A clamp kept the jacket and cell securely fastened together with two rubber gaskets for a water-tight seal. The jacket was provided with water pumped from a Tamson TE-Z9 water bath controlled to ±0.05°C.

The main cell connection to the RDE consisted of a 40 mm O-ring joint in the centre of the cell. This joint was not off-centred because vortexing was not a problem at the speeds used in our experiments and because it was more convenient for construction. The RDE shaft protruded into the cell through this opening. On either side were two B10/19 cup cones for reference and counter electrode entry ports. A third B10/19 cup cone was positioned

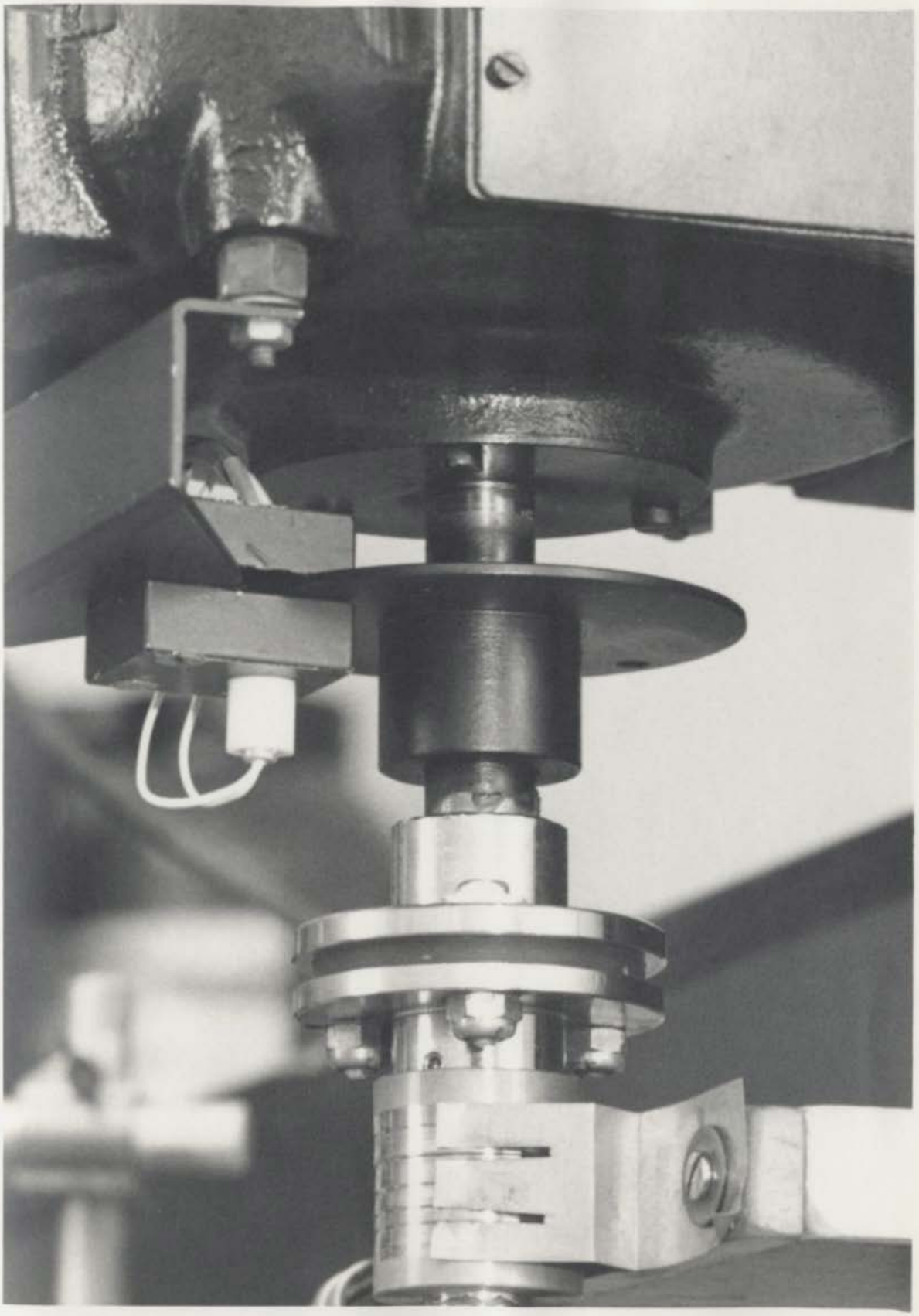

Fig. 3 Upper portion of electrode shaft illustrating plotting attachment, Tufnol coupler, and brass contact brush.

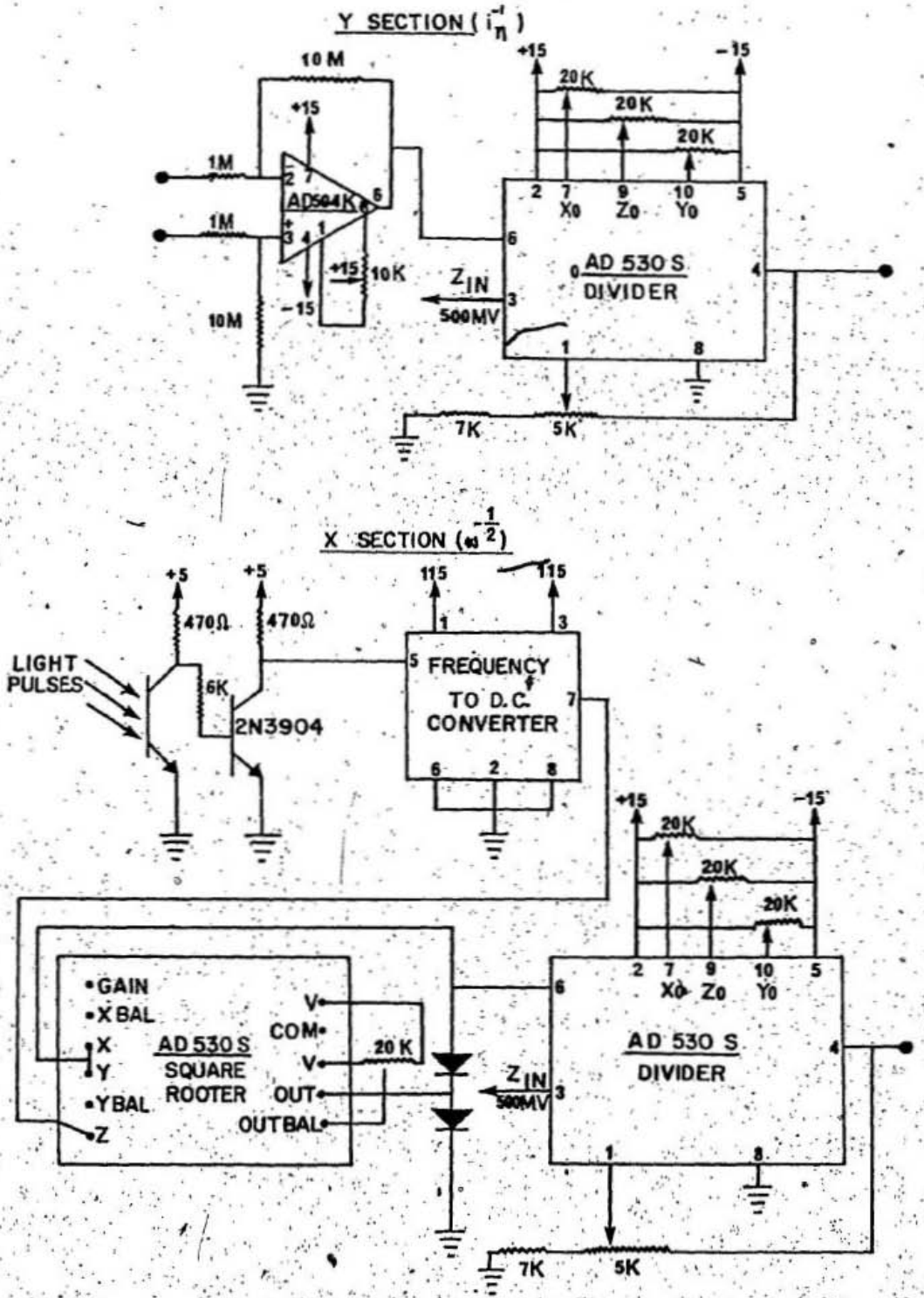

Fig. 4 Schematic diagram of device for direct plotting of inverse Levich plots.

Fig. 5 The cell.

Fig. 6 The cell, mounted in its thermostatting jacket.

between these two for the possible inclusion of other auxiliary electrodes (e.g. for oxidation purposes). A final B10/19 cone opposite, permitted entry of a nitrogen degassing tube. This tube was fitted with a two-way tap for purging the solution (degassing) or flowing over the surface (during measurements). A B14 socket with a thermometer well allowed the entry of a thermometer which measured the temperature of the experimental solution. An Ertco F series (-1°C to 51°C) thermometer was used for this purpose. Its calibration was checked against a platinum resistance thermometer using a Tinsley Wheatstone bridge. The corrections observed were so small that they had negligible effect on the relatively low activation energies observed. The Pyrex cell was raised and lowered by mounting it on a small scissors-jack support.

Reference and Counter Electrodes

The reference and counter electrodes for the cell were also constructed of Pyrex. Metals used in their preparation were of varying quality. The platinum counter and reference electrodes were prepared from 1 cm^2 Johnson Matthey and Mallory (J.M. & M.) Grade 2 platinum foils rolled in a cylindrical fashion. The palladium and gold counter and reference electrodes were constructed from 0.2 cm diameter J.M. & M. Grade 1 rod (see below). This was exactly the same material as used for the rotating discs. In each case, apparatus grade platimum (i.e. Grade 4, J.M. & M.) was employed as connecting leads to the counter and reference electrodes. In the palladium and gold cases, extreme care was taken so that no platinum was exposed to the solution

at the metal-in-glass sealed ends. For the gold electrodes special treatment was necessary. Because of its lower melting point, it was sealed into soda glass instead of Pyrex. Connection to the upper Pyrex tubing and socket was made with heat-shrinkable Teflon tubing. During experiments this seal was high enough on the electrode to be out of the solution.

Cleaning Procedures

During construction of mechanical apparatus, contact with organic materials (greases, oils, etc.) was minimized if not totally eliminated, where possible. However, all equipment received from the machine shop was initially degreased by treating with hot toluene to extract soluble organic matter, then hot ethanol to remove the toluene, followed by a number of washings with triple distilled water.

All newly constructed glassware was briefly treated with hot concentrated sodium hydroxide, then water. Before experimental use, all glassware was cleaned with boiling concentrated nitric acid. Several rinsings with triple distilled water followed. For the case of palladium reference and counter electrodes, a hot dilute nitric acid solution was the cleaning agent in place of concentrated nitric acid. Finally, just prior to an experimental run, all glassware and electrodes were given a thorough steaming.

Before each experiment, the RDE was stirred in hot concentrated caustic soda. The electrode was then treated several times with triple distilled water, washed with dilute perchloric acid, and finally washed several more times with water. This procedure was concluded by spinning the electrode at high speed for several minutes to dry it.

Materials

Perchloric Acid: 72% BDH ARISTAR $HClO_4$ (ClO_3^-, Cl^-, PO_4^{3-}, SiO_2, Ca, Mg, Sr, 1 ppm each; SO_4^{2-}, 2.5 ppm; Al, NH_3, Cl_2, Co, Cu, Pb, Li, Mn, Ni, K, Ag, Hg, Na, Zn, less than 0.5 ppm each;) was diluted to either 1.0 mol. l^{-1} or 0.1 mol. l^{-1} for the test solution.

Triple Distilled Water: Tap water was distilled, then redistilled over alkaline permanganate, followed by a final distillation under nitrogen with carbon dioxide prevented from entry by a soda lime trap.

Charcoal was prepared by reacting Sucrose with ARISTAR concentrated H_2SO_4, washed with water, then activated at red heat in air. The charcoal was then extracted with hot ethanol for three days and finally washed for six weeks with triple distilled water, renewed weekly. For use in solution purification, it was finally activated under nitrogen in an electrically heated silica test tube.

Iron: All iron perchlorate solutions were prepared by dissolving G.F. Smith Chemical Company 100.00% pure iron ("electrolytic, ignited in moist hydrogen") in ca. 6 mol.ℓ^{-1} perchloric acid at room temperature.

Nitrogen: Canadian Liquid Air, L-grade nitrogen (N_2, 99.99%; O_2, 20 ppm maximum; moisture, less than 10 ppm; Ar, 80 ppm;) was further purified by passing through a furnace at 140°C containing pre-reduced BTS catalyst from Badische-Anilin-und-Soda-Fabrik. This material is composed of 30% finely dispersed copper oxide, stabilized on a carrier, activated by reduction with hydrogen at 140°C. It diminishes oxygen to less than 0.1 ppm. The nitrogen was then passed through a solid carbon dioxide - ethanol trap and through two pre-saturators filled with triple distilled water and finally into the cell.

Platinum RDE: J.M. & M. Grade 1, 0.2 cm diameter rod was used for the platinum RDE (Cu, 3 ppm; Fe, Ni, Si, 2 ppm each; Au, Ag, 1 ppm each; Ca, Mg, Pd, less than 1 ppm each).

Gold RDE: J.M. & M. Grade 1, 0.2 cm diameter rod was used for all the gold electrodes (Ni, 7 ppm; Fe, 3 ppm; Ag, 2 ppm; Cu, 1 ppm; Mg, less than 1 ppm).

Palladium RDE: J.M. & M. Grade 1, 0.2 cm diameter rod was used for all the palladium electrodes as well as the RDE (Si, 4 ppm; Fe, 4 ppm; Ca, Cu, Mg, Ag, less than 1 ppm each).

Instrumentation

Potentiostats and Galvanostats: For determining current-over-potential relations a very precise (± 0.02 mV) custom built low voltage potentiostat (± 100 mV maximum output, linearity ± 0.1%) was used. Another custom made potentiostat, with a maximum range of ± 5V and resolution to 1 mV was used for limiting current measurements. This equipment could also serve as a two electrode galvanostat with current control on various ranges up to a maximum of 100 mA at an applied potential difference of 13 volts.

A Princeton Applied Research, Model 174 polarographic analyzer was used in determining real surface areas. It had high accuracy (± 0.25%) as well as a built-in potential scanning capability. This was used in conjunction with a Houston HR-2000 X - Y recorder for recording current-potential scans.

An Exact T301 function generator coupled with a battery-operated adjustable low voltage source was used for activation of the test electrode.

Voltmeters and Ammeters: Currents were measured with a Model 163 Keithley digital voltmeter shunted by a 1 KΩ General Radio standard resistor. A Keithley Model 602 Electrometer (± 2% accuracy) was used for potential measurements during cyclic activation and in the limiting current measurements. Various current-potential curves were recorded on the X - Y recorder previously mentioned. This recorder was later used with the automatic plotting device. This was used in some of the work for providing direct plots of i^{-1} vs. $\omega^{-1/2}$. It embodied the principles of the circuit designed by Kretschmer, Hamann, and Fassbender[46]. In our work the accuracy of the device was improved by replacement of their photodiode and multivibrator with a phototransistor and frequency to D.C. converter, respectively.

The entire experimental set-up is illustrated in Fig. 7.

METHOD

A usual experimental run was of one week's duration. Solutions were prepared and then passed into the cleaned apparatus through activated charcoal. The prepared ferrous perchlorate solution was potentiostatically oxidized to bring the ferrous and ferric ions to equal concentrations (in 24 to 48 hours). The progress of the potentiostatic oxidation was monitored by measuring the mass transport-limited currents. Alternatively, the current was measured as a function of time during the electrolysis so that an estimate of the total charge passed could be made. In any event, final verification of concentration, for purposes of calculation, was made following the experiment by analyzing a sample of the test solution potentiometrically on platinum against a standard Fisher certified 0.1 mol.ℓ^{-1} $Ce(SO_4)_2$ titrant.

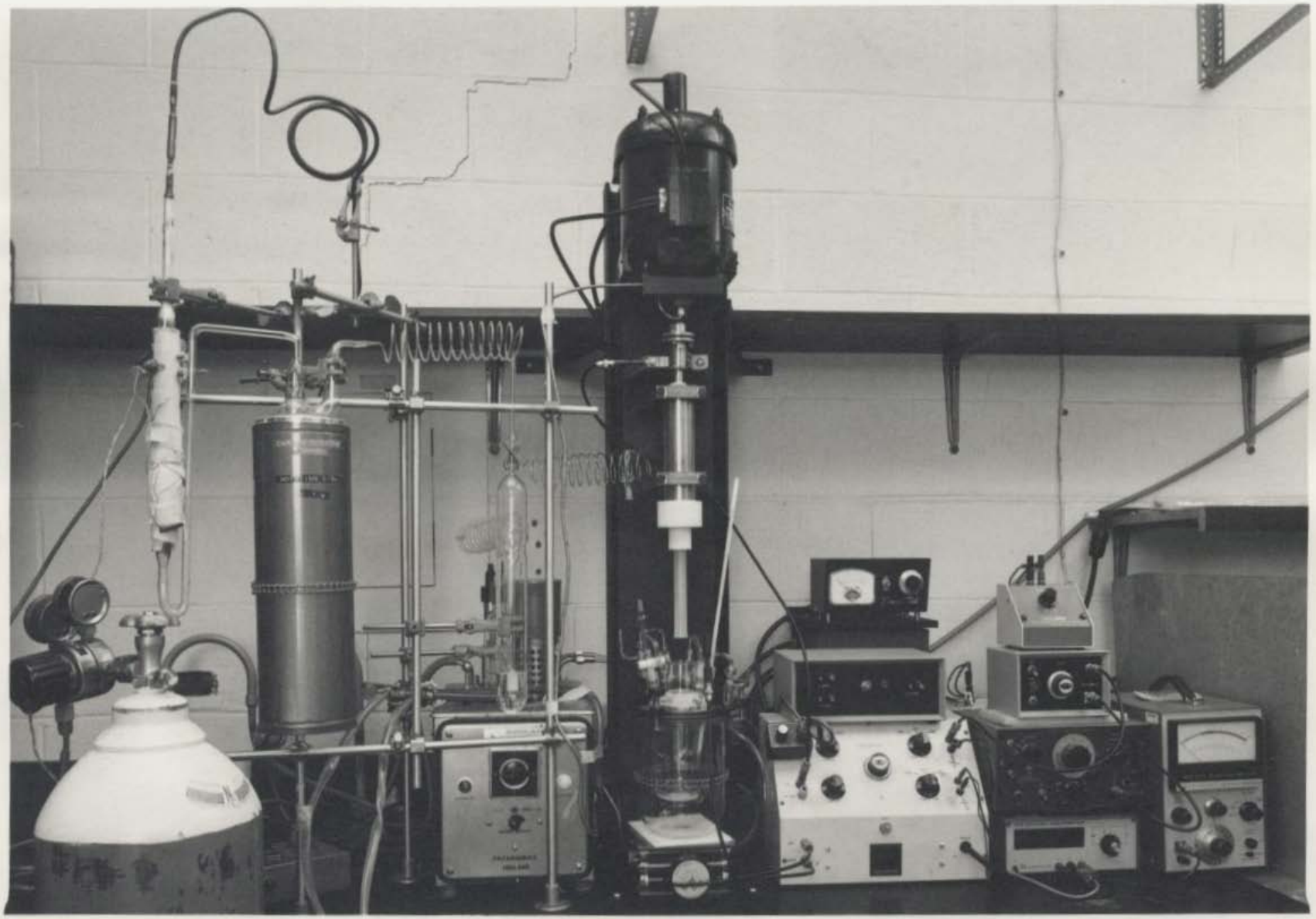

Fig. 7 The rotating disk electrode assembly with the cell, electronic equipment, water bath, and nitrogen purification system.

When oxidation was complete a 48 hour pre-electrolysis was performed. This was done galvanostatically, and was carried out at a current higher than any likely to be used in the experiment, and at room temperature, the highest working temperature.* The two electrode pre-electrolysis was concluded by simultaneously removing cathode and anode from the solution with current flowing, thus preventing deposited impurities from redissolving. The measurements then proceeded with fresh reference and counter electrodes.

The test electrode was activated "in situ" by cyclically varying its potential with time between set limits, depending upon the metal used. The sweep rate was 40 mV. s^{-1}. The cathodic and anodic limits of activation were chosen after reviewing the work of Rand and Woods[19]. These authors investigated the effect of cyclic activation of noble metal electrodes to certain anodic limits on the dissolution of these metals. On the basis of their results the following activation programs were chosen for the metals studies in the present work, such that no dissolution of the test electrode metal (and/or counter electrode) would occur: platinum (0.41 - 1.05 V versus NHE), gold (0.60 - 1.40 V), and palladium (0.33 - 0.95 V). By taking these precautions the possibility of electrode roughening was eliminated, as well as catalytic effects of dissolved noble metal ions or their electrodeposits. Extra care was taken in the case of the palladium electrode in that the cathodic limit, as well as the anodic limit was strictly adhered to, thus preventing possible hydrogen absorption into the palladium.

* In the later stages of the work.

Test electrodes were usually activated initially for a period of one hour. Each was then activated for a few minutes before each temperature of observation, in order to offset deactivation effects. In the case of platinum longer intermittent periods of activation were required to maintain the electrode at its maximal activity. The activation procedure was always halted on the cathodic side of the sweep, so that no oxide films would be present.

Kinetic data were measured by determining the slope of the current-potential relationship at various rotation speeds. Exchange current densities were calculated from equation (18) at each rotation speed. In the initial activation, potential cycling was repeated until measurements were reproducible. Plots of i_o^{-1} versus $\omega^{-1/2}$ were made at each temperature. Intercept, slope, and inherent errors were determined by a weighted least squares analysis. Data were interpreted by both the intercept and the Jahn-Vielstich techniques. Randles' method of analysis was also applied, considering current-overpotential relationships and limiting currents at each rotation speed separately. For convenience, a series of measurements of ferrous and ferric diffusion coefficients were made at a variety of concentrations on platinum. These were later confirmed using gold. For the lengthy series of calculations inherent in the Randles approach a computer program was utilized using a PDP-11 computer.

Experimental activation enthalpies* were determined from the temperature dependency of the exchange current density as follows:

* Since, in this case, the difference between internal energy changes and enthalpy changes is insignificant, the latter term was used for convenience.

$$\Delta H^{\ddagger} = -R\left(\frac{\partial \ln(i_o)_\infty}{\partial(1/T)}\right) \qquad (55)$$

Errors were estimated from the standard deviation of the slope obtained by weighted least squares. The pre-exponential factor $A^{\ddagger}$ was obtained from the intercept of the Arrhenius plot at $T^{-1} = 0$.

Real Surface Areas: The real surface area of each of the noble metal RDE's was determined by various techniques. In each case the real surface area was not determined until all the kinetic work had been concluded. This was due to the possibility that the procedure used for estimating these areas could cause metal dissolution and roughening of the electrode. This fear was greatest in the case of palladium. Surface area measurements were important since the kinetics of the ferrous-ferric system depend upon the real surface area.

For measuring the surface areas of each metal, the methods of Woods[47] were used. The platinum real surface area was determined by measuring the charge required to adsorb either a monolayer of hydrogen atoms or desorb a monolayer of oxygen atoms. Current-time sweeps were integrated according to the suggestions of Woods. The hydrogen method was preferred for platinum and real surface areas were calculated by dividing the integrated charge by 210 $\mu C/cm^2$.

For real surface area measurements on palladium and gold, areas were calculated by oxygen desorption alone. These were estimated by dividing the integrated charges for palladium and gold by 424 and 386 $\mu C/cm^2$, respectively[47].

RESULTS AND CALCULATIONS

Preliminary Work

The initial stage of the research involved exploratory experiments, performed using the platinum RDE of the old apparatus. During this period, data points were collected over a wider temperature range (288 - 338 K) than for most of the later work. In addition, the electrode was activated over two different potential ranges, one being the conventional range +0.4 to +1.42 V and the other, +0.4 to +1.05 V, resulting from an examination of Rand and Woods' experiments[19].

These experiments were informative with respect to the performance of the old experimental equipment as well as to the general use of a RDE in interfacial kinetics. According to equation (42), the technique relies upon a long extrapolation to infinite rotation speed for determination of the true exchange current density or heterogeneous rate constant. Data taken over a range of temperatures would yield a family of plots (see Fig. 8) whose y-intercepts increase with decreasing temperature. It was generally observed from our results that, for a particular family of curves, the absolute error associated with the deviation of the data points from perfect linearity, and calculated in the statistical treatment of the extrapolation, was roughly the same for all temperatures studied. But in contrast, the relative error increased with increasing temperature due to the diminishing intercept (i.e. the rate was increasing). It was found that at temperatures exceeding about 298 K, the errors associated with such intercepts were often greater than the exchange current density indicated. The difficulty was compounded because the poor speed control of this old

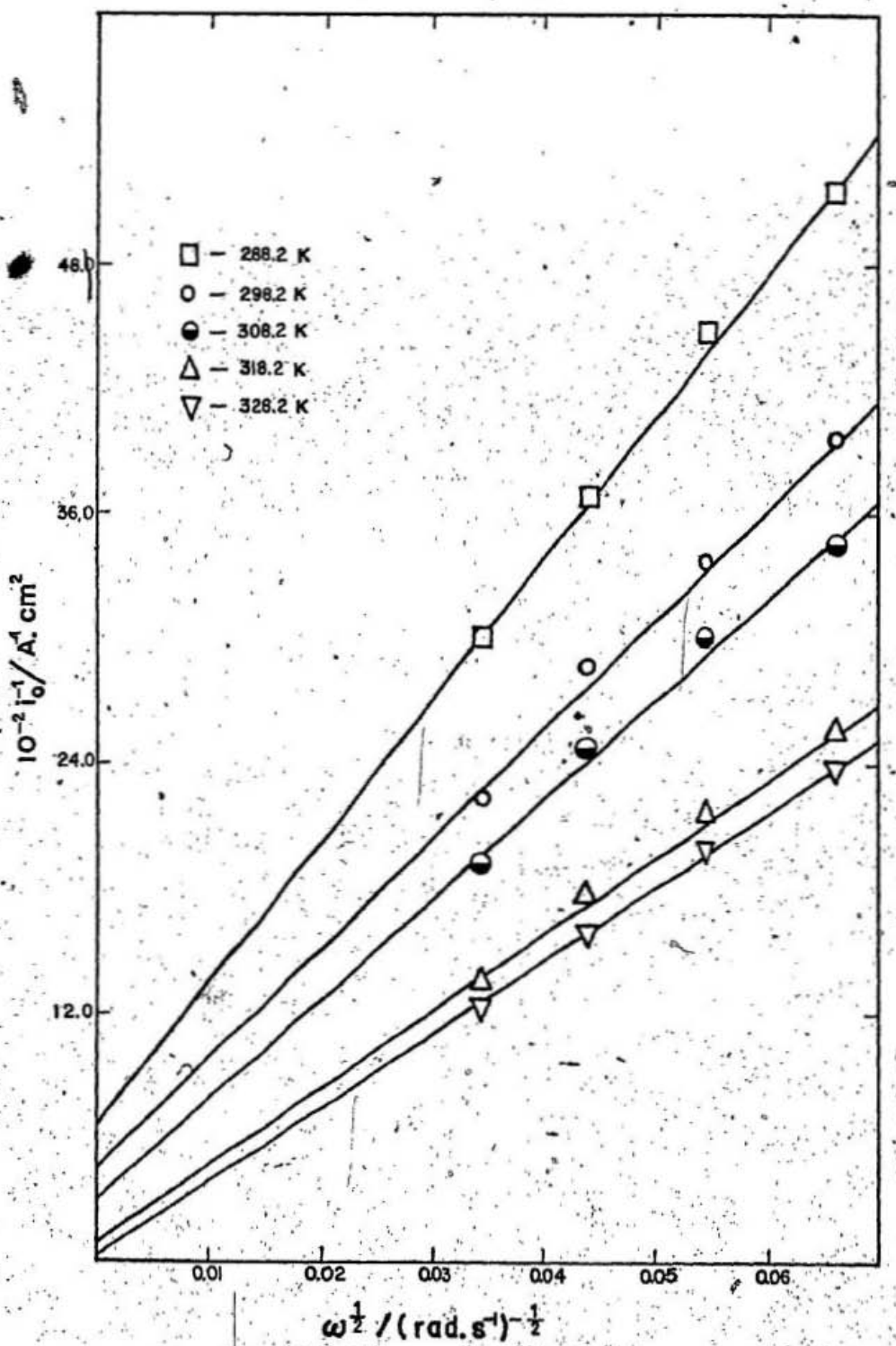

Fig. 8 Inverse Levich plots, Pt, 10^{-6} mol. cm^{-3} Fe^{2+}, Fe^{3+} in 10^{-4} mol. cm^{-3} $HClO_4$; experiment no. 9.

apparatus increased the generated error. In some high temperature experiments, ca. 328 - 338 K, either a negative intercept or an error limit extending below zero was observed. These results were extraneous and could not be interpreted in physical terms. In his book, "Electrochemical Kinetics", Albery[36] considers the relative rates of mass transport and of electron transfer and estimates the maximum heterogeneous rate constant measurable by a RDE to be ca. 0.01 $cm.s^{-1}$. In most of these initial experiments, the apparent rate constants observed at temperatures above 298 K exceed this value. Thus the reaction rate exceeded the limit imposed by the experimental method chosen for its study. A typical Arrhenius plot obtained from these early data is seen in Fig. 9. The error bars illustrate the problems previously mentioned, especially with respect to the negative intercepts and error limits which extend off the graph. By considering all the points of this plot a $\Delta H^{\ddagger}$ of approximately 48 - 60 $kJ.\ mol^{-1}$ is deduced. This wide variation illustrates the large and excessive errors involved in such a long extrapolation at higher temperatures. Considering Fig. 9 qualitatively, we may conservatively apply Albery's limit (i.e. to the three lower temperatures) as indicated by the dotted line to obtain a revised $\Delta H^{\ddagger}$ of about 36 $kJ.\ mol^{-1}$. Lower temperature Arrhenius plots took on greater significance later in the work. Many of the results in the preliminary work were similar to Fig. 9 and were not very reliable. From these results, the course for the remainder of the research was clear, namely to obtain data at lower temperatures using a servo-controlled RDE.

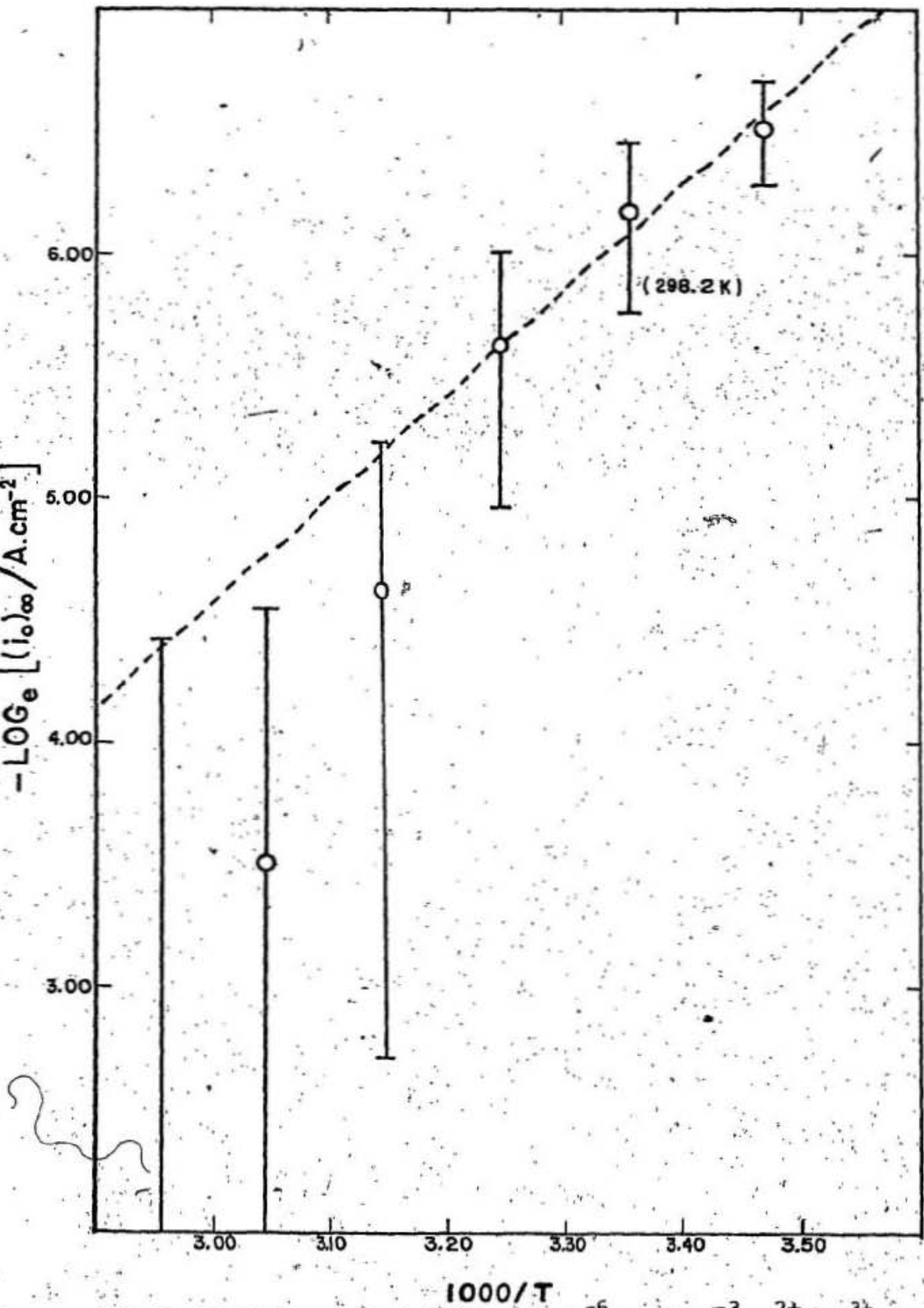

Fig. 9 Arrhenius plot of $(i_o)_\infty$, Pt, 10^{-6} mol. cm^{-3} Fe^{2+}, Fe^{3+} in 10^{-4} mol. cm^{-3} $HClO_4$; experiment no. 9, $\Delta H^{\ddagger}$ determined at lower temperatures, ca. 36 kJ. mol^{-1}.

Because of the drawbacks inherent in these early results, it was difficult to discern whether changing the activation potential limits had any effect upon the true rate parameters. Rand and Woods[19] have clearly demonstrated the occurrence of metal dissolution at higher anodic sweeping limits (above +1.05 V for platinum). During the initial series of runs, the maximum anodic limit was diminished and the rate constant (298 K) recorded in each experiment thereafter showed a gradual non-linear decline in magnitude, illustrating the effects of possibly "overactivating" the RDE in earlier trials. Any solid electrode kineticist must recognize the role of the electrode's activity and its history in studying electrocatalysis. This activity was identified in this work as the most important single factor contributing to irreproducibility of results. This is true for all the metals studied in this work, but is especially important for platinum. The greatest obstacle in determining rate parameters on solid electrodes is the maintenence of the electrode in a state of constant maximum activity.

In one experiment, (see Table 1) performed on a new platinum disc, (never activated) a perfectly linear Arrhenius plot was obtained (see Fig. 10). This linearity was possibly indicative of constant activity throughout the temperature range. The extrapolations relevant to Table 1(b) are shown in Fig. 11. Note that the observed $\Delta H^{\ddagger}$ is quite comparable to the value obtained from the low temperature points of Fig. 9. However the observed rates differ by several orders of magnitude. These early results, even though very qualitative, hint that $\Delta H^{\ddagger}$ is possibly independent of the activity of the electrode,

Table 1(a) Exchange current density:- rotation speed dependence. Experiment No 1: unactivated Pt, 10^{-6} mol.cm^{-3} Fe^{2+}, Fe^{3+} in 10^{-4} mol.cm^{-3} $HClO_4$. Data presented in order of measurement.

301.0 K		308.4 K		321.0 K	
ω/rpm	$10^5 i_o$/A.cm^{-2}	ω/rpm	$10^5 i_o$/A.cm^{-2}	ω/rpm	$10^5 i_o$/A.cm^{-2}
7500	1.46*	1360	1.77	2460	2.92
1500	1.43	2200	1.85	3400	3.02
1800	1.44	3500	1.88	4200	3.10
2850	1.45	4300	1.92	5300	3.13
4050	1.45	5600	1.92	6500	3.14
4900	1.45	7200	1.93	7800	3.15
6100	1.46	3850	1.87	4100	3.11

* Relative precision for i_o measurement assessed to be ± 0.3%.

Table 1(b) Exchange current densities extrapolated to infinite rotation speed, from Fig. 11, Experiment No. 1. Activation enthalpy from Fig. 10.

T/K	$10^5 (i_o)_\infty$/A.cm^{-2}
301.0	1.49 ± 0.05
308.4	2.08 ± 0.03
321.0	3.55 ± 0.08
$\Delta H^{\ddagger}$ =	(34.9 ± 0.7) kJ.mol^{-1}

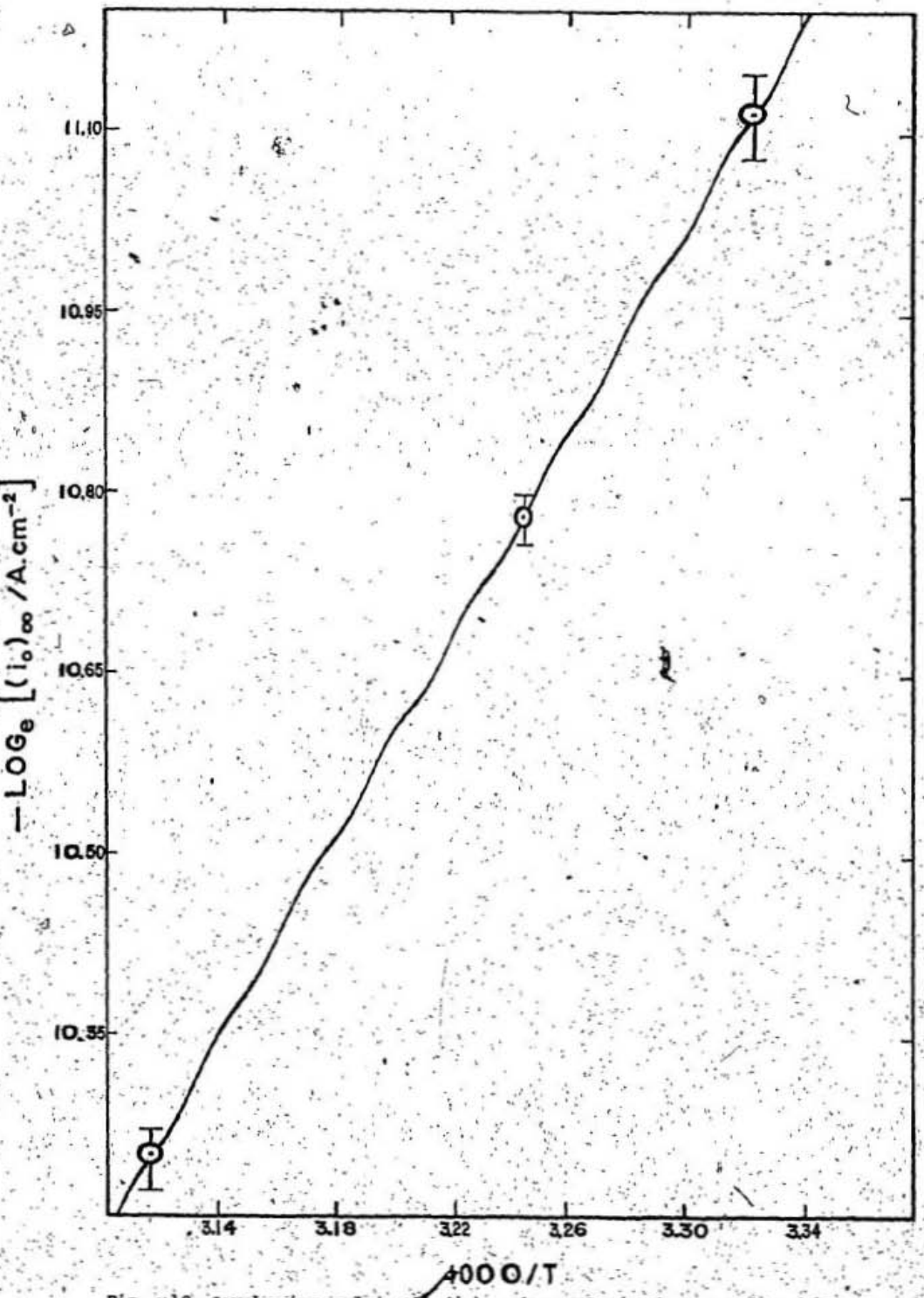

Fig. 10 Arrhenius plot of $(i_o)_\infty$ (see Fig. 11), unactivated Pt, 10^{-6} mol. cm^{-3} Fe^{2+}, Fe^{3+} in 10^{-4} mol. cm^{-3} $HClO_4$; experiment no. 1, data from Table 1(b), $\Delta H^{\ddagger}$ = (34.9 ± 0.7) kJ. mol^{-1}.

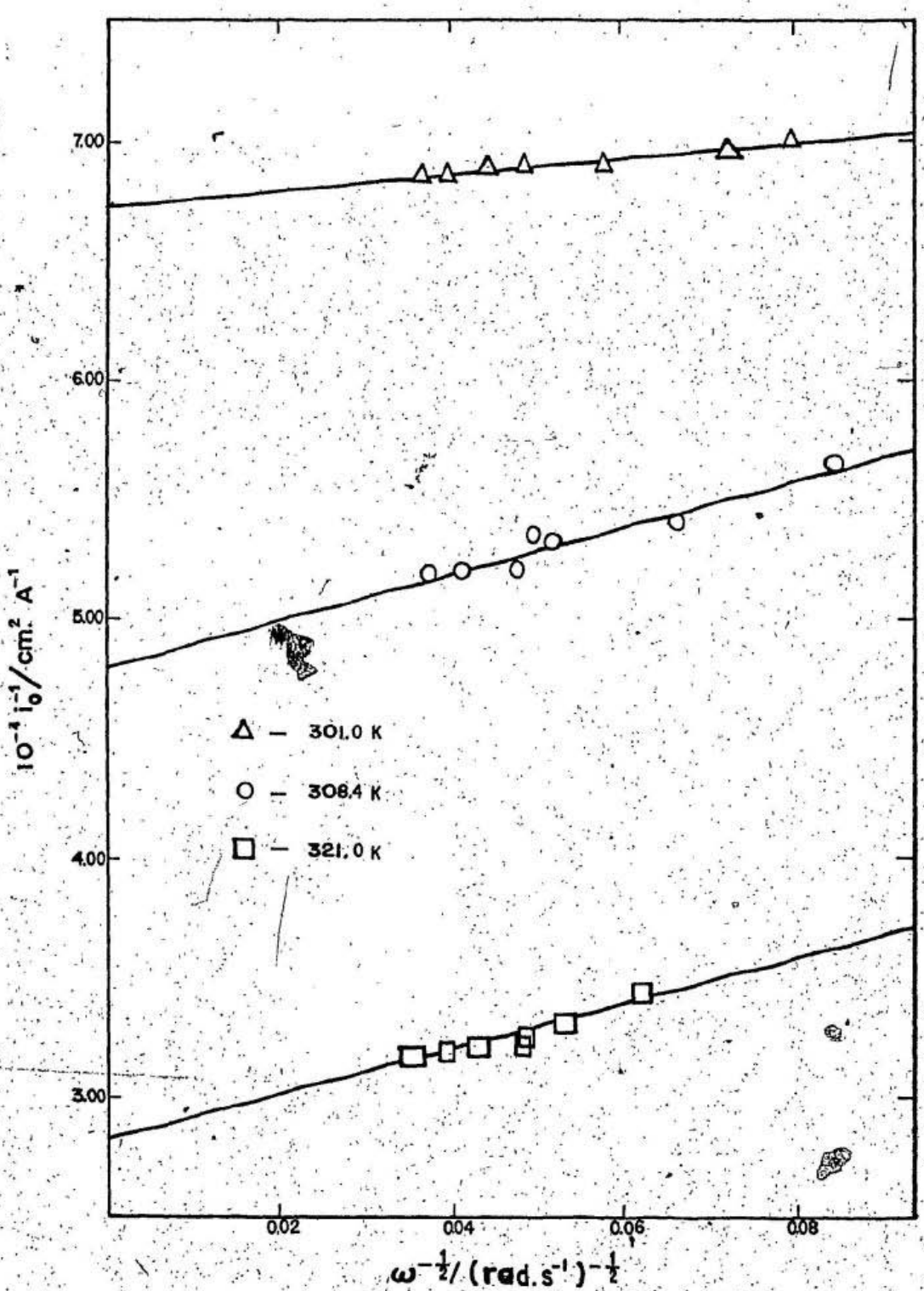

Fig. 11 Inverse Levich plots of $(i_o)_\infty$, unactivated Pt, 10^{-6} mol. cm^{-3} Fe^{2+}, Fe^{3+} in 10^{-4} mol. cm^{-3} $HClO_4$; experiment no. 1, data from Table 1(a).

provided that its activity is constant during the short term of the experimental measurement. The rate constant is obviously not independent of electrode activity. No firm conclusions concerning this matter could be made on the basis of these preliminary results. Some of these preliminary results are listed in Table 2, the $\Delta H^{\ddagger}$'s of which were originally widely variant but were reevaluated for low temperatures only. These results indicate the effects of activating the electrode as a function of both the anodic limit and also time. The gradual non-linear decrease of the rate constant was observed after the activation limits were changed. In summary, these data were only useful in illustrating the problems to be overcome in the later work.

The remaining major portion of the research was performed with a view to clarifying the results for platinum, and of studying two other noble metals, palladium and gold, to determine if any relationship existed between rate parameters and the nature of the metal. Rates were measured over the lower temperature range, 273 - 298 K in the remainder of the work.

Diffusion Coefficients

In order to apply the methods of data analysis outlined in the theoretical background section, utilizing equations (42) and (43) and (49) and (50), respectively, the diffusion coefficients for ferrous and ferric species were needed and anodic and cathodic limiting currents were determined.

$D_{Fe^{2+}}$ and $D_{Fe^{3+}}$ were obtained by measuring mass transport-limited currents at high overpotentials (η = ±455 mV). A Levich plot of i_{LIM}

Table 2 Some early experimental results using the old apparatus, 10^{-6} mol.cm^{-3} Fe^{2+}, Fe^{3+} in 10^{-4} mol.cm^{-3} $HClO_4$; all on Pt.

Expt. No.	$10^3 k_o$/cm.s^{-1} at 298.2 K	$\Delta H^{\ddagger}$/ kJ.mol^{-1}	$A^{\ddagger}$/ cm.s^{-1}	Activation Program* Limits Volts vs. NHE
1	0.13††	34.9	1.69×10^{2}	None
2	2.59	8.4	7.67×10^{-2}	A - just at the start
3	2.53	11.7	2.84×10^{-1}	A - just at the start
4	23.6	35.1	3.33×10^{4}	A - continuously while changing T
5	39.9	27.6	2.73×10^{2}	A - continuously while changing T
6†	36.5	45.2	3.03×10^{6}	A - continuously while changing T
7†	50.0	61.1	2.53×10^{9}	A - continuously while changing T
8	42.6	35.6	7.35×10^{4}	B - continuously while changing T
9	36.1	34.3	3.69×10^{4}	B - continuously while changing T

*A: +0.4 to +1.42; B: +0.4 to +1.05

† Following kinetic determinations, these test solutions were analyzed for dissolved platinum by the stannous chloride method of Sandell[71]. Levels of dissolved platinum were found to be below the limit of detection, i.e. < 4 ppb.

†† Data in Table 2 are preliminary. Therefore, no estimate of error has been assigned.

versus $\omega^{1/2}$ yields a straight line with a slope dependent on the diffusion coefficient. A family of cathodic (Fig. 12) and anodic (Fig. 13) plots at various temperatures was obtained for each species. Diffusion coefficients were calculated using the expression of Bruckenstein[40] (equations (32) and (33)) from the Levich plot slopes evaluated by a linear least squares computation. Kinematic viscosities for aqueous perchloric acid were interpolated from the compilations of Landolt and Börnstein[51]. The temperature dependencies of D_{Fe}^{2+} and D_{Fe}^{3+} were found by a $\ln D_{Fe}^{n+}$ versus T^{-1} plot. These were reported in the form $D = D_o \exp(-E_D/RT)$ where E_D/R is the slope of the Arrhenius plot and D_o the intercept at $T^{-1} = 0$. All results were obtained using 10^{-3} mol.cm^{-3} $HClO_4$ since all of the later kinetic data were obtained in this medium.

Typical values of the diffusion coefficients are listed in Table 3, which include results obtained on both platinum and gold. No diffusion coefficients were determined on palladium due to the high risk of dissolution at high anodic overpotentials.

The temperature dependency of each diffusion coefficient was determined on platinum, the Arrhenius parameters, summarized in Tables 4 and 5, having been determined from plots exemplified by Fig. 14.

The Arrhenius parameters for D_{Fe}^{2+} do not show any trend with varying concentration, which agrees with the general assumption that the diffusion coefficient is concentration independent. However a slight trend is evident for the D_{Fe}^{3+} measurements which seem to increase slightly with increasing concentration of Fe^{3+} ions.

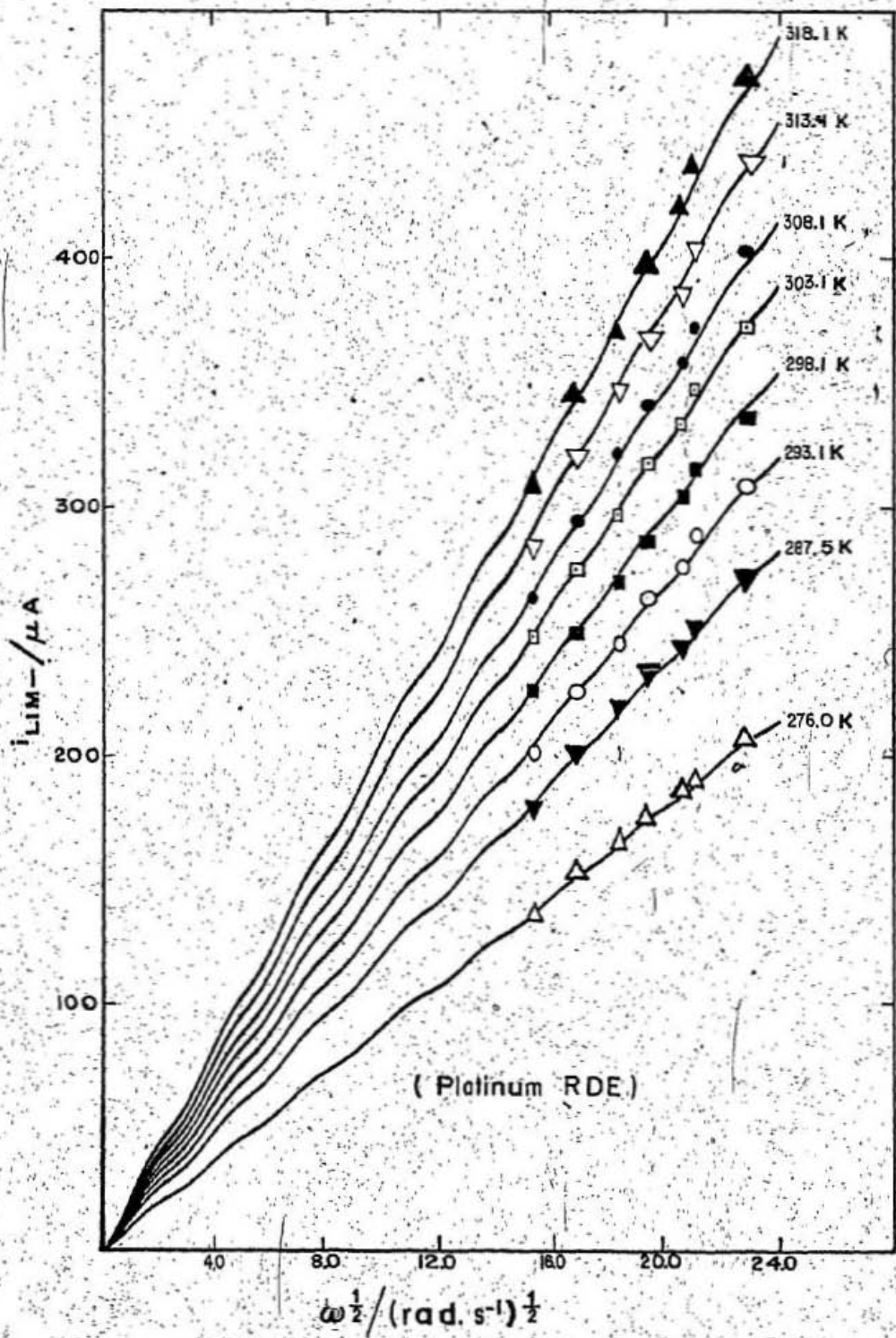

Fig. 12 Levich plots for $D_{Fe^{3+}}$ determination; Fe^{3+}; 10^{-5} mol. cm^{-3} in 10^{-3} mol. cm^{-3} $HClO_4$; obtained at η = -455 mV.

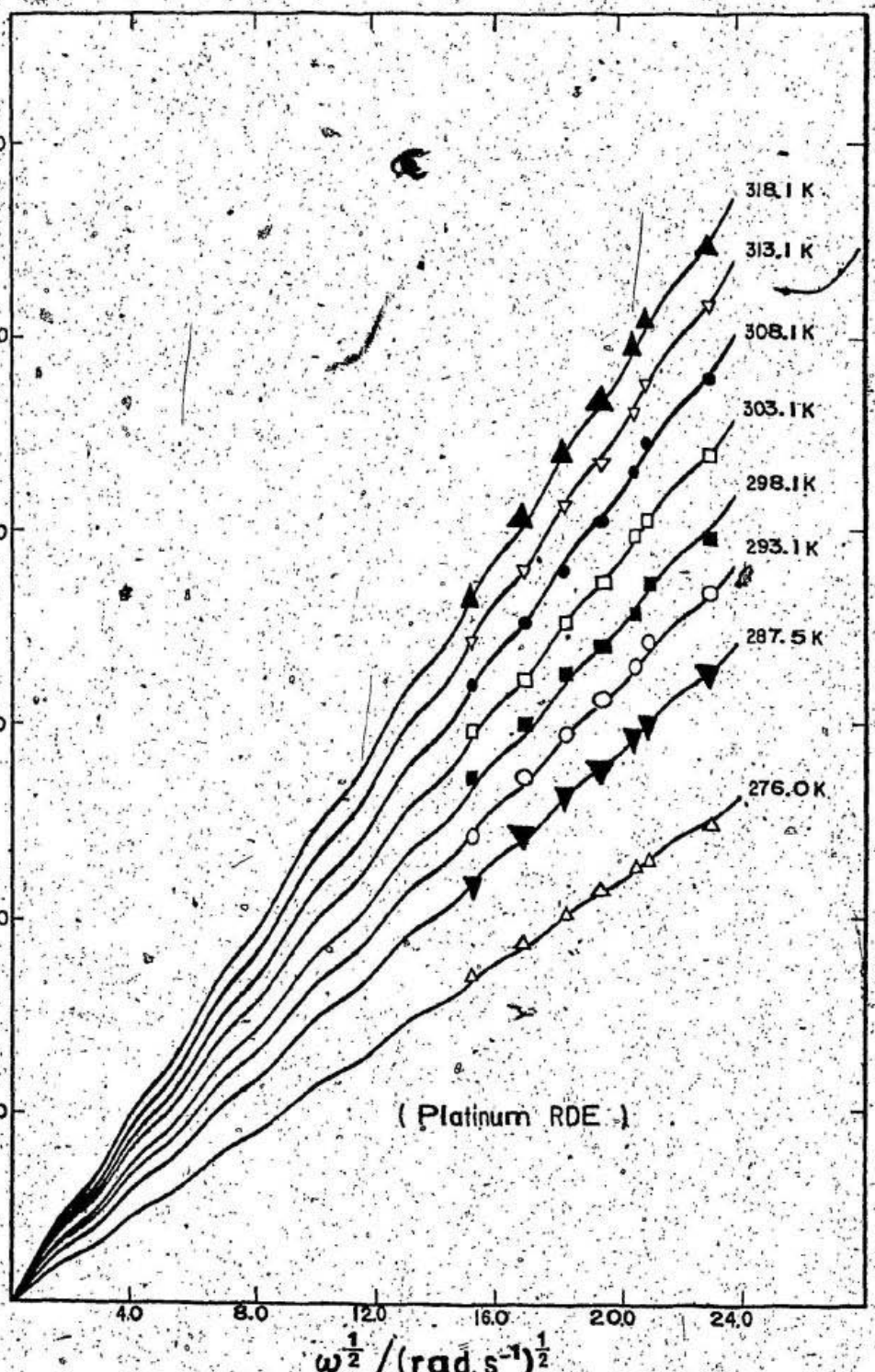

Fig. 13 Levich plots for $D_{Fe^{2+}}$ determination; Fe^{2+}: 10^{-5} mol. cm^{-3} in 10^{-3} mol. cm^{-3} $HClO_4$; obtained at η = +455 mV.

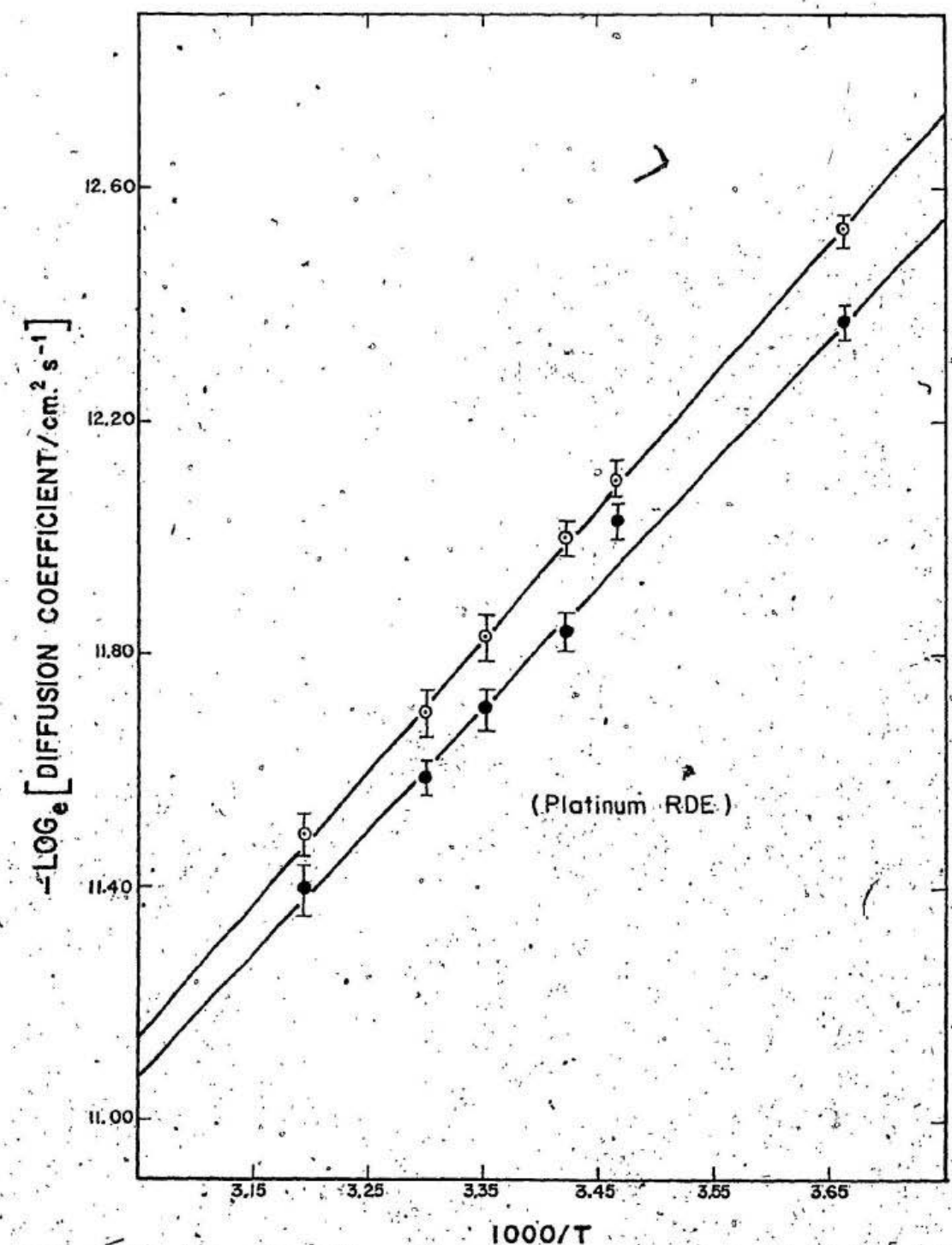

Fig. 14 Diffusion coefficient temperature dependencies; 10^{-5} mol. cm^{-3} Fe^{2+}, Fe^{3+} in 10^{-3} mol. cm^{-3} $HClO_4$; Fe^{2+} (●), E_D = (18.2 ± 1.0) and Fe^{3+} (○), E_D = (18.7 ± 0.2) kJ. mol^{-1} respectively.

Table 3 Concentration and temperature dependence of diffusion coefficients of Fe^{2+} and Fe^{3+} in 10^{-3} mol.cm^{-3} $HClO_4$ using rotating disc electrodes of the metals indicated.

T/K	Redox ion concentration/mol.cm^{-3}			Metal
	10^{-6}	10^{-5}	2×10^{-5}	
	$10^5 D_{Fe^{2+}}$/cm.^{2}s^{-1}			
273.2	0.50_1	0.44_3	0.50_4	Pt
298.2	0.90_8	0.86_1	0.93_1	Pt
323.2	1.50_0	1.51_0	1.57_0	Pt
298.2	-	0.82_7	-	Au
	$10^5 D_{Fe^{3+}}$/cm.^{2}s^{-1}			
273.2	0.34_2	0.36_9	0.32_0	Pt
298.2	0.65_9	0.73_7	0.69_2	Pt
323.2	1.15_0	1.32_0	1.33_0	Pt
298.2	-	0.66_4	-	Au

Table 4 Arrhenius parameters for $D_{Fe^{2+}}$ in 10^{-3} mol.cm^{-3} $HClO_4$ using a Pt RDE.

[Fe^{2+}]/mol.cm^{-3}	$10^4 D_o$/cm^{2}s^{-1}	E_D/kJ.mol^{-1}
10^{-6}	60.3 ± 3.6	16.1 ± 0.8
10^{-5}	113 ± 7.9	17.8 ± 0.8
10^{-5}	132 ± 12.8	18.2 ± 1.0
2×10^{-5}	77.0 ± 4.2	16.7 ± 0.7

Table 5 Arrhenius parameters for $D_{Fe^{3+}}$ in 10^{-3} mol.cm^{-3} $HClO_4$ using a Pt RDE.

$[Fe^{3+}]$/mol.cm^{-3}	$10^4 D_o$/cm^{2}s^{-1}	E_D/kJ.mol^{-1}
10^{-6}	78.3 ± 2.6	17.6 ± 0.4
10^{-6}	92.7 ± 5.4	17.9 ± 0.7
10^{-5}	142 ± 2.2	18.7 ± 0.2
10^{-5}	134 ± 7.6	18.7 ± 0.6
2×10^{-5}	320 ± 29	20.9 ± 0.8

Rate Measurements with Platinum

The results obtained using platinum were by far the most difficult to reproduce even with the use of the new improved RDE. Again, this problem was undoubtedly associated with the activity of the electrode surface. Data were obtained by repetitive measurements at a variety of temperatures ranging back and forth between ca. 273 and 298 K. Even during a single experiment, the rate was observed to vary by a factor of two. Behaviour of this sort was even seen in experiments (e.g. Experiment No. 24) in which the test solution was pretreated with activated charcoal. All results are reported as the heterogeneous rate constant k_o in cm.s^{-1}. Results expressed as i_o were converted to k_o using equation (16) i.e. $k_o = i_o/FC_i^{\infty}$.

Table 6 lists the data of a typical experiment. Exchange current densities, i_o, were calculated from the $i - \eta$ slope using equation (18) at various rotation speeds and temperatures. An inverse Levich plot

Table 6 Exchange current densities as functions of rotation speed and temperature in Experiment No. 24: Pt, 10^{-5} mol.cm^{-3} Fe^{2+}, Fe^{3+} in 10^{-3} mol.cm^{-3} $HClO_4$.

	10^3 i_o/A.cm^{-2}									
ω/rpm	355	429	530	715	895	1080	1430	2150	2842	3550
T/K										
298.2*	1.37†	1.48	1.63	1.86	2.06	2.22	2.53	3.00	3.38	3.66
298.2	1.38	1.49	1.64	1.85	2.03	2.20	2.48	2.92	3.29	3.58
293.1	1.21	1.32	1.45	1.63	1.79	1.94	2.17	2.56	2.87	3.13
288.5	1.09	1.18	1.31	1.48	1.63	1.75	1.98	2.35	2.60	2.82
284.1	1.01	1.09	1.18	1.33	1.45	1.54	1.73	2.02	2.23	2.41
278.2	0.87	0.93	1.02	1.13	1.23	1.32	1.47	1.69	1.88	2.01
277.3	0.85	0.91	0.99	1.10	1.20	1.28	1.41	1.62	1.78	1.91
299.1	1.37	1.49	1.64	1.86	2.04	2.22	2.51	2.98	3.32	3.58
289.2	1.13	1.22	1.34	1.49	1.63	1.74	1.95	2.28	2.53	2.75
283.8	0.98	1.05	1.15	1.28	1.40	1.51	1.67	1.95	2.16	2.34
280.5	0.89	0.96	1.05	1.16	1.26	1.36	1.50	1.74	1.92	2.07
288.5	0.97	1.05	1.15	1.30	1.43	1.53	1.74	2.04	2.27	2.47

* Results from top to bottom of table in order of measurement.

† Relative precision for i_o measurement assessed to be ± 0.3%

of some of this data (i_o^{-1} vs $\omega^{-1/2}$) is shown in Fig. 15. (Some data were omitted from the plot, for clarity). The data were analyzed by both the intercept and Jahn-Vielstich methods. In addition, the i - η relationship was examined at each rotation speed and temperature by means of Randles' approach. The results of all three methods of analysis are summarized in Table 7.

Table 7 Rate Constants with standard deviations from a typical experiment. 10^{-5} mol.cm^{-3} Fe^{2+}, Fe^{3+} in 10^{-3} mol.cm^{-3} $HClO_4$ using a Pt RDE. Experiment No. 24.

T/K	$10^3 k_o$/cm.s^{-1}			
	Intercept	Jahn, Vielstich	Randles (extrap.)	Randles† (mean)
298.2*	18.1 ± 0.5	18.1 ± 0.5	17.7 ± 0.6	17.0 ± 0.4
298.2	14.3 ± 0.6	13.9 ± 0.7	16.1 ± 0.4	15.3 ± 0.2
293.1	11.9 ± 0.4	11.7 ± 0.5	12.8 ± 0.4	12.0 ± 0.3
288.5	11.0 ± 0.3	10.9 ± 0.3	11.4 ± 0.4	11.1 ± 0.3
284.1	7.0 ± 0.2	6.6 ± 0.3	7.5 ± 0.3	8.65 ± 0.5
278.2	5.3 ± 0.1	4.9 ± 0.2	5.8 ± 0.1	6.66 ± 0.3
277.3	4.7 ± 0.1	4.2 ± 0.1	4.8 ± 0.1	5.45 ± 0.6
299.1	15.3 ± 0.3	15.3 ± 0.5	15.0 ± 0.4	15.0 ± 0.4
289.2	8.3 ± 0.3	7.8 ± 0.4	8.9 ± 0.4	9.80 ± 0.6
283.8	6.7 ± 0.2	6.3 ± 0.3	7.2 ± 0.1	7.32 ± 0.4
280.5	5.5 ± 0.2	5.3 ± 0.2	5.9 ± 0.1	6.60 ± 0.6
288.5	9.0 ± 0.3	10.0 ± 0.4	9.6 ± 0.4	8.37 ± 0.6

* Results from top to bottom of table in order of measurement.

† If theory is correct, this is the normal data treatment.

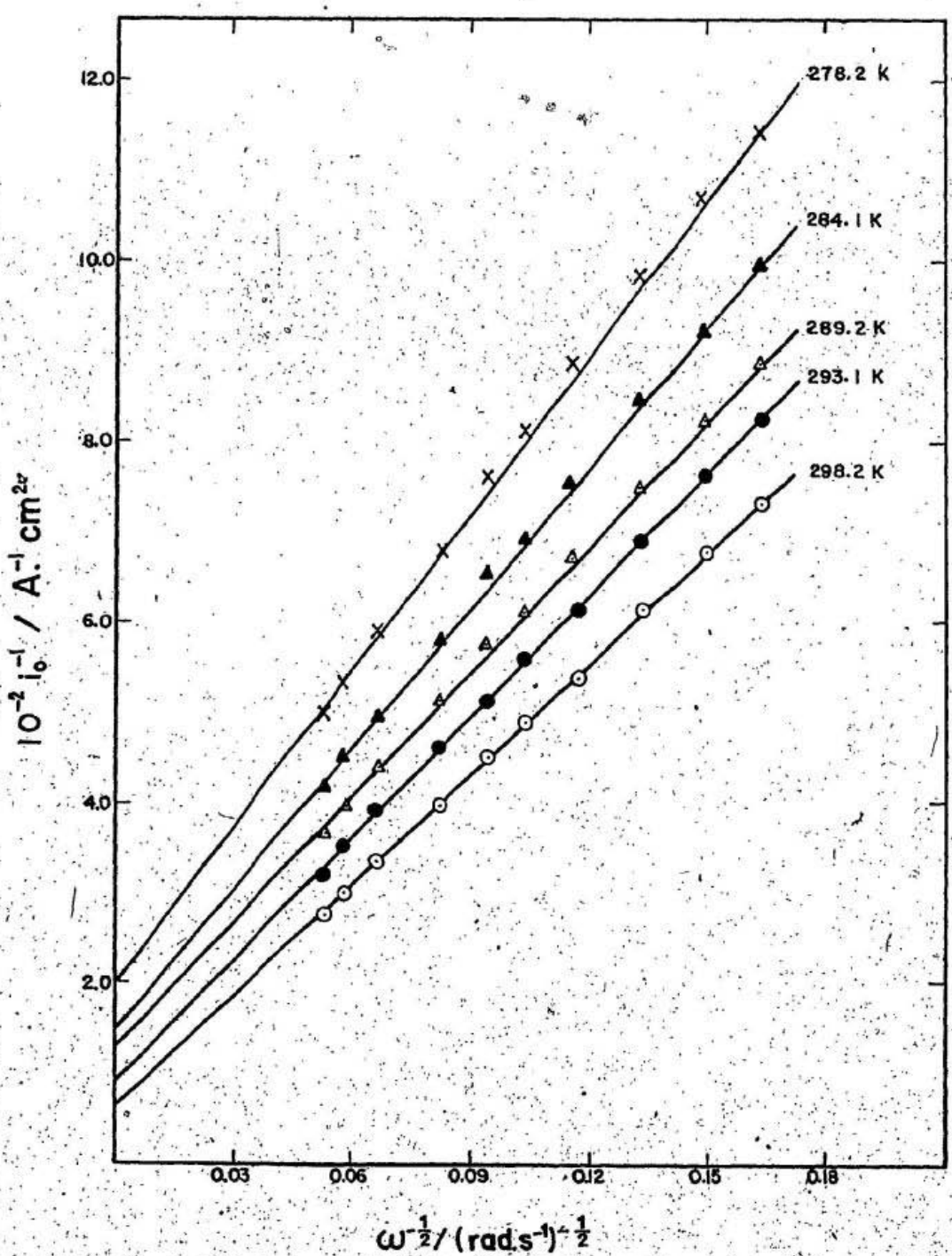

Fig. 15 Inverse Levich plots, Pt, 10^{-5} mol. cm^{-3} Fe^{2+}, Fe^{3+} in 10^{-3} mol. cm^{-3} $HClO_4$; experiment no. 24, with some data of Table 6 omitted for clarity.

An Arrhenius plot of results obtained by the intercept method is contained in Fig. 16. The scatter of points in Fig. 16 is indicative of the problems involved in measuring rates on platinum. Because it appears to be difficult to obtain a long term stable surface, each experiment must be repeated at several temperatures so that a reasonable Arrhenius plot could be obtained. The best values of the rate constants at 298.2 K and the derived kinetic parameters obtained by three methods are summarized in Table 8.

Table 8 Summarized kinetic data from Table 7 analyzed by three methods; Pt, 10^{-5} mol.cm^{-3} Fe^{2+}, Fe^{3+} in 10^{-3} mol.cm^{-3} $HClO_4$. Experiment No. 24.

Kinetic Parameters	Intercept	Jahn, Vielstich	Randles (extrap.)	Randles (mean)
$10^3 k_o$/cm.s^{-1} best value at 298.2 K	15.7 ± 2.7	16.3 ± 2.7	15.9 ± 0.6	15.4 ± 0.4
$\Delta H^{\ddagger}$/kJ. mol^{-1}	40.0 ± 2.4	43.1 ± 2.9	37.5 ± 2.0	30.6 ± 2.4
$\ln(A^{\ddagger}$/cm.s$^{-1})$	12.0 ± 1.0	13.3 ± 1.2	11.0 ± 0.8	8.16 ± 1.0

As seen in Table 8 all three methods yield essentially the same kinetic parameters. However, some difficulties in respect of use of the Randles method must be mentioned, especially concerning the results obtained with platinum. In some experiments the method could not be applied because the calculated value of the right hand side of either equation (49) or (50), referred to as $\log_e Y$, became negative due to the

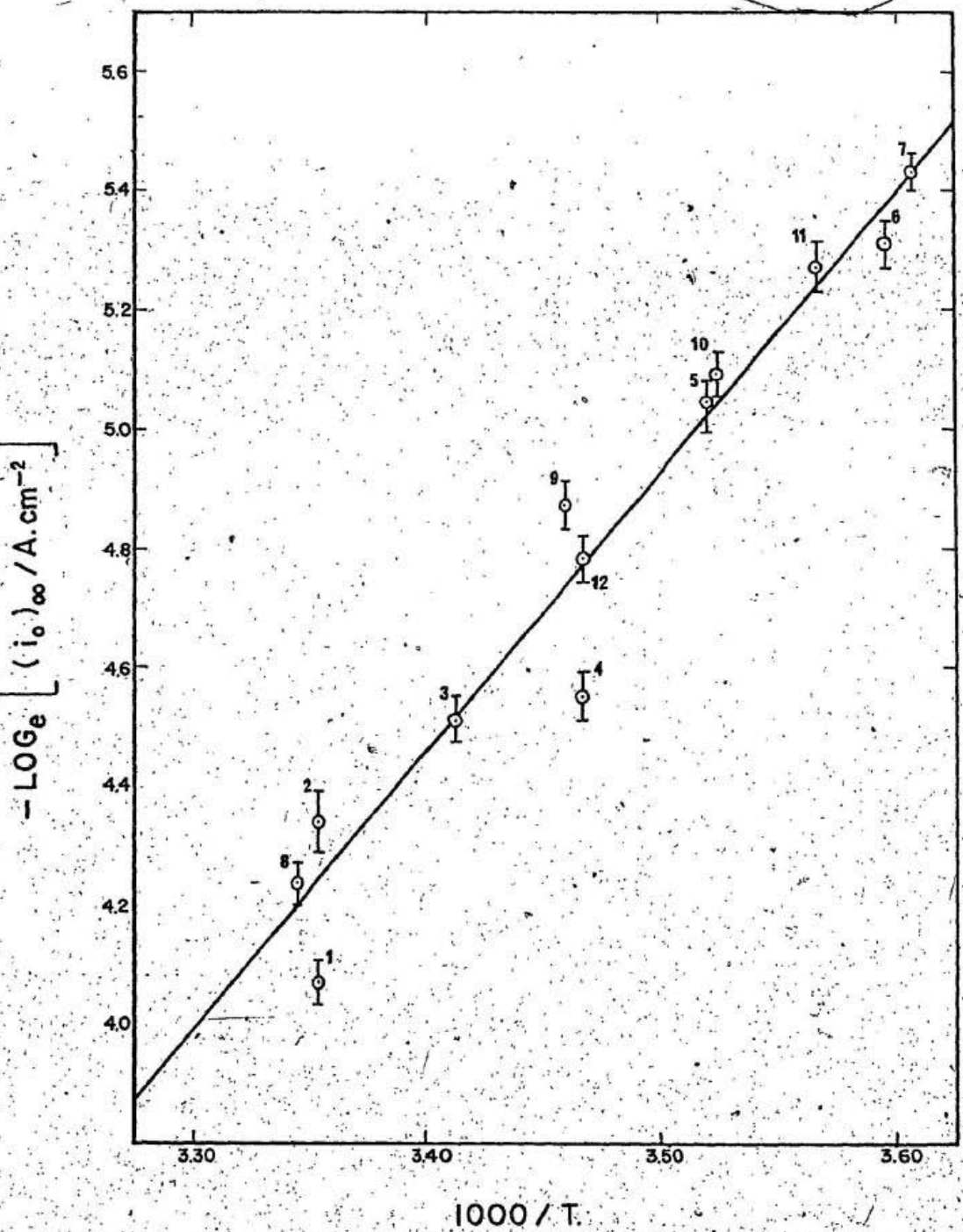

Fig. 16 Arrhenius plot of $(i_o)_\infty$, Pt, 10^{-5} mol.cm^{-3} Fe^{2+}, Fe^{3+} in 10^{-3} mol.cm^{-3} $HClO_4$; experiment no. 24, data from Table 6, extrapolated as in Fig. 15; $\Delta H^{\ddagger} = (40.0 \pm 2.4)$ kJ.mol.$^{-1}$

exponential growth of the second or third term relative to the first. Obviously in these cases a semi-logarithmic plot could not be made (i.e. $\log_e Y$ versus η). The Randles approach was only successful for a small number of experiments on platinum. Similar behaviour was not observed in later experiments on palladium and gold.

Fig. 17, however, shows a typical successful Randles analysis with platinum. These particular results were obtained at 277.3 K at various rotation speeds. Since Randles' approach predicted a constant value for the exchange current density, i_o, regardless of rotation speed, all lines should in theory coincide in a single point at $\eta = 0$. A study of Fig. 17 suggests trends both of the intercept at $\eta = 0$ (the exchange current) and of the slope (which is proportional to α). As an empirical approach, the reciprocal exchange current density from the Randles analysis, i.e. $(i_{oR})_\omega^{-1}$, was plotted against $\omega^{-1/2}$ for every temperature of measurement in Experiment 24. These plots are shown in Fig. 18, from which it is evident that at 288 K and above, no dependence of $(i_{oR})_\omega$ on ω exists, whereas fluctuations of $(i_{oR})_\omega^{-1}$ with $\omega^{-1/2}$ at lower temperatures possibly suggest that extrapolation to $\omega = \infty$ yields a more useful result. Since it appeared that the Randles approach had failed to completely eliminate rotation speed dependence under these conditions, such an empirical plot was performed in each case. It is interesting to observe that the extrapolated value (e.g. from Fig. 18) usually yielded rate constants comparable to the other two methods. This comparison has already been made in Table 7 for one experiment, as well as including a simple average of the rates for the various rotation speeds at each temperature. The non-ideal behaviour (ω dependence of i_{oR}) was slightly evident

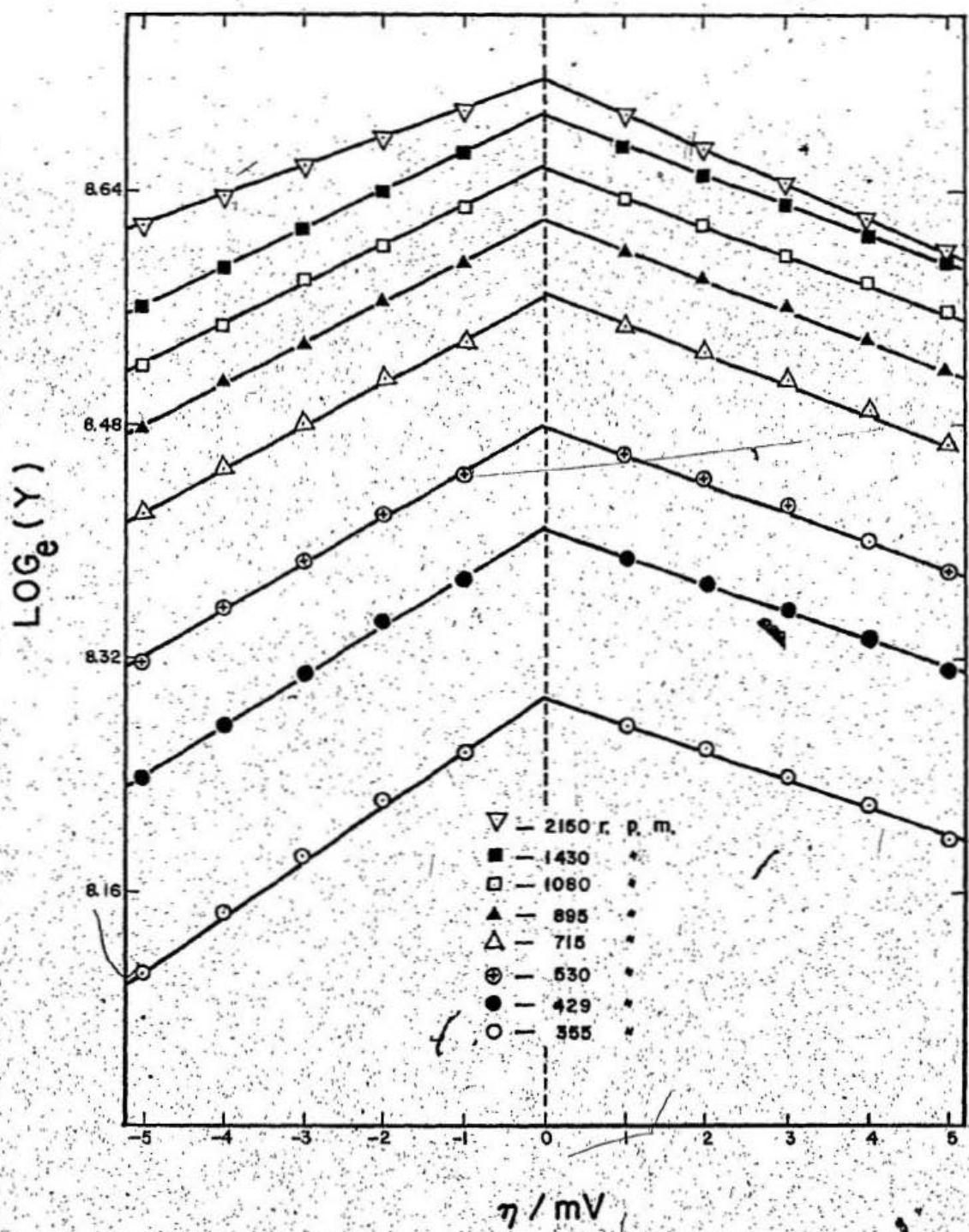

Fig. 17 Randles approach to data of experiment no. 24, 277.3 K, Table 6; Pt, 10^{-5} mol.cm^{-3} Fe^{2+}, Fe^{3+} in 10^{-3} mol.cm^{-3} $HClO_4$.

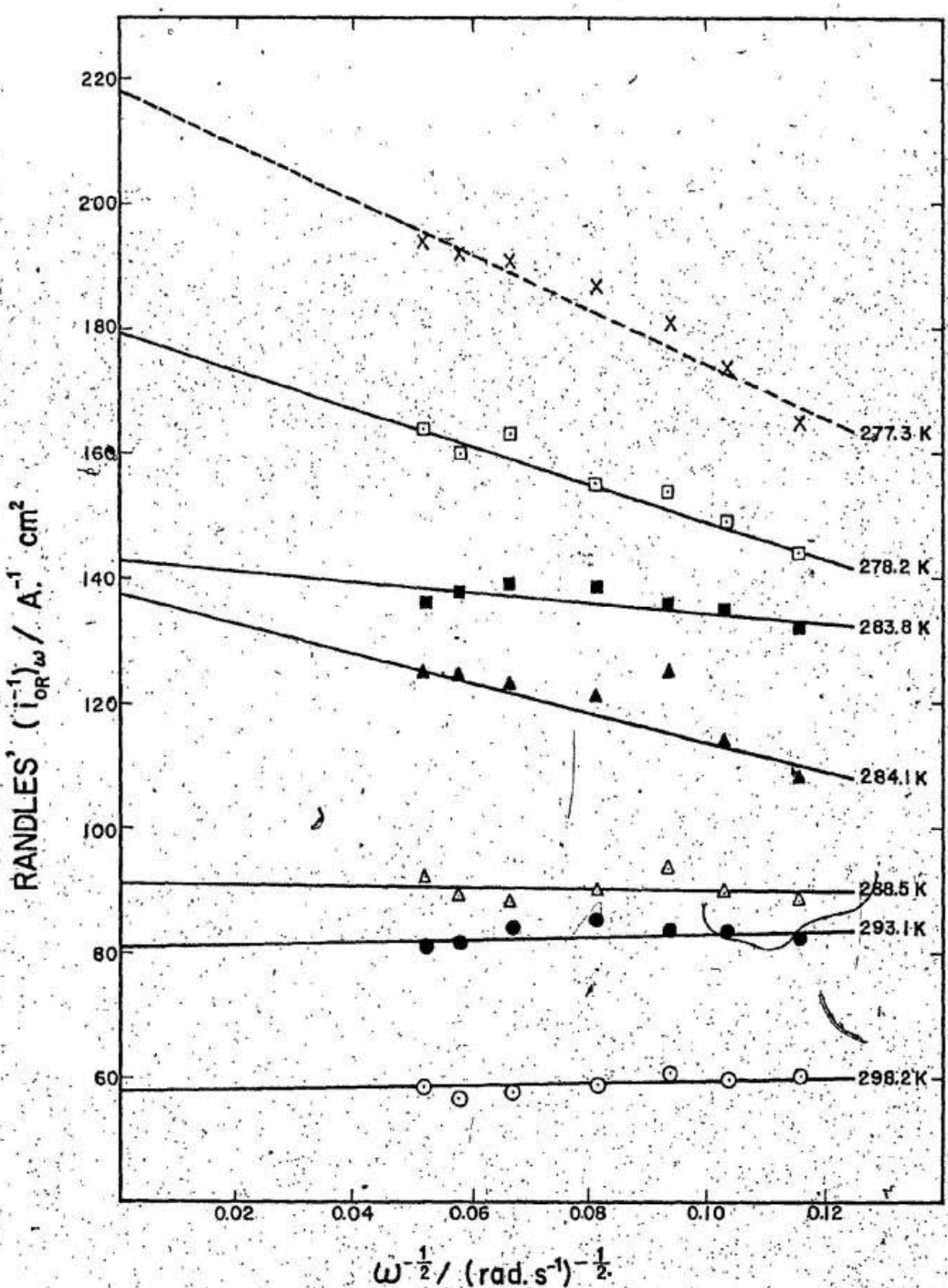

Fig. 18. Dependence of $(i_{oR})_\omega$ on rotation speed for experiment no. 24; Pt, 10^{-5} mol.cm^{-3} Fe^{2+}, Fe^{3+} in 10^{-3} mol.cm^{-3} $HClO_4$.

with the other metals, sometimes yielding positive and sometimes negative deviations from anticipated behaviour.

A definite dependence of α upon rotation speed could also not be overlooked. Transfer coefficients are obtainable from the slopes of plots such as those in Fig. 17. In Fig. 19 empirical plots of α from these slopes versus $\omega^{-1/2}$ are shown. They are reasonably linear and extrapolate to close to 0.50 as $\omega \to \infty$. The α's used for plots such as those of Fig. 19 were mean values from the anodic and cathodic Randles plots at particular rotation speeds. All metals studied exhibited the same behaviour. It is noteworthy that in the case of α the greatest dependency is at the highest temperatures studied but the ω- dependence even at 277 K is quite strong. Ideality is approached but not reached at the lowest temperatures of our study. This contrasts with the behaviour of i_{oR} as a function of ω. This matter will be discussed in the final chapter.

In obtaining the data, all systematic errors arising from electrical, mechanical, and thermal measurements were minimized. However, it is especially evident from the platinum data that the greatest residual error arises from the varying activity of the platinum electrode. This was overcome by taking many data points up and down the Arrhenius plot and choosing the best fit. The standard deviation of the slope arising from such a regression was much greater than the relatively negligible probable contributions to error from measuring instruments. A summary of the data obtained from the more reliable experiments is given in Table 9. Most experiments in this stage of the work on

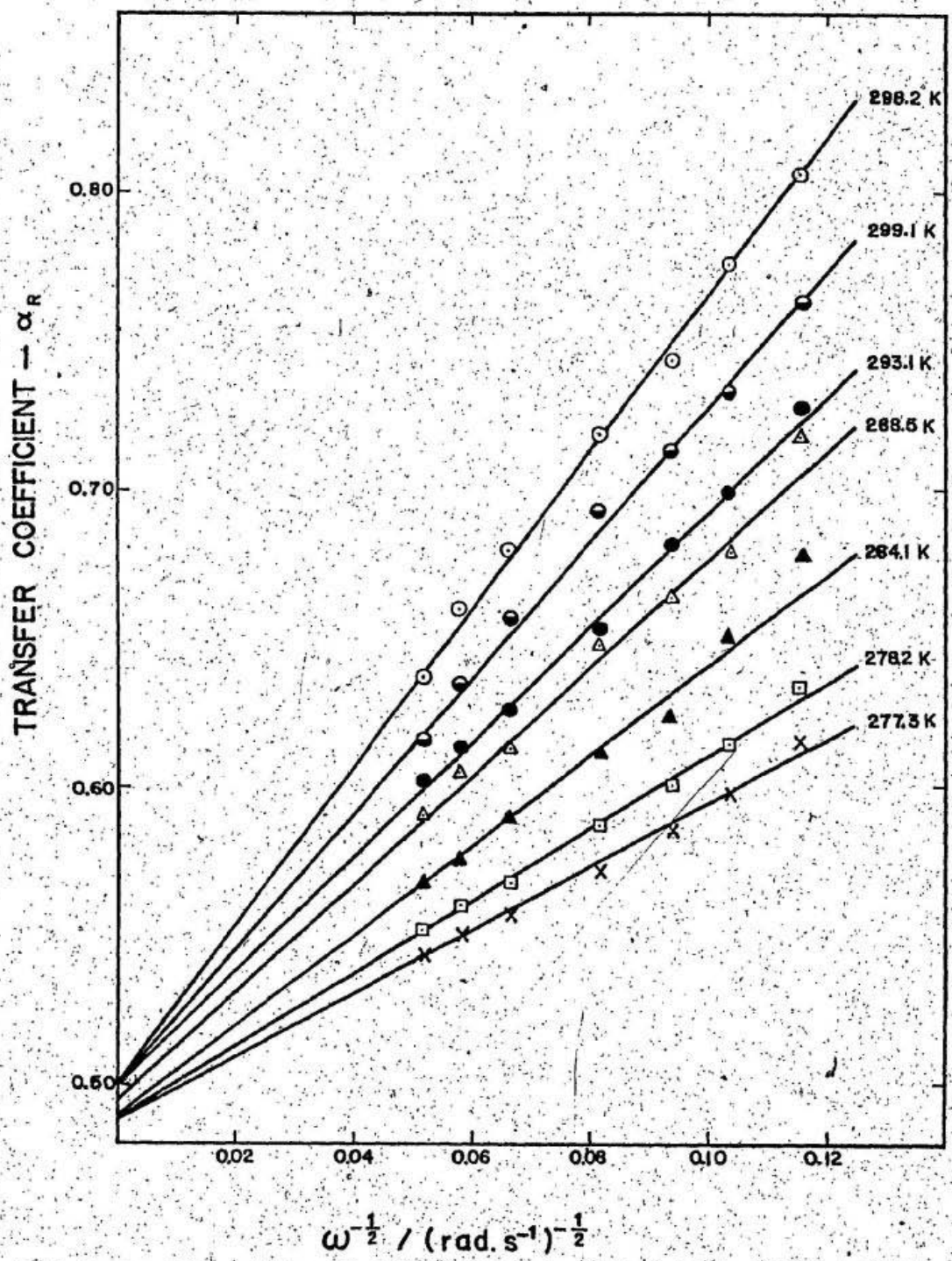

Fig. 19 Dependence of α_R on rotation speed for experiment no. 24; Pt, 10^{-5} mol.cm^{-3} Fe^{2+}, Fe^{3+} in 10^{-3} mol.cm^{-3} $HClO_4$.

platinum were performed using 10^{-5} mol.cm^{-3} ferrous and ferric ions. The concentration of reactive species was kept within that range so that the most kinetically desirable data could be obtained, free from any complexation or reactant adsorption effects and also because analogous homogeneous experiments are performed at even lower concentrations (See e.g. Silverman and Dodson[53]; Fukushima and Reynolds[54]). As a further support to this approach Anson[11] showed that the exchange current density varied linearly with concentration up to 2×10^{-5} mol.cm^{-3}.

Table 9 Summary of preferred rate constants and Arrhenius parameters: Fe^{2+}, Fe^{3+} electron transfer at a platinum RDE in 10^{-3} mol.cm^{-3} $HClO_4$.

Expt. No.	[Redox] mol.cm^{-3} $[Fe^{2+}]=[Fe^{3+}]$	$10^3 k_o$/cm.s^{-1} at 298.2 K	$\Delta H^{\ddagger}$ kJ.mol^{-1}	$\ln(A^{\ddagger}$/cm.s$^{-1})$
15*	10^{-6}	29.7 ± 8.4†	35.1 ± 10	10.6 ± 3.87
19	10^{-5}	21.2 ± 4.1	27.8 ± 3.5	7.36 ± 1.44
20	10^{-5}	32.6 ± 7.8	36.8 ± 7.5	11.4 ± 3.14
21	10^{-5}	16.1 ± 2.1	29.9 ± 3.3	7.93 ± 1.37
22	10^{-5}	17.1 ± 3.0	49.6 ± 3.1	15.9 ± 1.31
23	10^{-5}	23.3 ± 3.2	43.7 ± 1.1	13.9 ± 0.47
24	10^{-5}	15.7 ± 2.7	40.0 ± 2.4	12.0 ± 1.00

* old apparatus, low temperature data only.

† error for rate constants estimated from observed ranges within each experiment.

The data of Table 9 were treated by two different statistical methods. One involved averaging the rate parameters via a weighted mean ($\Sigma W_i x_i / \Sigma W_i$) and calculating the standard weighted error of the mean, $((\Sigma W_i (x_i - \bar{x})^2 / (n-1)\Sigma W_i)^{1/2})$, the weight, W_i, being the square of the inverse variance. The other approach involved combining all the data points for the experiments indicated, and performing just one multi-point Arrhenius plot using the error as calculated from the weighted regression analysis. This involved over 80 rate determinations on platinum between 273 and 298 K. The approaches are compared in Table 10, which summarizes the experiments on platinum, uncorrected for real surface areas.

Table 10 Summary of experiments with platinum.

$10^3 k_o / cm.s^{-1}$ at 298.2 K (weighted mean)	18.4 ± 1.6
Range of values for rate constant at 298.2 K, $10^3 k_o / cm.s^{-1}$	16 – 33
$\Delta H^{\ddagger} / kJ.mol^{-1}$ (weighted mean)	41.5 ± 3.0
$\Delta H^{\ddagger} / kJ.mol^{-1}$ (one Arrhenius plot for all experiments)	38.6 ± 3.2
Weighted mean $[\ln(A^{\ddagger} / cm.s^{-1})]$	12.48 ± 1.17
$\ln(A^{\ddagger} / cm.s^{-1})$ (one Arrhenius plot for all experiments)	11.40 ± 1.33

Rate Measurements with Gold

Initial experiments on gold were beset with difficulties. Galvanostatic oxidation of the ferrous solution led to partial dissolution of the gold counter and reference electrodes. The dissolved gold species was reduced by the ferrous ions and precipitated out as gold dust. For this reason, oxidations were performed potentiostatically with magnetic stirring. In addition, pretreatment of test solutions with activated charcoal invariably led to the presence of some fine charcoal dust in the experimental cell. Either the gold dust or the charcoal (or both) appeared to adhere to the RDE surface, thus giving it a tarnished appearance as well as producing severely anomalous results, i.e. negative intercepts of i_o^{-1} vs $\omega^{-1/2}$ plots. The dust was removed by polishing with a non-abrasive optical lens tissue. Because of the relative softness of gold, the gold disc became slightly rougher than the platinum and palladium discs.

For the majority of experiments the charcoal purification step was omitted. Following this omission, more conformable results were obtained.

Table 11 summarizes the exchange current densities from a typical experiment on gold, the i_o's having been obtained from $i - \eta$ curves at each temperature and rotation speed.

An inverse Levich plot of some of these i_o's are shown in Fig. 20. The results were as usual analyzed by the three methods used for the platinum work. Table 12 summarizes these comparative calculations.

Table 11 Exchange current densities as functions of rotation speed and temperature. Experiment No. 32: Au, 10^{-6} mol.cm^{-3} Fe^{2+}, Fe^{3+} in 10^{-3} mol.cm^{-3} $HClO_4$.

	$10^4\, i_o$/A.cm^{-2}									
ω/rpm	360	432	536	720	900	1080	1440	2160	2860	3560
T/K										
298.2*	1.32†	1.45	1.58	1.77	1.94	2.09	2.38	2.79	3.12	3.44
295.2	1.23	1.33	1.46	1.65	1.81	1.96	2.19	2.60	2.93	3.21
292.2	1.16	1.25	1.37	1.54	1.69	1.82	2.04	2.39	2.69	2.90
289.2	1.09	1.16	1.26	1.43	1.56	1.68	1.88	2.20	2.47	2.68
285.2	0.99	1.07	1.16	1.29	1.41	1.53	1.70	1.98	2.22	2.41
279.6	0.85	0.90	0.97	1.09	1.18	1.27	1.41	1.63	1.82	1.97
289.2	1.08	1.17	1.27	1.43	1.55	1.68	1.86	2.18	2.45	2.64
295.1	1.26	1.34	1.48	1.65	1.80	1.94	2.17	2.53	2.83	3.09

* Results from top to bottom in order of measurement.

† Relative precision for i_o measurement assessed to be ± 0.3%.

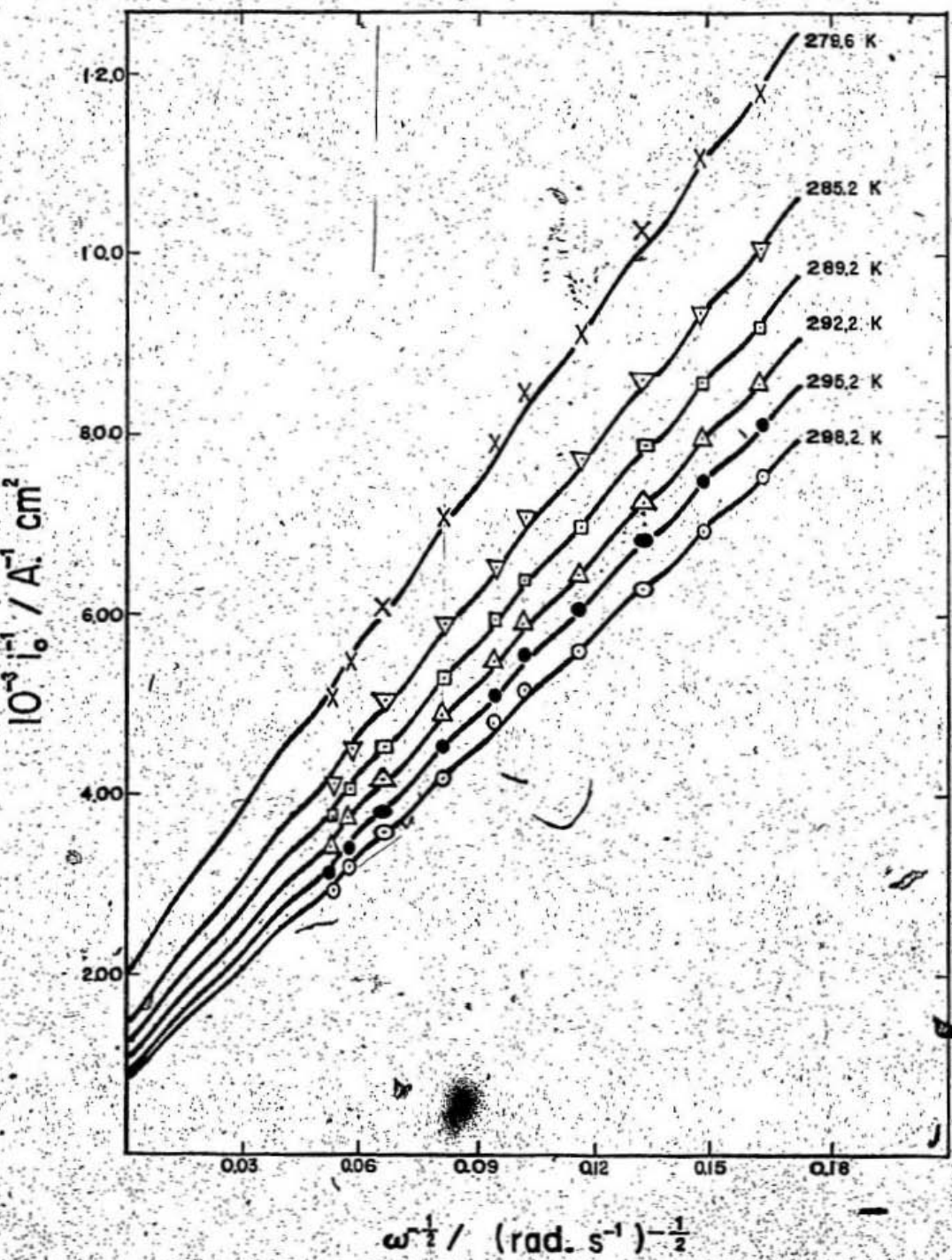

Fig. 20 Inverse Levich plots, Au, 10^{-6} mol. cm^{-3} Fe^{2+}, Fe^{3+} in 10^{-3} mol. cm^{-3} $HClO_4$; experiment no. 32, Table 11.

Table 12 Rate constants with standard deviations from a typical experiment. 10^{-6} mol.cm^{-3} Fe^{2+}, Fe^{3+} in 10^{-3} mol.cm^{-3} $HClO_4$ using a Au RDE. Experiment No. 32.

T/K	10^3 k_o/cm.s^{-1}			
	Intercept	Jahn, Vielstich	Randles (extrap.)	Randles (mean)
298.2*	13.2 ± 0.73	13.4 ± 0.88	12.6 ± 0.76	12.2 ± 0.79
295.2	12.9 ± 0.58	13.3 ± 0.72	12.1 ± 0.57	11.0 ± 0.61
292.2	10.0 ± 0.33	10.0 ± 0.42	9.55 ± 0.34	9.97 ± 0.42
289.2	8.82 ± 0.39	8.89 ± 0.49	8.28 ± 0.43	8.64 ± 0.40
285.2	7.44 ± 0.38	7.41 ± 0.47	6.95 ± 0.39	7.59 ± 0.54
279.6	5.37 ± 0.27	5.38 ± 0.33	5.04 ± 0.25	5.34 ± 0.24
289.2	8.27 ± 0.30	8.21 ± 0.39	7.88 ± 0.30	8.57 ± 0.46
295.1	9.24 ± 0.44	9.59 ± 0.54	9.26 ± 0.46	10.98 ± 1.05

*Results from top to bottom of table in order of measurement.

Fig. 21 is an Arrhenius plot of the data of Table 12 obtained by the intercept method. Rate parameters from the three methods of analysis are summarized in Table 13.

Results with gold appeared to be more reliable, but probably due to the experimental dexterity gained through previous experiences on platinum. Randles' method was successfully applied to all experiments on gold. Measurements of i_o obtained by Randles' method did not show any definite dependence on the rotation speed, but neither were they completely independent. As such, a simple average would probably be more significant. For comparison, this has already been included in Table 12.

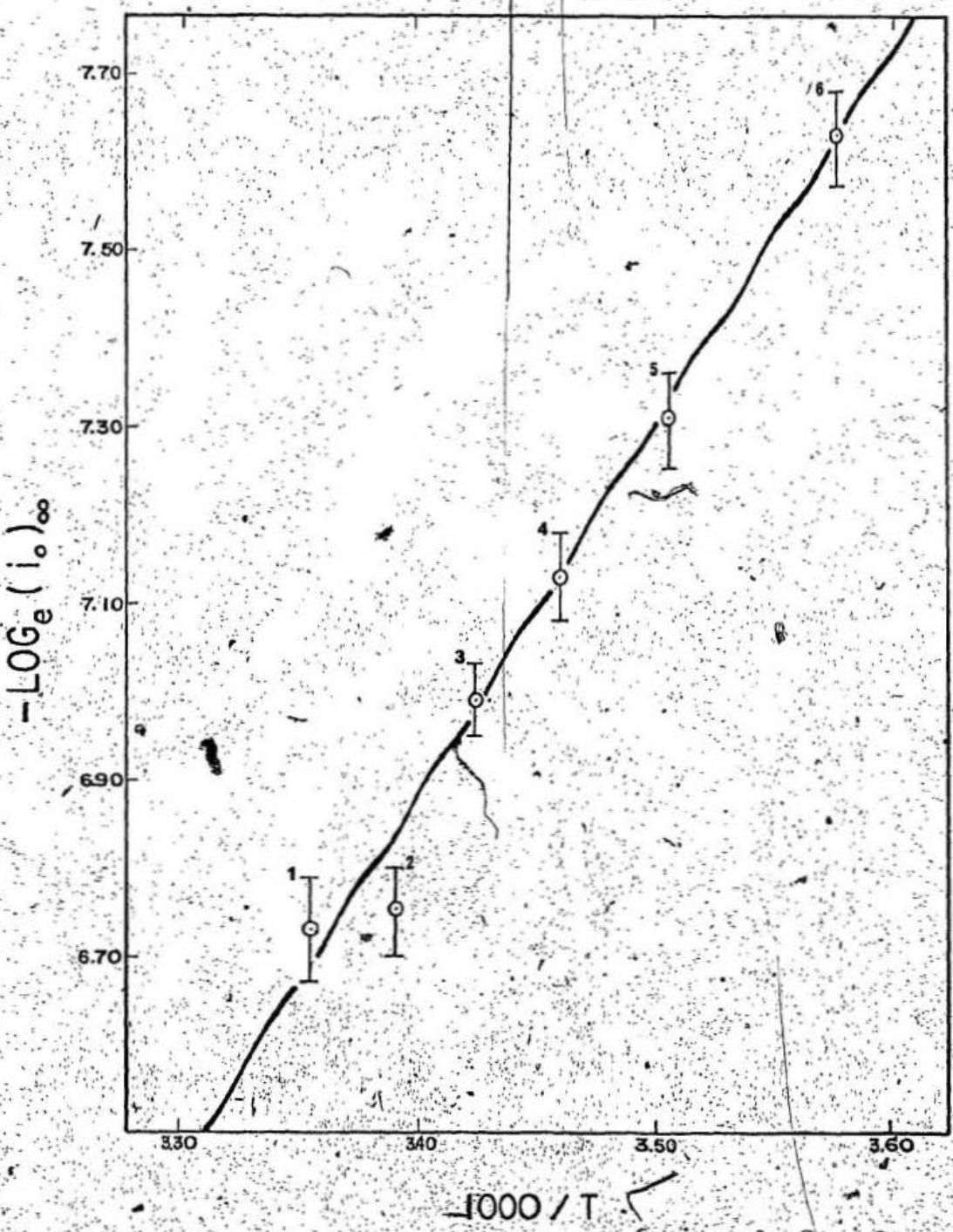

Fig. 21 Arrhenius plot of $(i_o)_\infty$, Au, 10^{-6} mol.cm^{-3} Fe^{2+}, Fe^{3+} in 10^{-3} mol.cm^{-3} $HClO_4$; experiment no. 32, Table II; extrapolated as in Fig. 20; $\Delta H^{\ddagger}$ = (35.1 ± 2.7) kJ. mol.$^{-1}$

Table 13 Summarized kinetic data from Table 12 analyzed by three methods. Au, 10^{-6} mol.cm^{-3} Fe^{2+}, Fe^{3+} in 10^{-3} mol.cm^{-3} $HClO_4$. Experiment No. 32.

Kinetic Parameter	Intercept	Jahn, Vielstich	Randles (extrap.)	Randles (mean)
$10^3 k_o$/cm.s^{-1} best value at 298.2 K	13.9 ± 1.3	13.9 ± 0.9	12.9 ± 0.7	12.7 ± 0.8
$\Delta H^{\ddagger}$/kJ.mol^{-1}	35.1 ± 2.7	36.2 ± 3.4	35.6 ± 2.4	31.3 ± 1.4
$\ln(A^{\ddagger}$/cm.s$^{-1})$	9.9 ± 1.1	10.3 ± 1.4	10.0 ± 1.0	8.26 ± 0.47

A typical empirical plot of the type used with platinum is shown in Fig. 22. As with platinum, nearly ideal behaviour is observed at the higher temperatures, whereas the low temperature data show a lot of scatter.

The Randles transfer coefficient, α_R, also showed a strong dependence on ω in the gold work (see Fig. 23) but once again convergence to $\alpha = 0.5$ at infinite rotation speed is found for all temperatures studied.

A summary of the data for the more reliable experiments on gold is included in Table 14. Also included in this table are data for two experiments where anomalous rate constants were observed, possibly due to the charcoal dust problem previously mentioned. Because the Arrhenius plots were linear even though the rates were exceptionally high, the temperature dependencies were thought significant and were therefore included.

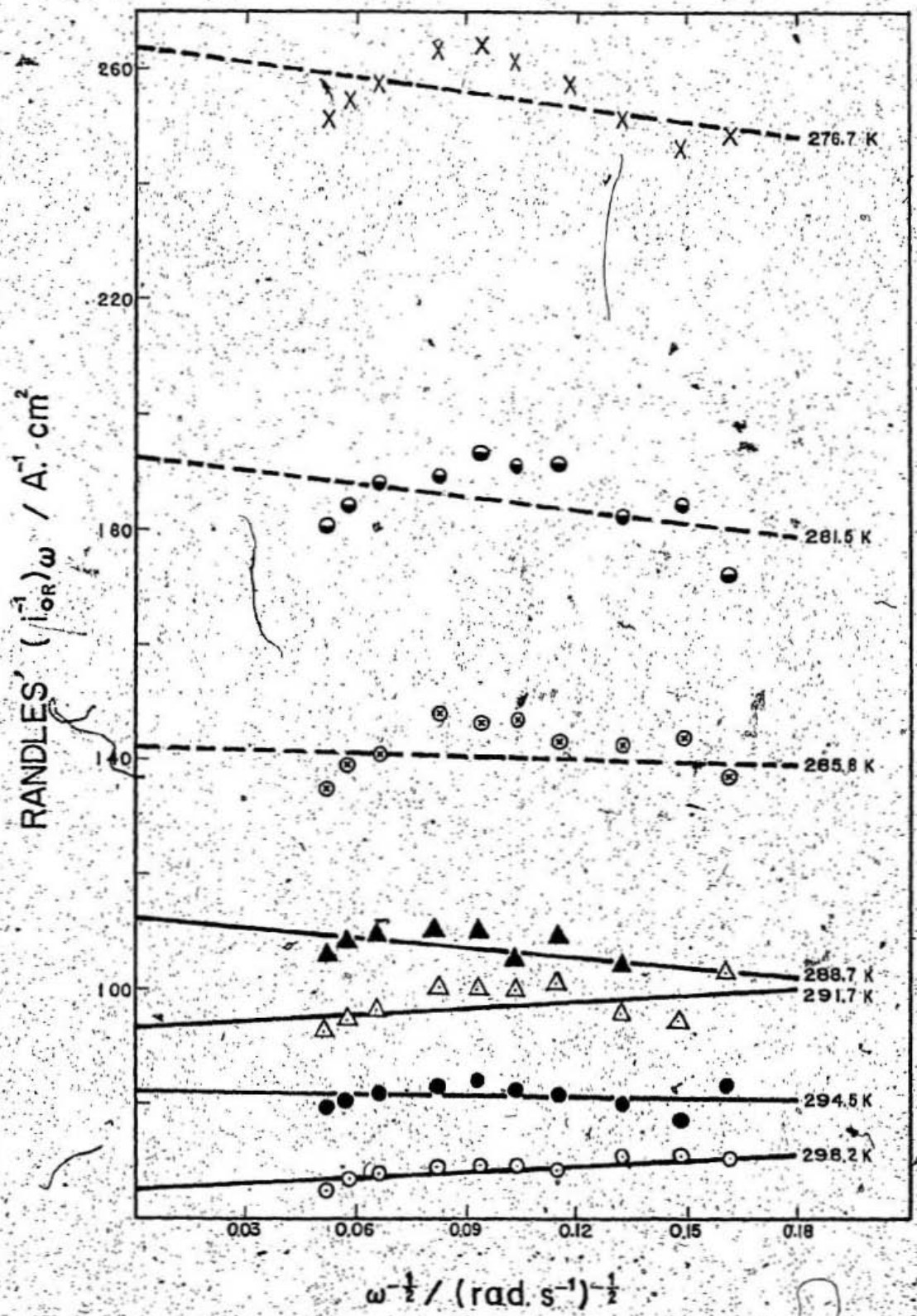

Fig. 22 Dependence of $(i_{OR})_\omega$ on rotation speed for experiment no. 30; Au, 10^{-5} mol.cm^{-3} Fe^{2+}, Fe^{3+} in 10^{-3} mol.cm^{-3} HClO$_4$

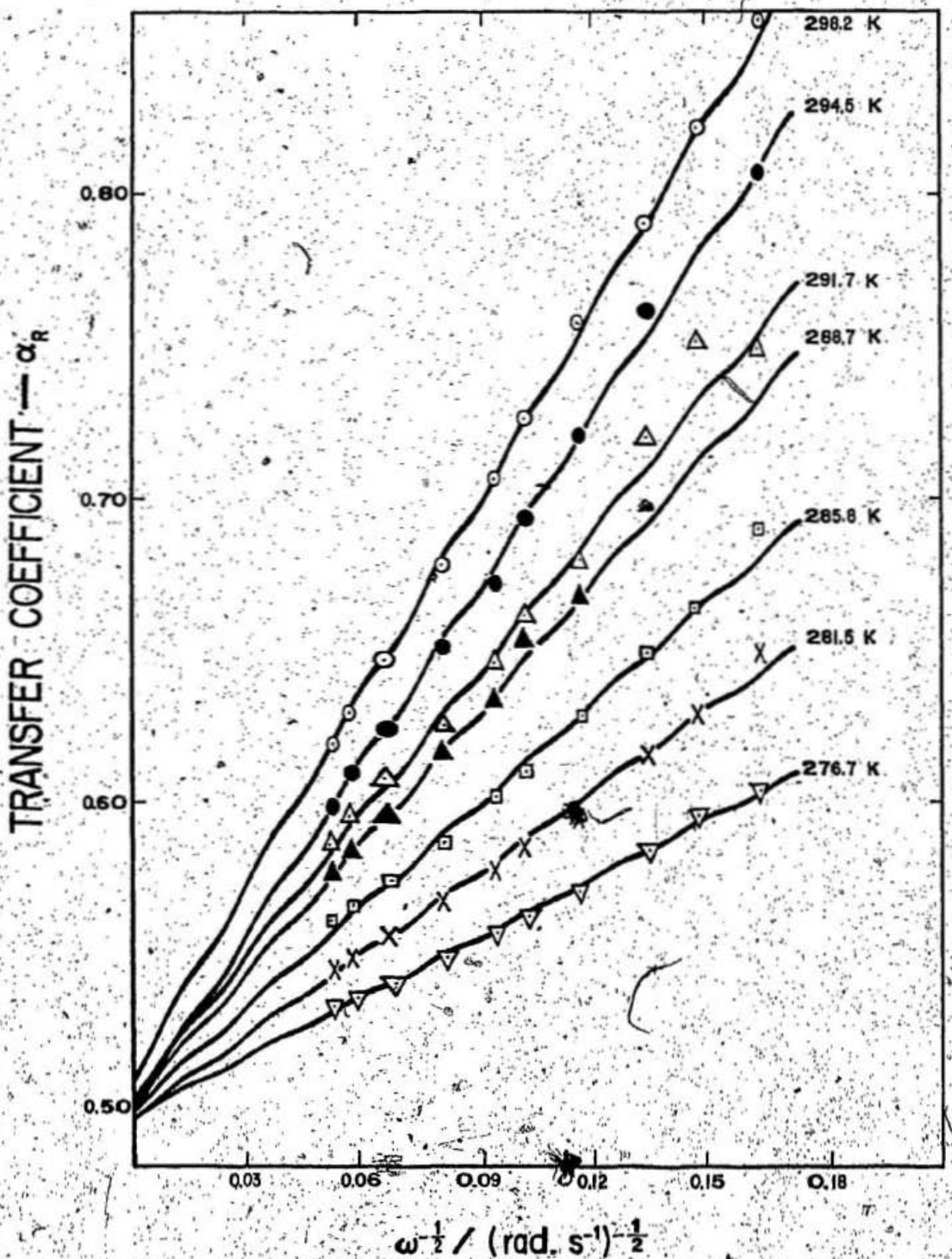

Fig. 23 Dependence of α_R on rotation speed for experiment no. 30; Au, 10^{-5} mol.cm^{-3} Fe^{2+}, Fe^{3+} in 10^{-3} mol.cm^{-3} $HClO_4$.

Table 14 Summary of preferred rate constants and Arrhenius parameters; Fe^{2+}, Fe^{3+} electron transfer at a Au RDE in 10^{-3} mol.cm^{-3} $HClO_4$.

Expt. No.	$[Fe^{2+}]=[Fe^{3+}]$ mol.cm^{-3}	$10^3 k_o$/cm.s^{-1} at 298.2 K	$\Delta H^{\ddagger}$/ kJ.mol^{-1}	$\ln(A^{\ddagger}$/cm.s$^{-1})$
25	10^{-5}	12.5 ± 2.4	33.4 ± 3.6	9.09 ± 1.52
26	10^{-5}	-	41.1 ± 4.5	-
27	10^{-5}	-	41.5 ± 4.7	-
28	10^{-6}	8.57 ± 1.0	29.3 ± 1.1	7.06 ± 0.48
30	10^{-5}	16.4 ± 0.8	44.2 ± 0.6	13.7 ± 0.24
31	10^{-5}	14.1 ± 1.9	41.9 ± 2.6	12.6 ± 1.09
32	10^{-6}	13.9 ± 1.3	35.1 ± 2.7	9.88 ± 1.13

These data were handled in a similar manner to the platinum data except that the rates for Expts. 26 and 27 were not included in the all-points Arrhenius calculation for gold. Table 15 summarizes the best results.

Table 15 Summary of experiments with gold.

$10^3 k_o/cm.s^{-1}$ at 298.2 K (weighted mean)	13.5 ± 1.6
Range of values for rate constant at 298.2 K, $10^3 k_o/cm.s^{-1}$	8 - 16
$\Delta H^{\ddagger}/kJ.mol^{-1}$ (weighted mean)	38.9 ± 2.5
$\Delta H^{\ddagger}/kJ.mol^{-1}$ (one Arrhenius plot for all experiments)	42.9 ± 1.7
Weighted mean $[\ln(A^{\ddagger}/cm.s^{-1})]$	12.26 ± 1.31
$\ln(A^{\ddagger}/cm.s^{-1})$ (one Arrhenius plot for all experiments)	13.10 ± 0.70

Rate Measurements with Palladium

In the platinum and gold experiments all electrodes used for oxidation, pre-electrolysis, and rate measurements were constructed of the same metal as the RDE. Unfortunately, this was not possible during the oxidation of solutions for palladium experiments. The currents were so small on palladium (at η = +150 mV) that about one month would have been required for each experiment. A compromise was made by substituting platinum electrodes for the oxidation process only, carried out with the palladium RDE completely excluded from the solution. During pre-electrolysis and rate measurements, however,

all electrodes were of palladium construction. During data collection the potentials of all palladium electrodes were frequently monitored.

Although palladium was considered to be a more difficult metal to study, necessitating changes from the usual procedure, the results with this metal were more consistent than those obtained with platinum and gold. Reproducibility within a particular experiment was within a few percent, unlike the factors of two seen with the previously studied metals.

Table 16 lists the data of a typical experiment on palladium.

Table 16 Exchange current densities as functions of rotation speed and temperature in Experiment No. 33: Pd, 10^{-5} mol.cm^{-3}, Fe^{2+}, Fe^{3+} in 10^{-3} mol.cm^{-3} $HClO_4$.

	$10^3 i_o$/A.cm^{-2}									
ω/rpm	362	434	537	715	900	1080	1440	2163	2860	3565
T/K										
298.2*	1.22†	1.32	1.42	1.57	1.71	1.82	2.01	2.29	2.49	2.65
294.1	1.07	1.15	1.25	1.37	1.49	1.57	1.73	1.95	2.11	2.24
291.6	1.01	1.07	1.16	1.27	1.38	1.46	1.59	1.80	1.94	2.06
288.6	0.91	0.97	1.05	1.16	1.24	1.32	1.43	1.62	1.74	1.83
285.6	0.84	0.89	0.97	1.05	1.13	1.19	1.30	1.45	1.55	1.64
282.1	0.75	0.80	0.85	0.94	1.00	1.05	1.14	1.26	1.36	1.42
279.5	0.68	0.71	0.77	0.84	0.89	0.94	1.01	1.12	1.19	1.25

* Results from top to bottom of table in order of measurement.

† Relative precision for i_o measurement assessed to be ± 0.3%.

The inverse Levich plots of these data are given in Fig. 24. As before three evaluation methods were applied. A comparison is performed in Table 17.

Table 17 Rate constants with standard deviations from a typical experiment. 10^{-5} mol.cm^{-3} Fe^{2+}, Fe^{3+} in 10^{-3} mol.cm^{-3} $HClO_4$ using a Pd RDE; Experiment No. 33.

T/K	$10^3 k_o$/cm.s^{-1}			
	Intercept	Jahn,Vielstich	Randles (extrap.)	Randles (mean)
298.2*	6.09 ± 0.07	5.90 ± 0.10	6.03 ± 0.09	6.73 ± 0.30
294.1	4.71 ± 0.04	4.59 ± 0.06	4.69 ± 0.05	5.04 ± 0.16
291.6	4.15 ± 0.04	3.96 ± 0.06	4.12 ± 0.05	4.47 ± 0.15
288.6	3.58 ± 0.03	3.45 ± 0.04	3.57 ± 0.03	3.76 ± 0.09
285.6	3.03 ± 0.03	2.88 ± 0.05	3.00 ± 0.03	3.23 ± 0.10
282.1	2.53 ± 0.02	2.46 ± 0.03	2.52 ± 0.02	2.65 ± 0.06
279.5	2.14 ± 0.02	2.09 ± 0.03	2.13 ± 0.02	2.19 ± 0.04

*Results from top to bottom of table in order of measurement.

An Arrhenius plot of the intercept data appears in Fig. 25. The excellent linearity and small deviations exhibited by these data was found in all palladium experiments. Summarized results of the three methods of data analysis are presented in Table 18.

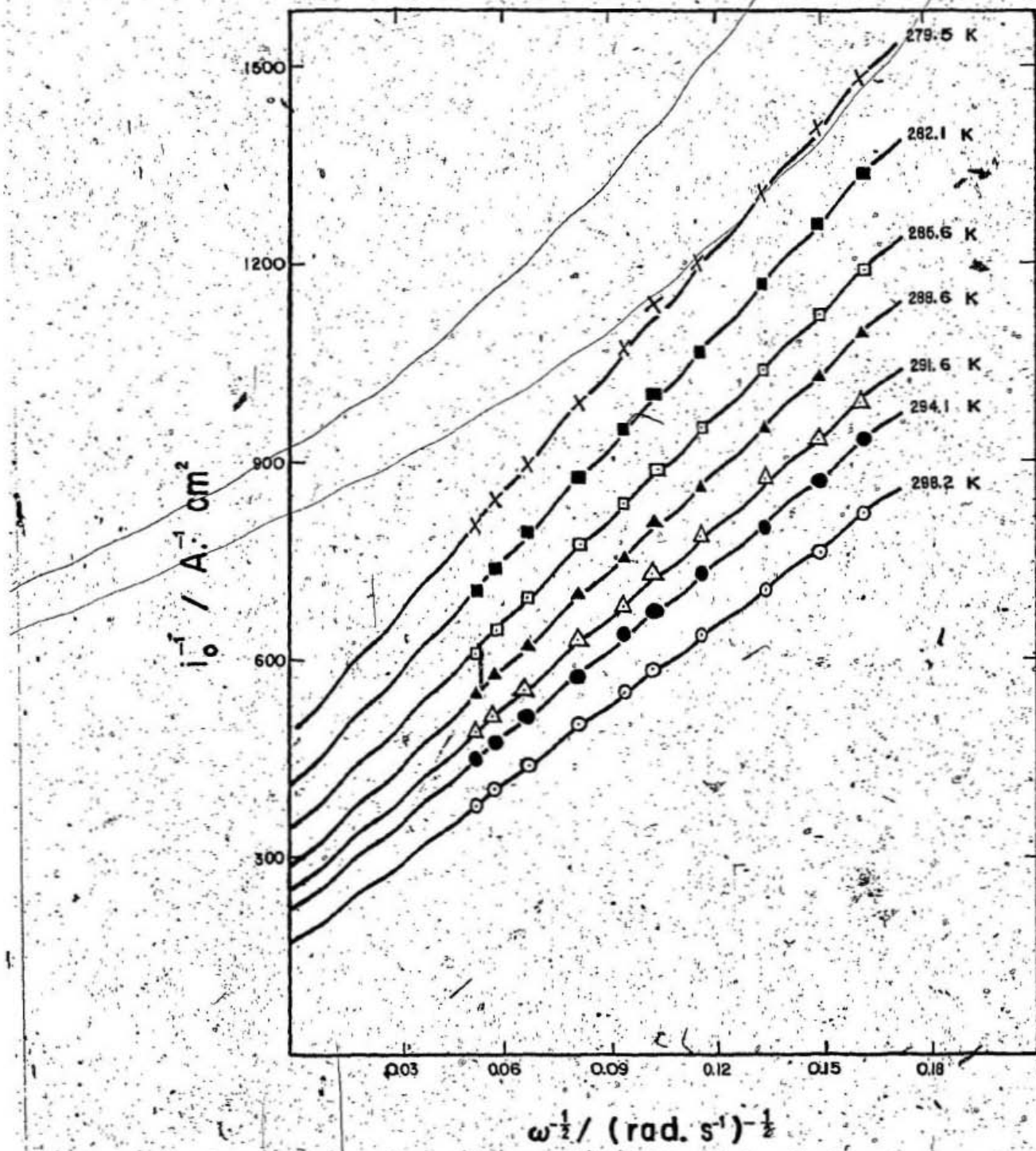

Fig. 24. Inverse Levich plots, Pd, 10^{-5} mol. cm^{-3} Fe^{2+}, Fe^{3+} in 10^{-3} mol. cm^{-3} $HClO_4$; experiment no. 33, Table 16.

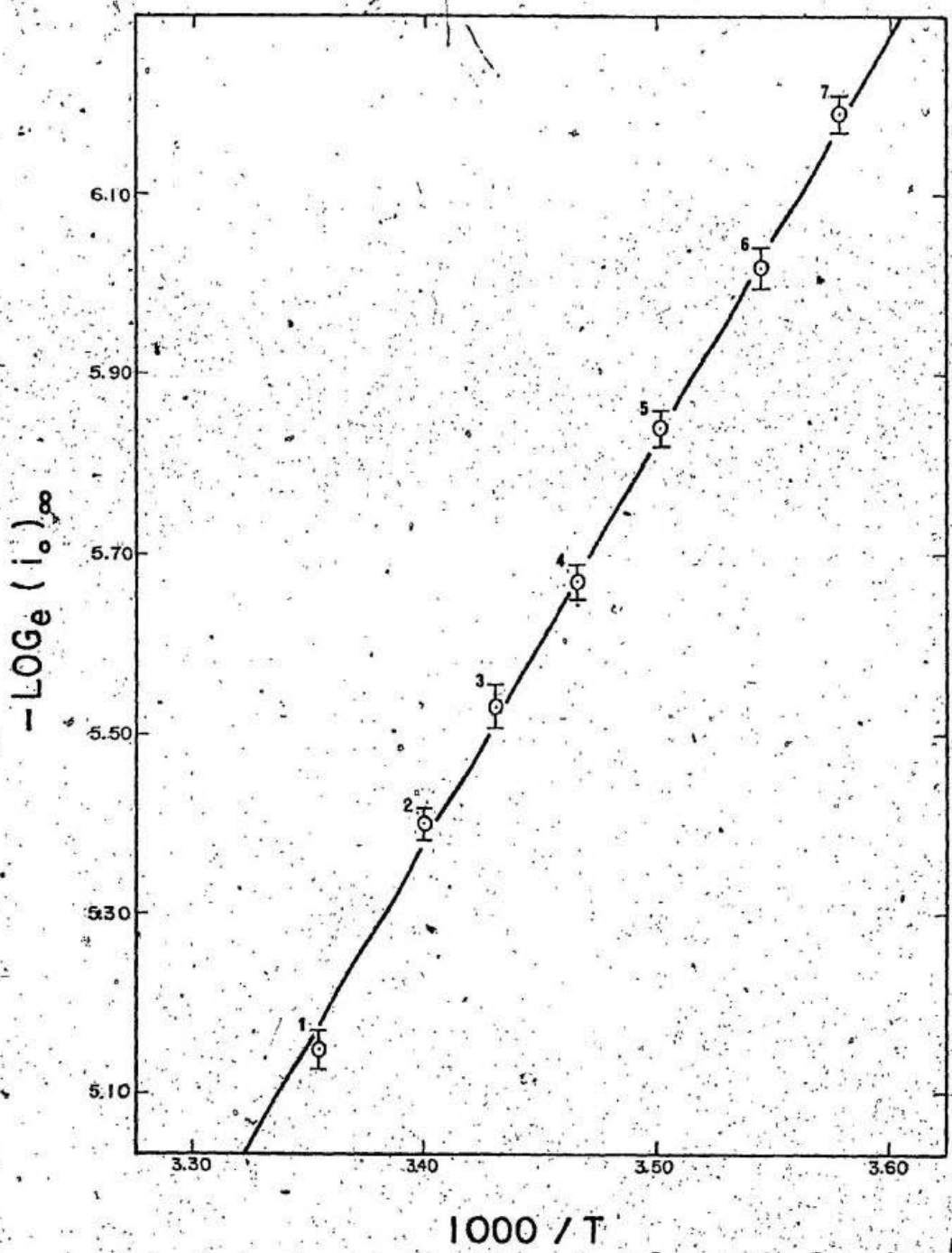

Fig. 25 Arrhenius plot of $(i_o)_\infty$, Pd, 10^{-5} mol.cm^{-3} Fe^{2+}, Fe^{3+} in 10^{-3} mol.cm^{-3} $HClO_4$; experiment no. 33, Table 16; extrapolated as in Fig. 24; $\Delta H^{\ddagger}$ = (37.2 ± 0.7) kJ. mol.$^{-1}$

Table 18 Summarized kinetic data from Table 17 analyzed by three methods. Pd, 10^{-5} mol.cm^{-3} Fe^{2+}, Fe^{3+} in 10^{-3} mol.cm^{-3} $HClO_4$. Experiment No. 33.

Kinetic Parameter	Intercept	Jahn, Vielstich	Randles (extrap.)	Randles (mean)
$10^3 k_o$/cm.s^{-1} best value at 298.2 K	5.88 ± 0.08	5.74 ± 0.07	5.85 ± 0.08	6.44 ± 0.3
$\Delta H^{\ddagger}$/kJ.mol^{-1}	37.2 ± 0.7	37.6 ± 0.9	37.3 ± 0.7	39.7 ± 0.9
$\ln(A^{\ddagger}$/cm.s$^{-1})$	9.87 ± 0.3	9.99 ± 0.4	9.89 ± 0.3	11.0 ± 0.34

Results for palladium yielded a small but unmistakable dependence on rotation speed for charge transfer exchange current densities calculated by Randles' method. A typical empirical plot of Randles $(i_{oR})^{-1}$ versus $\omega^{-1/2}$ is presented in Fig. 26. The dependence on rotation speed in this case is more pronounced, and it will be noted that the same apparent slope for each plot is indicated at each temperature, indicating similar non-ideal behaviour. Again exchange current densities extrapolated versus $\omega^{-1/2}$ to $\omega = \infty$ always agreed with those obtained by the two other methods. The results of Table 17 have been obtained in this way and the Randles results then agree very well.

A similar dependency of the transfer coefficient, from Randles' treatment was observed in experiments with palladium just as with platinum and gold, namely that as ω increased, $\alpha_{apparent}$ decreased,

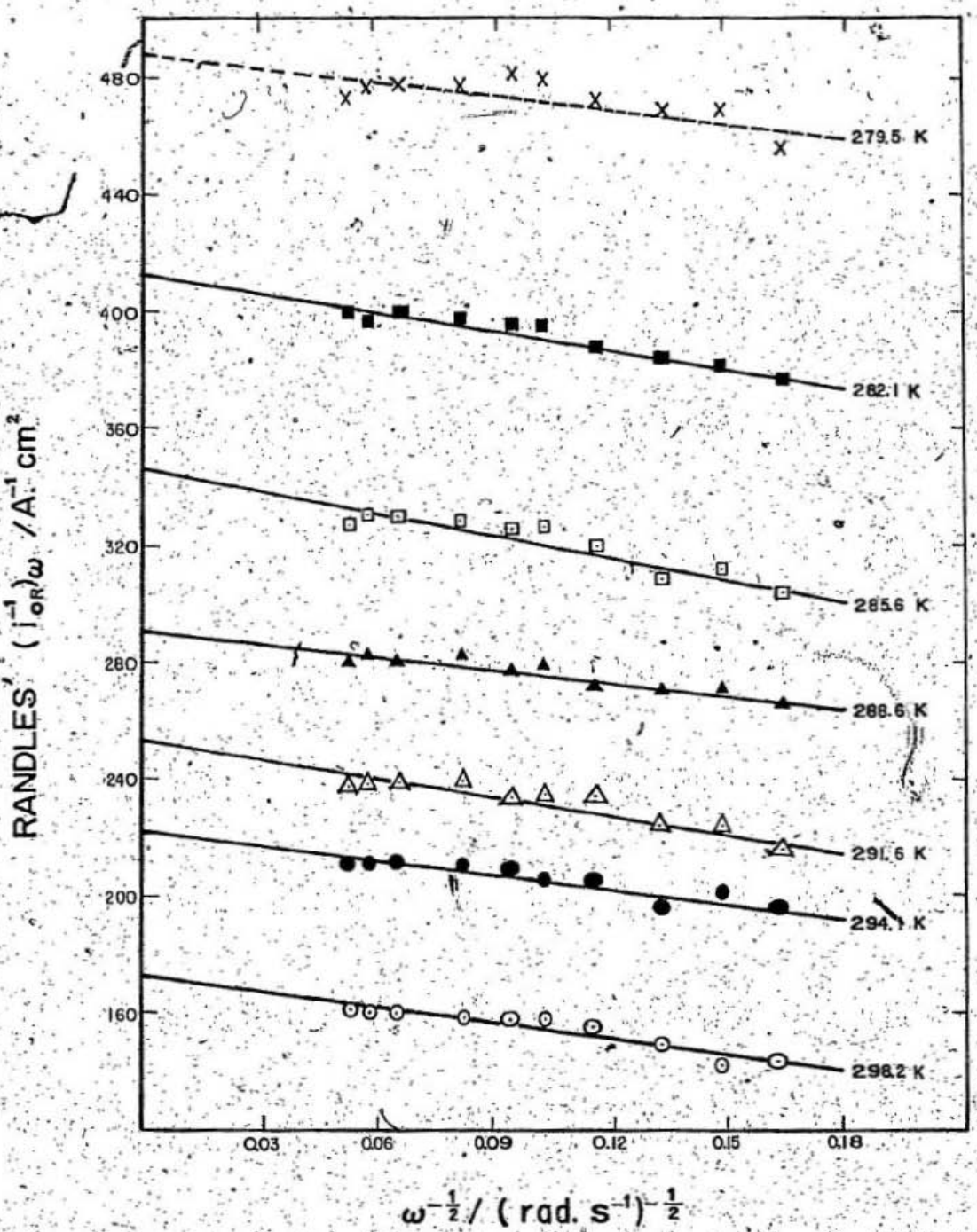

Fig. 26 Dependence of $(i_{oR})_{\omega}$ on rotation speed for experiment no. 33; Pd, 10^{-5} mol.cm^{-3} Fe^{2+}, Fe^{3+} in 10^{-3} mol.cm^{-3} $HClO_4$.

the relationship being linear between α and $\omega^{-1/2}$. An example of this is shown in Fig. 27. Notice the near perfect convergence of all curves to $\alpha = 0.5$ at infinite rotation speed.

Results with palladium varied within only a narrow range. Therefore, only a few experiments were required to establish confidence limits. These are listed in Table 19.

Table 19 Summary of preferred rate constants and Arrhenius parameters; Fe^{2+}, Fe^{3+} electron transfer at a Pd RDE in 10^{-3} mol.cm^{-3} $HClO_4$.

Expt. No.	$[Fe^{2+}]=[Fe^{3+}]$ mol.cm^{-3}	$10^3 k_o$/cm.s^{-1} at 298.2 K	$\Delta H^{\ddagger}$/ kJ.mol^{-1}	$\ln(A^{\ddagger}$/cm.s$^{-1})$
33	10^{-5}	5.88 ± 0.08	37.2 ± 0.7	9.87 ± 0.28
34	10^{-5}	7.77 ± 0.11	28.8 ± 1.4	6.76 ± 0.58
35	10^{-6}	5.32 ± 0.10	34.1 ± 0.6	8.44 ± 0.26
36	10^{-6}	5.63 ± 0.09	32.6 ± 1.8	7.97 ± 0.73

These data were handled in a similar way to those obtained using platinum and gold, a summary being available in Table 20.

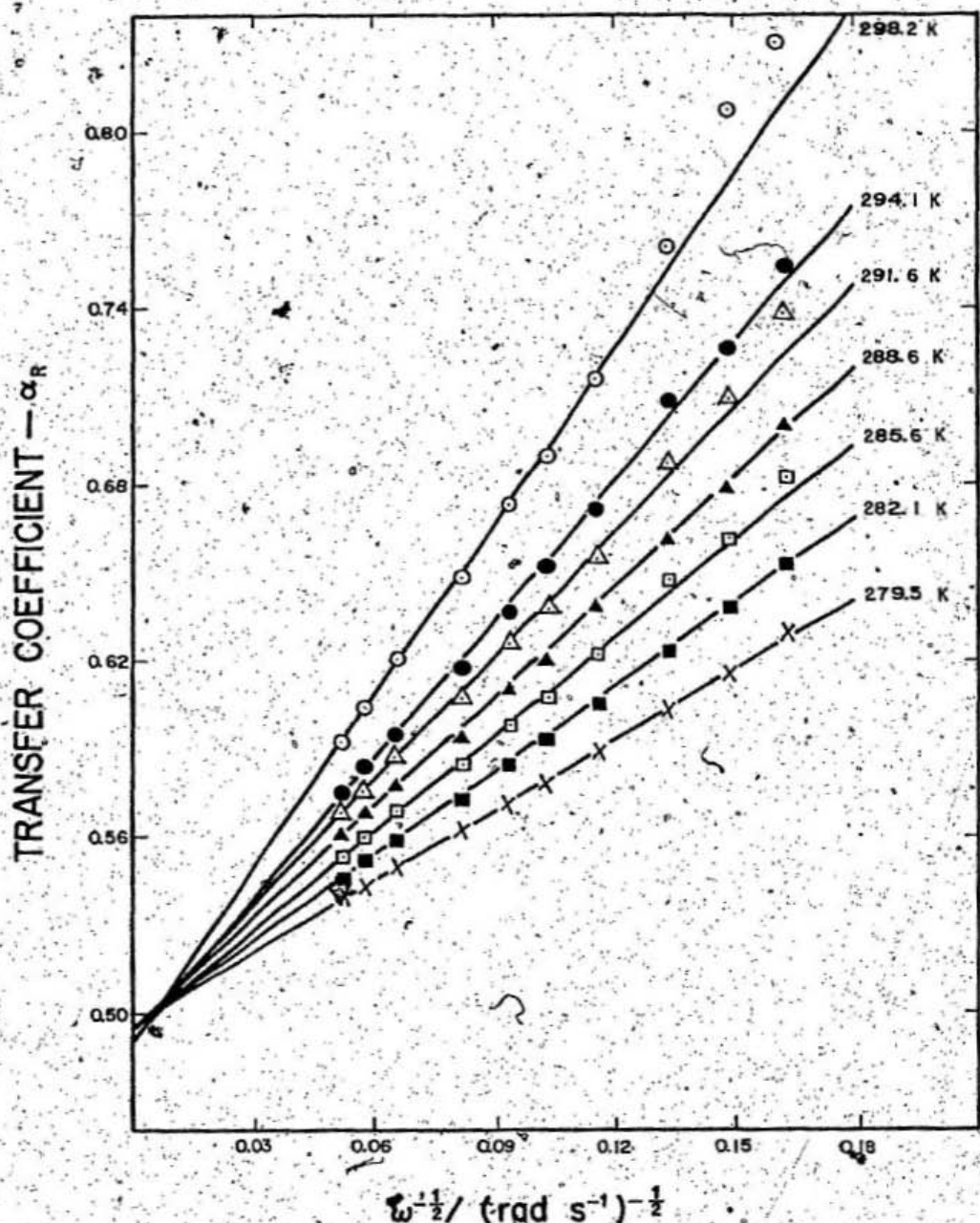

Fig. 27 Dependence of α_R on rotation speed for experiment no. 33; Pd, 10^{-5} mol.cm^{-3} Fe^{2+}, Fe^{3+} in 10^{-3} mol.cm^{-3} $HClO_4$.

Table 20 Summary of experiments with palladium.

$10^3 k_o/cm.s^{-1}$ at 298.2 K (weighted mean)	6.03 ± 0.48
Range of values for rate constant at 298.2 K, $10^3 k_o/cm.s^{-1}$	5 - 8
$\Delta H^{\ddagger}/kJ.mol^{-1}$ (weighted mean)	34.8 ± 1.4
$\Delta H^{\ddagger}/kJ.mol^{-1}$ (one Arrhenius plot for all experiments)	37.0 ± 3.0
Weighted mean $[\ln(A^{\ddagger}/cm.s^{-1})]$	8.81 ± 0.59
$\ln(A^{\ddagger}/cm.s^{-1})$ (one Arrhenius plot for all experiments)	8.05 ± 1.45

Correction of Rates for Real Areas

The real surface areas of the platinum, palladium and gold working electrodes were measured according to the procedures of Woods[47] previously described. The surface area of the platinum was measured using both oxygen desorption and hydrogen adsorption techniques, the latter being preferred. Palladium and gold real areas were determined through oxygen desorption. Results of these measurements and corresponding roughness factors are listed in Table 21.

Table 21 Determination of real surface areas.

Metal	Geometric Area = 0.0314 cm^2 based on 0.2 cm. diameter, as manufactured by J.M. and M.		
	H_{ads}	O_{desorp}	Roughness Factor*
Pt	0.10 cm^2	0.11 cm^2	3.2 to 3.5
Au	–	0.20 cm^2	6.4
Pd	–	0.11 cm^2	3.4

*Precision estimated to be ±5%.

Corrected Results

Using the roughness factors of Table 21 (3.4 for platinum) the true rate constants and consequent pre-exponential factors were calculated. These results are summarized in Table 22.

Table 22 Best values of corrected rate constants at 298.2 K for Pt, Au, and Pd and Arrhenius parameters.

Metal	$10^3 k_o/cm.s^{-1}$	$\Delta H^{\ddagger}/kJ.mol^{-1}$		$\ln(A^{\ddagger}/cm.s^{-1})$	
		All Pts.	Weighted Mean	All Pts.	Weighted Mean
Pt	5.41 ± 0.47	38.6 ± 3.2	41.5 ± 3.0	10.18 ± 1.33	11.26 ± 1.17
Au	2.11 ± 0.25	42.9 ± 1.7	38.9 ± 2.5	11.24 ± 0.70	10.40 ± 1.31
Pd	1.77 ± 0.14	37.0 ± 3.0	34.8 ± 1.4	8.54 ± 1.28	7.59 ± 0.59

Measurement of Chloride Impurity Concentration

Because chloride ion was recognized as a possible impurity arising from the dissolution of the iron and also from the acid used, as will be discussed in the next section, attempts were made to estimate the chloride concentration of the actual test solution containing the ferrous and ferric ions. From the manufacturer's specification for the perchloric acid we estimated the diluted acid (10^{-3} mol.cm^{-3}) to contain 2×10^{-9} mol.cm^{-3} chloride. This estimate excludes any chloride arising from the dissolution or from the activation process.

Solutions of ferrous and ferric perchlorate were analyzed by a coulometric titration using electrolytically generated mercurous ion, a technique similar to that of Lingane[70]. The iron was removed by precipitating out as the hydrated ferrous and ferric oxides by adding aqueous sodium hydroxide. Following separation, the solution was reacidified and analyzed. Titrations were performed in 80% methanol. A similar procedure was performed on a sample of the background electrolyte acting as a blank. The difference (Δt in seconds at constant current) between potentiometric titration curves at the inflection point for the sample and blank yielded the chloride content of the solution. Four separately prepared test solutions were found to be 6.48×10^{-7}, 5.24×10^{-7}, 5.70×10^{-7}, and 5.48×10^{-7} mol.cm^{-3} in chloride respectively, much higher than had been anticipated. If we consider the possible interference of ferrous ion, resulting from the solubility of ferrous hydroxide ($K_{sp} = 1.64 \times 10^{-14}$, 291 K), the

resulting ferrous ion concentration would be 2×10^{-8} mol.cm^{-2} which could give rise to about a 4% error due to its reaction with mercurous ion. However, this is only a conservative estimate. Since the exact concentration of chloride impurity may not be that critical, we can reasonably assume the chloride concentration to be in the range 10^{-7} to 10^{-8} mol.cm^{-3}. It may be noted that the G.F. Smith Chemical Co. impurity limit for their commercially prepared iron perchlorates would result in a chloride concentration of 2×10^{-8} mol.cm^{-3} for the same concentration of test solution.

DISCUSSION

Effect of Chloride Impurity

The present research has as its objective the examination of the kinetics of the ferrous-ferric reaction in perchloric acid, that is to say under conditions in which it might reasonably be expected that the participating species were the hexa-aquo complexes of ferrous and ferric ions. Unfortunately, the perchlorate ion is unstable with respect to its decomposition to chloride ion and water under certain conditions which may have been encountered in the work:

$$ClO_4^-(aq) + 8H^+(aq) + 8e^- \rightleftharpoons Cl^-(aq) + 4H_2O(l) \quad E^\circ = +1.37\ V$$

This half-reaction, combined with half-reaction

$$Fe^{3+}(aq) + e^- \rightleftharpoons Fe^{2+}(aq) \qquad E^\circ = +0.771\ V$$

or with

$$Fe^{2+}(aq) + 2e^- \rightleftharpoons Fe(c) \qquad E^\circ = -0.44\ V$$

makes an overall reaction which is thermodynamically feasible and therefore capable of actual realisation, e.g.

$$4Fe(c) + ClO_4^-(aq) + 8H^+(aq) \rightleftharpoons 4Fe^{2+}(aq) + Cl^-(aq) + 4H_2O(l)$$
$$E^\circ = +1.81\ V$$

Chloride ions are also actual or potential impurities in metal per-

chlorates and in perchloric acid, itself. Chloride concentrations were minimized by use of ARISTAR perchloric acid and, it was at first thought, by preparing solutions of the dissolved iron species from pure metallic iron. Estimating from the manufacturer's specifications, the chloride concentration expected after dilution would be $[Cl^-] = 2 \times 10^{-9}$ mol.cm^{-3} in 10^{-3} mol.cm^{-3} $HClO_4$ or $[Cl^-] = 2 \times 10^{-10}$ mol.cm^{-3} in 10^{-4} mol.cm^{-3} $HClO_4$. The possibility of electrolytic reduction at the potential of the dissolving iron was not contemplated but the work of Johnson and Resnick[28] indicated that such a process was not only possible but difficult to prevent. This has also been recognized in the most recent work by Horanyi and Inzelt[64] who studied the adsorption of chloride ion on platinum as a function of potential by a radiotracer technique. Even during adsorption measurements these workers observed slow reduction of perchlorate to chloride ion. Doubtless the existence of "nascent" atomic hydrogen at the surface of the dissolving metal may be responsible for facilitating this reduction as well. A search for chloride ions, by a method outlined previously, after anodic oxidation of half of the ferrous ions to ferric revealed concentrations of the order of 5×10^{-7} mol.cm^{-3} in our prepared solutions. However, the analytical method was not perfect, as remaining trace amounts of ferrous ions could interfere slightly. In any case, the purity of our iron perchlorate solutions should be at least comparable with that of manufacturers of iron perchlorates, (e.g. G.F. Smith Chemical Co., ferrous perchlorate hexahydrate, contains 0.01% Cl^- yielding 2×10^{-8} mol.cm^{-3} for the solutions required for

this work). We can reasonably estimate the chloride ion content on this basis to be in the range of 10^{-7} to 10^{-8} mol.cm^{-3}. The activation process for all three metals may be a source of chloride ions, the counter electrode in each case becoming negative enough to cause electroreduction of the perchlorate. Indeed, Horanyi and Inzelt[64] have observed generation of chloride from perchlorate at zero volts (NHE).

Johnson and Resnick's work[28] may be utilized to estimate chloride ion concentrations in their solutions and also the kinetic effects of such adsorbed chloride. In their work the half-wave potential $E_{1/2}$ of a platinum RDE was observed to be time dependent in the ferrous-ferric system in perchlorate medium, both with and without added halides (chloride, bromide, or iodide). They analyzed the $E_{1/2}$ versus time curves in terms of a transition time τ, related to the apparent heterogeneous rate constant, $k_{o,app}$, for electron transfer[28]. An equation relating τ to $k_{o,app}$ and the rate constant k_2, for the reaction occurring on a platinum surface with a monolayer coverage with chloride ($\theta_{Cl^-} = 1$) was developed:

$$\tau = \frac{\alpha F k_{o,app} \Gamma_{max} E_{1/2}}{0.62RT\, k_2 AD^{2/3} \nu^{-1/6} \omega^{1/2} C^{\infty}_{Cl^-}} \qquad (56)$$

where Γ_{max}/A is the saturation chloride coverage of the surface (mol.cm^{-2}), calculable from the number of platinum surface atoms per square centimetre, viz 1.3×10^{15}, $C^{\infty}_{Cl^-}$ is the bulk concentration of chloride ions and other terms have their usual meanings. For a surface devoid of adsorbed chloride ions, a rate constant k_1 is applicable which is related to $k_{o,app}$ and k_2 by:

$$k_{o,app} = (1 - \theta_{Cl^-}) k_1 + \theta_{Cl^-} k_2 \quad (57).$$

Johnson and Resnick[28,62] found that a log τ versus log $(C^{\infty}_{Cl^-})_{added}$ was linear with slope = −1 as expected from equation (56) but departed from linearity at low or zero added chloride concentration. For our purposes, we use Johnson and Resnick's data to estimate the chloride concentration in the "pure" perchlorate solution and, checking that a plot of log τ versus $(C^{\infty}_{Cl^-})_{true}$ is linear down to the lowest concentrations, after these had been corrected, we estimate a residual chloride concentration of about 10^{-9} mol.cm^{-3}.

When we substitute reasonable values of the variables and $\alpha = 0.5$ into equation (56) for the various chloride concentrations of their work, with $k_{o,app}$ and k_2 the only unknowns, we obtain the ratio $k_{o,app}/k_2$. In this way, for $(C^{\infty}_{Cl^-})_{true}$ values estimated to be 1.1×10^{-9} mol.cm^{-3} (zero added chloride[28]) and 9.1×10^{-9} mol.cm^{-3} (8×10^{-9} mol.cm^{-3} added chloride[28]), the rate constant ratios are 0.01383 and 0.01686, respectively: not a very large difference for a nearly tenfold change of concentration. On this basis, the rate constant k_2, applicable to a surface fully covered with adsorbed chloride, is expected to be 60 or 70 fold greater than $k_{o,app}$ under these experimental conditions.

Balashova and Kazarinov[27] have also studied the adsorption of halide ions on platinum by radioactive tracer methods, both as a function of halide concentration and of electrode potential. According to Balashova's work, the coverage of halides on smooth platinum increases linearly with the logarithm of the bulk halide concentration.

These radioactive tracer studies show that the extent of halide ion adsorption decreases from iodide to bromide to chloride. Although Balashova's data places most emphasis upon the adsorption of iodide ions, sufficient information is available to allow an estimate of the chloride coverage on platinum. Using a solution containing 1×10^{-6} mol.cm^{-3} HCl and 1×10^{-6} mol.cm^{-3} NaCl, Balashova and Kazarinov[55] have investigated the adsorption of chloride as a function of potential. By using platinized platinum electrodes, corrected for real surface area, they have shown that at 0.77 V (NHE), the redox potential of the ferrous-ferric reaction, the chloride surface concentration is 2.5×10^{-10} mol.cm^{-2}. In terms of fractional coverage, we deduce this to be $\theta_{Cl^-} = 0.11$. Similarly Horanyi and Inzelt[64] have observed 50,000 cpm of ^{36}Cl disintegration per apparent cm^2 as the coverage at the same potential for a 10^{-3} mol.cm^{-3} $HClO_4$ solution containing 2×10^{-8} mol.cm^{-3} chloride ion. By using a radioactive decay constant of 3×10^{-12} min^{-1} (for ^{36}Cl, half life = 4.4×10^5 years) and assuming a roughness factor of 300 for platinized platinum[65], an average value of those measured by these authors, we calculate a coverage of $\theta_{Cl^-} = 0.35$. This is inconsistent with the Balashova work at the higher concentration (2×10^{-6} mol.cm^{-3} Cl^-). If we examine the coverage - potential curves of both works, we observe that, at the highest potential of +0.800 V, Balashova's curve[55] is approaching a plateau, whereas Horanyi's surface concentrations do not appear to be near saturation. Because Balashova's value of chloride surface concentration has reached a constant value as a function of potential, we conclude that θ_{Cl^-} in her case may be much larger than the 0.11 deduced above. On this basis the results of both works become complementary.

If we reconsider Johnson and Resnick's work, we can estimate θ_{Cl^-} at the residual chloride concentration of 1.1×10^{-9} mol.cm^{-3} by extrapolating from the data of both Balashova (here we assume $\theta_{Cl^-} \simeq 1$ at $[Cl^-] = 2 \times 10^{-6}$ mol.cm^{-3}) and Horanyi (we calculate θ_{Cl^-} to be 0.35 at $[Cl^-] = 2 \times 10^{-8}$ mol.cm^{-3}). By this means we estimate a coverage of $\theta_{Cl^-} \leq 0.01$ for Johnson and Resnick's solution with no added chloride provided that the semi-logarithmic relationship of Balashova is valid in this region.

We now consider the electrocatalytic effect of this coverage by rearranging equation (57) to obtain,

$$\frac{k_1}{k_2} = \frac{k_{o,app}}{k_2(1-\theta_{Cl^-})} - \frac{\theta_{Cl^-}}{(1-\theta_{Cl^-})} \qquad (58)$$

where by the definitions of k_1 and k_2, their ratio must be a constant, whereas $k_{o,app}/k_2$ depends upon θ_{Cl^-} as already illustrated. We then use the value of $k_{o,app}/k_2$ (i.e. 0.01383) obtained at the residual chloride concentration of 1.1×10^{-9} mol.cm^{-2} (as we interpret the data of Johnson and Resnick), and a value of $\theta_{Cl^-} = 0.01$, as we estimated, to calculate k_1/k_2 to be 3.87×10^{-3}. This value describes the total catalytic effect that adsorbed chloride has on the rate of this reaction going from zero to saturation coverage. Thus the rate constant at complete coverage, k_2, is 258 times the rate constant at zero coverage, k_1. We may now use this relationship ($k_2 = 258k_1$) with equation (57) and the $k_{o,app}$ magnitudes observed in this work to estimate the true uncatalyzed rate constants

for the ferrous-ferric reaction. If we use the general relationship $\theta_{Cl^-} = a \log C^{\infty}_{Cl^-} + b$, where a and b are constants, then the data of both Balashova et al. and Horanyi et al. may be interpolated for the chloride concentration of our test solutions, which could have been as high as 5×10^{-7} mol.cm^{-3} after prolonged activation. This interpolation yields a probable coverage of $\theta_{Cl^-} = 0.8$ for our experiments. If we then substitute this coverage and the corrected $k_{o,app}$ (see Table 22) for platinum into equation (57) we find k_1 to be 2.62×10^{-5} cm.s^{-1}. The coverage we have used in this calculation can only be considered an estimate since it depends on a judgement on our part that the coverage at 2×10^{-6} mol.cm^{-3} chloride approaches unity. The fully catalyzed rate constant, k_2, at monolayer coverage would then be 6.76×10^{-3} cm.s^{-1}, a value not much greater than the k's observed in the present work. Unfortunately, not knowing the relative extents of adsorption of chloride on palladium and gold, we cannot really compare the rates on all three metals for zero chloride adsorption.

The above arguments are confirmed if we consider the results of kinetic studies of this system by Su[16], using concentrated (up to 6×10^{-3} mol.cm^{-3}) chloride medium (see Table 26). These are within an order of magnitude of the rate constants reported here for the perchlorate medium. If we correct the rate constants of Su's work for real surface areas (using real surface areas measured here), then no appreciable difference between the rate constants of ferrous-ferric electron transfer in perchlorate and concentrated chloride

medium is evident. This is more easily understood if we consider that the chloride coverage in the perchlorate medium could be as high as 0.8. Then the difference between the two media is only 20% with respect to chloride surface coverage.

To properly verify any of the aforementioned discussion, experiments really should be undertaken in the absence of chloride, This poses an insuperable experimental problem, since, as is apparent from the previous observations, one is faced with the prospect of having finally purified the solution of chloride impurity only to have it regenerated during the activation of the electrode. In this regard it is perhaps significant to recall that for platinum, activating the electrode increased the rate constant one hundred fold, for an experimental range was observed, from 10^{-5} cm.s^{-1} for unactivated platinum (Figs. 10 or 11) to 6×10^{-3} cm.s^{-1} for activated platinum (Table 22). Considering the combined effect of both activation and chloride impurity one can understand the possible causes of the irreproducibility of results observed with platinum, in particular.

With respect to the possibility of adsorption of chloride impurity on the metal, we must now encompass the role of the pre-exponential factor, $A^{\ddagger}$ into the discussion. In this work we report the rates as

$$k_o = A^{\ddagger} \exp(-\Delta H^{\ddagger}/RT) \qquad (59)$$

where $A^{\ddagger}$, the experimental pre-exponential factor is related to the true pre-exponential factor by an exponential entropy term. However,

on the basis of the chloride adsorption discussion above, two parallel paths for electron transfer are operative which may be expanded in Arrhenius form from equation (57), i.e.

$$k_{o,app} = A_1^{\ddagger} e^{-\Delta H_1^{\ddagger}/RT} (1 - \theta_{Cl^-}) + A_2^{\ddagger} e^{-\Delta H_2^{\ddagger}/RT} \theta_{Cl^-} \qquad (60)$$

where $\Delta H_1^{\ddagger}$, $A_1^{\ddagger}$ and $\Delta H_2^{\ddagger}$, $A_2^{\ddagger}$ are the Arrhenius parameters for the respective uncatalyzed and catalyzed processes. Such an expression does not, in general, yield a linear Arrhenius plot. However, experimental Arrhenius plots have been presented here which are linear. Such linearity may be possible because a relatively short temperature range was studied, or as is suggested, the electrode is almost covered with chloride causing the first term in equation (60) to be negligible. If this were the case the rate parameters measured, would be those for the predominating chloride catalyzed process, since at the coverage of 0.8 as estimated, the uncatalyzed rate would be contributing barely 0.1% to the total current. Since the experimental system of this work is not capable of determining θ_{Cl^-}, any temperature dependency of this quantity is not calculable and must be overlooked in the present discussion. However, it may be tentatively assumed that temperature will have little effect on an electrode nearly saturated by chloride.

With respect to chloride adsorption, the pre-exponential factor may be further included in an alternate approach involving experimental variations with $\Delta H^{\ddagger}$. In a study by Joshi, Mehl, and Parsons[63] on V^{2+}, V^{3+} kinetics on mercury, they showed that both $\ln A^{\ddagger}$ and $\Delta H^{\ddagger}$ increased

linearly with the concentration of various tetra alkyl ammonium ions which were adsorbed onto the electrode surface. Such an adsorption model implies the possible effect, that chloride (in our case) could have on the rates. Since both ln A and $\Delta H^{\ddagger}$ are individually proportional to the concentration of the adsorbed species then a plot of ln A vs $\Delta H^{\ddagger}$ from a series of experiments at possible different concentrations of chloride impurity would be linear, if such a model were valid. On this premise, two approaches are possible. Firstly, a plot of this sort can be made for all the experiments performed on an individual metal, the linearity of such plots attesting to the variability of the chloride impurity concentration, since it may arise from several sources. Secondly, we may plot the best values of ln $A^{\ddagger}$ versus the best values of $\Delta H^{\ddagger}$ for each metal against each other. If such a plot were linear, it would then indicate by its slope, how much the adsorbed chloride coverage changed from metal to metal. Plots of the first kind are seen in Figs. 28, 29, and 30 for platinum, gold, and palladium, respectively. A plot of the second kind is illustrated in Fig. 31. These plots seem to be linear which validates the existence of a compensation effect where the same rate constant is observed due to a mutual compensation of the individual Arrhenius parameters.

The theoretical basis to this observed compensation effect must be speculative. Two explanations are possible. One explanation of an increasing $\Delta H^{\ddagger}$ with $A^{\ddagger}$ may be given in terms of the chloride ions being more strongly adsorbed than the reactants, thus forcing up the energy barrier but simultaneously offering an alternative mode of electron transfer through a chloride ion bridge, thereby increasing the frequency

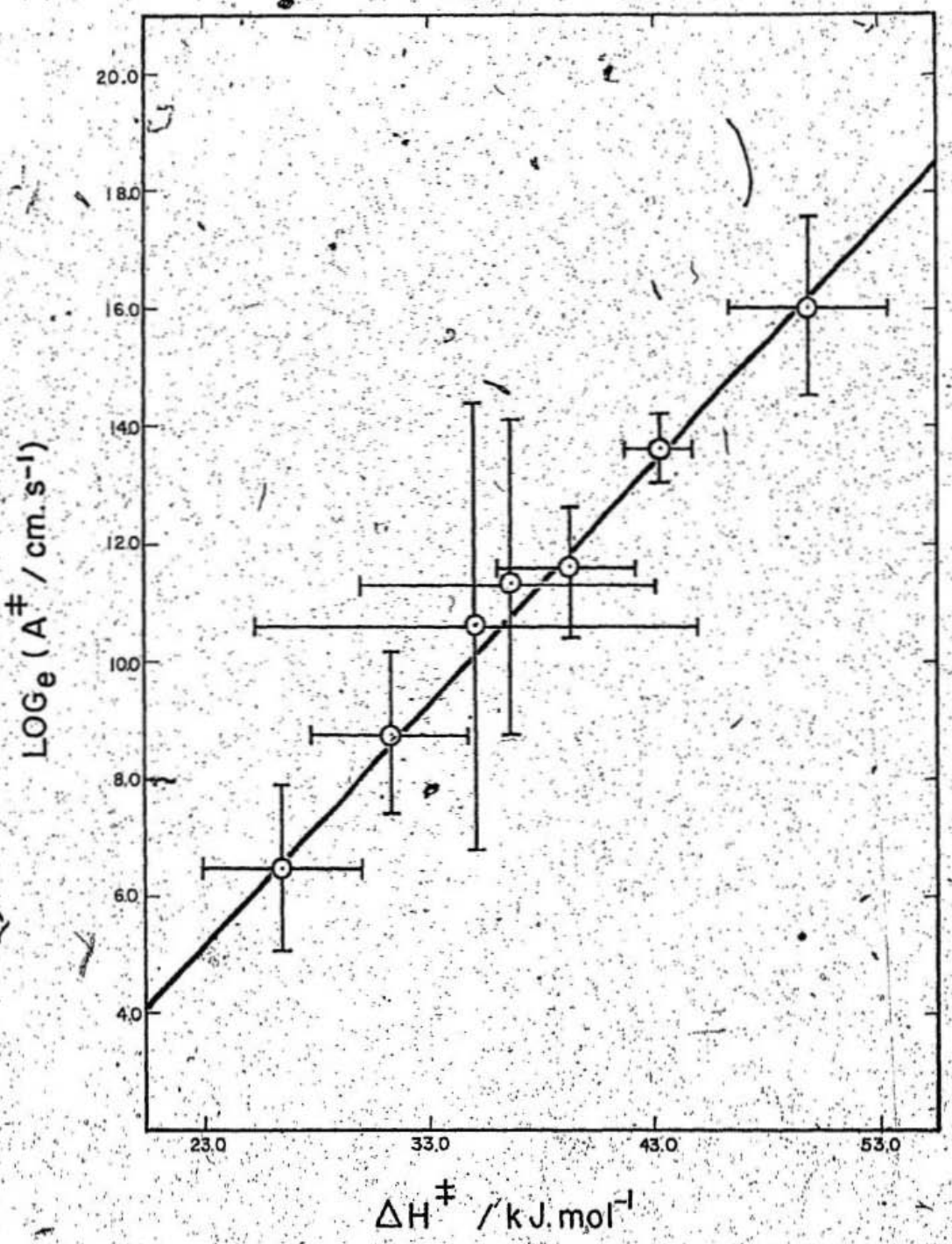

Fig. 28 Compensation effect for platinum; data from Table 9.

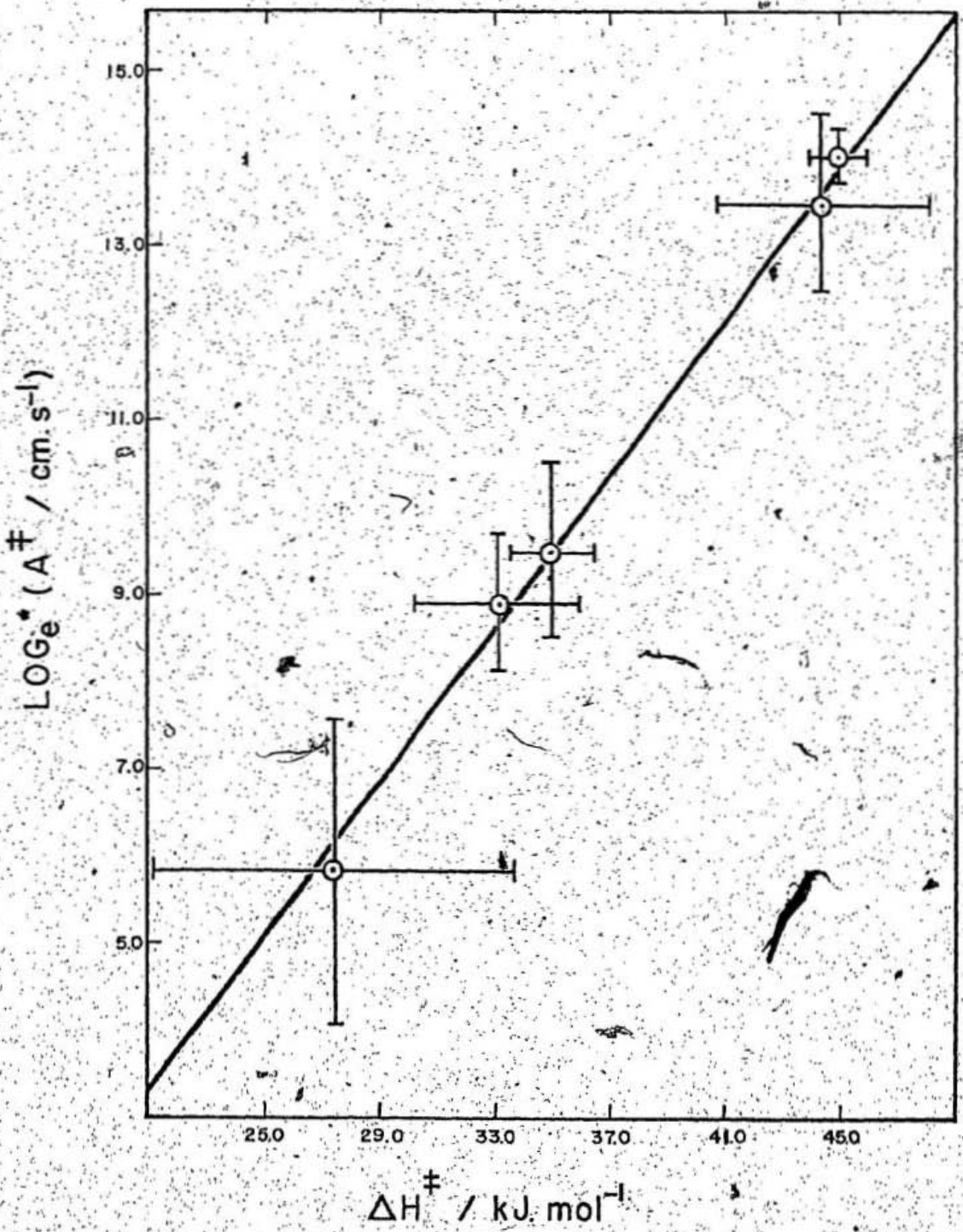

Fig. 29 Compensation effect for gold; data from Table 14.

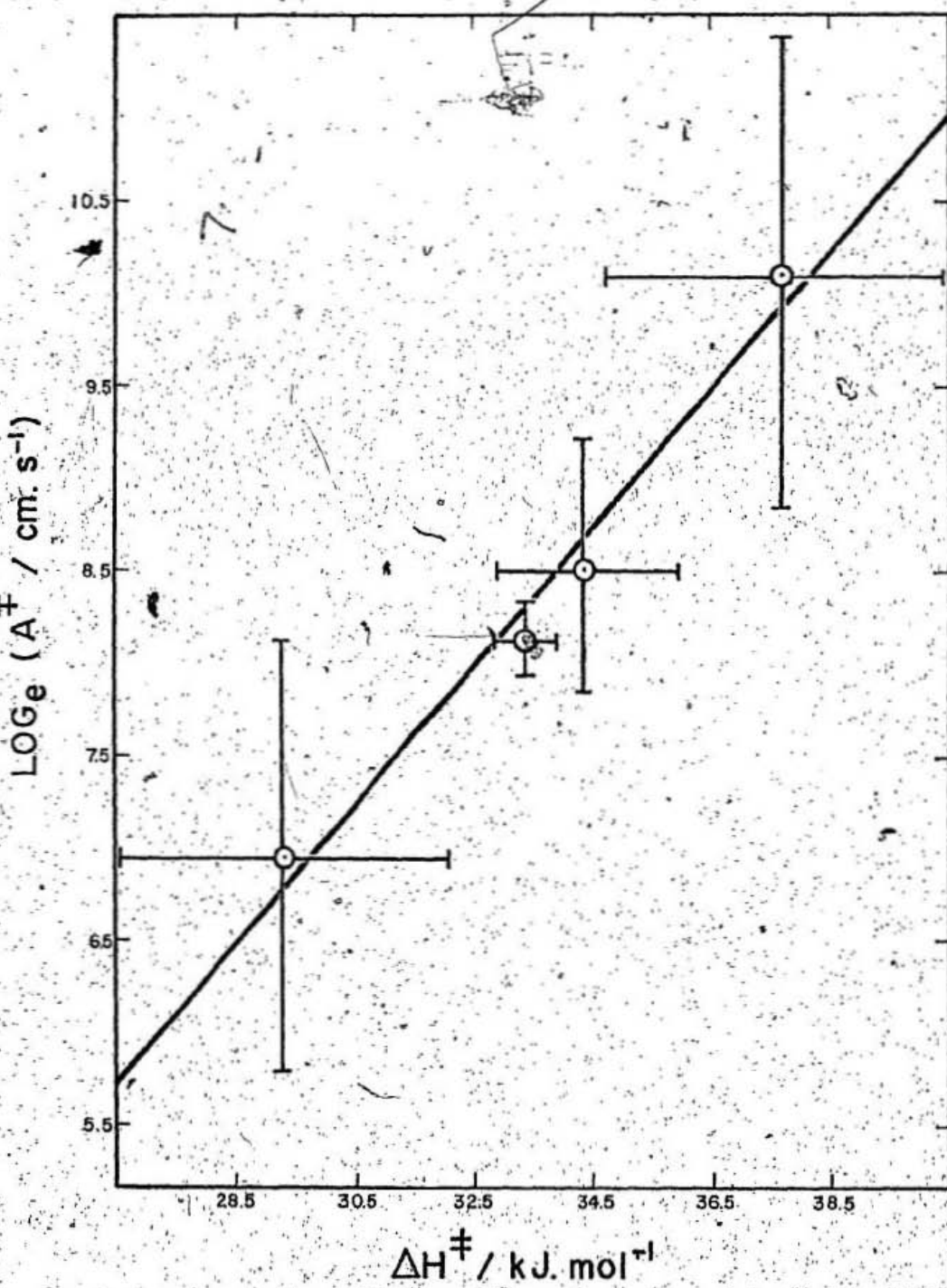

Fig. 30 Compensation effect for palladium; data from Table 19.

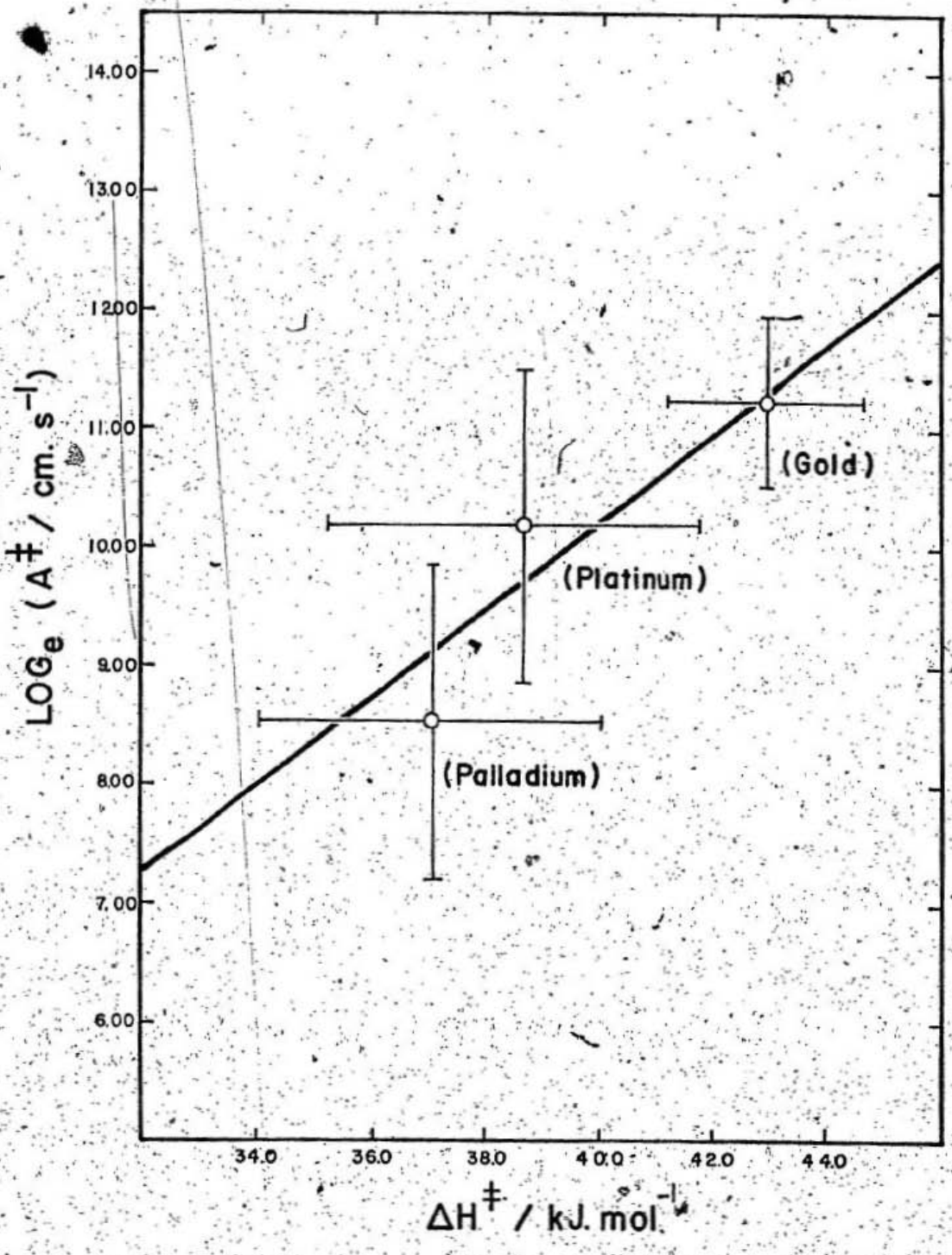

Fig. 31. Compensation effect for all metals studied; data from Table 22.

factor as observed. This prediction could be tested as could the effect of adsorbed chloride on the rate by combined rate measurements and radioactive chloride studies. The other explanation of compensation effects involves a consideration in terms of random errors only. The slope (1/RT) of such a compensation plot yields the "isokinetic temperature" which has been evaluated[72,73] to see if compensation effects are real or an extraneous artifact of the data due to random experimental errors. If these slopes yield a temperature approximate to what has been encountered in the experimental temperature range, then no physical meaning may be inferred. Thus the slopes of Figs. 28, 29, 30 and 31 (as evaluated by a double weighted least squares method) yield 302K, 276K, 328K, and 284K respectively. Because of the poor linearity of Fig. 31, the indicated slope had a high standard error (±10%). (The errors on the other slopes were lower, being ±4, ±2, and ±5% for Pt, Au, and Pd respectively.) The proximity of these isokinetic temperatures to the experimental temperature range suggests that these plots may not be used as a strong basis for extricating information concerning the chloride adsorption process.

Activation Enthalpies - Homogeneous and Heterogeneous Reactions

The activation enthalpies for the ferrous-ferric reaction listed in Table 22 have a median value close to 39 $kJ.mol^{-1}$. On the basis of the "weighted mean" data, there is a small systematic trend, in the same fashion as that of the rate constants, from palladium to gold to platinum. No such trend exists if the "all points" data are used instead. One might even argue that since no strong dependence of the activation enthalpy on the nature of the metal electrode exists, no dependence whatsoever is observable. This would certainly be true if the experimental errors were somewhat larger than our estimates of them. An attempt to correlate the rate parameters of this work (including activation enthalpy) to metal properties will be considered more quantitatively in the next section.

Bockris, Mannan, and Damjanovic[6] earlier suggested that $\Delta H^{\ddagger}$ for this reaction was independent of the metal, their work providing the stimulus for the present investigation. Both they and Trasatti et al.[4,56], who studied other metals and metal oxides as electrocatalysts, made an error in using simple linear $i - \eta$ plots to determine i_o's, assumed to refer exclusively to charge transfer, without eliminating by one means or another significant mass transport hindrance of the reaction. The reaction velocities measured by these workers were mass transport-limited and should not have been used in an Arrhenius plot to determine activation enthalpies of the charge transfer process. The temperature dependencies so measured refer, therefore, to a convective diffusion-controlled process, as we shall demonstrate. The work of Vojnovic and Sepa[61] on the ferrocyanide-

ferricyanide reaction on tungsten bronzes at one temperature suffers from the same drawback. To estimate the possible effect of ignoring the mass transport contribution, all one has to do is consider any of the inverse Levich plots (Figs. 15, 20 and 24) illustrated previously. Upon extrapolation to infinite rotation speed, the apparent exchange current density increased by a factor of 4 - 6 fold at 298.2 K. The assumption, that the enthalpy of activation indicated by measurements at other than kinetically controlled conditions is the same as under strictly kinetically controlled conditions is entirely false, as will be demonstrated.

The magnitudes of $\Delta H^{\ddagger}$ reported by Bockris et al. (i.e. Pt, 21; Rh, 26; Ir, 23; Au, 22; Pd, 10 $kJ.mol^{-1}$) and by Gallizioli and Trasatti[4] (Pt, 23; Ru, 21; Ta, 23 $kJ.mol^{-1}$) compare reasonably with the E_D's reported for $D_{Fe^{2+}}$ and $D_{Fe^{3+}}$ in Tables 4 and 5 (i.e., 16 - 20 $kJ.mol^{-1}$), indicating a diffusion controlled process. To demonstrate the point, the data of the present work can be analyzed under similar mass transport-controlled conditions, at the various experimental rotation speeds. If a plot is made of ln i_o, obtained at each rotation speed from the i - η slope, against reciprocal temperature, we can obtain a series of Arrhenius plots corresponding to each speed. To this purpose, and as a typical example the data of Table 6 (for platinum) are plotted in Fig. 32, and $\Delta H^{\ddagger}_{\omega}$ calculated at each rotation speed. The results of this graph are summarized in Table 23, together with corresponding calculations for gold and palladium, taken from Tables 11 and 16, respectively.

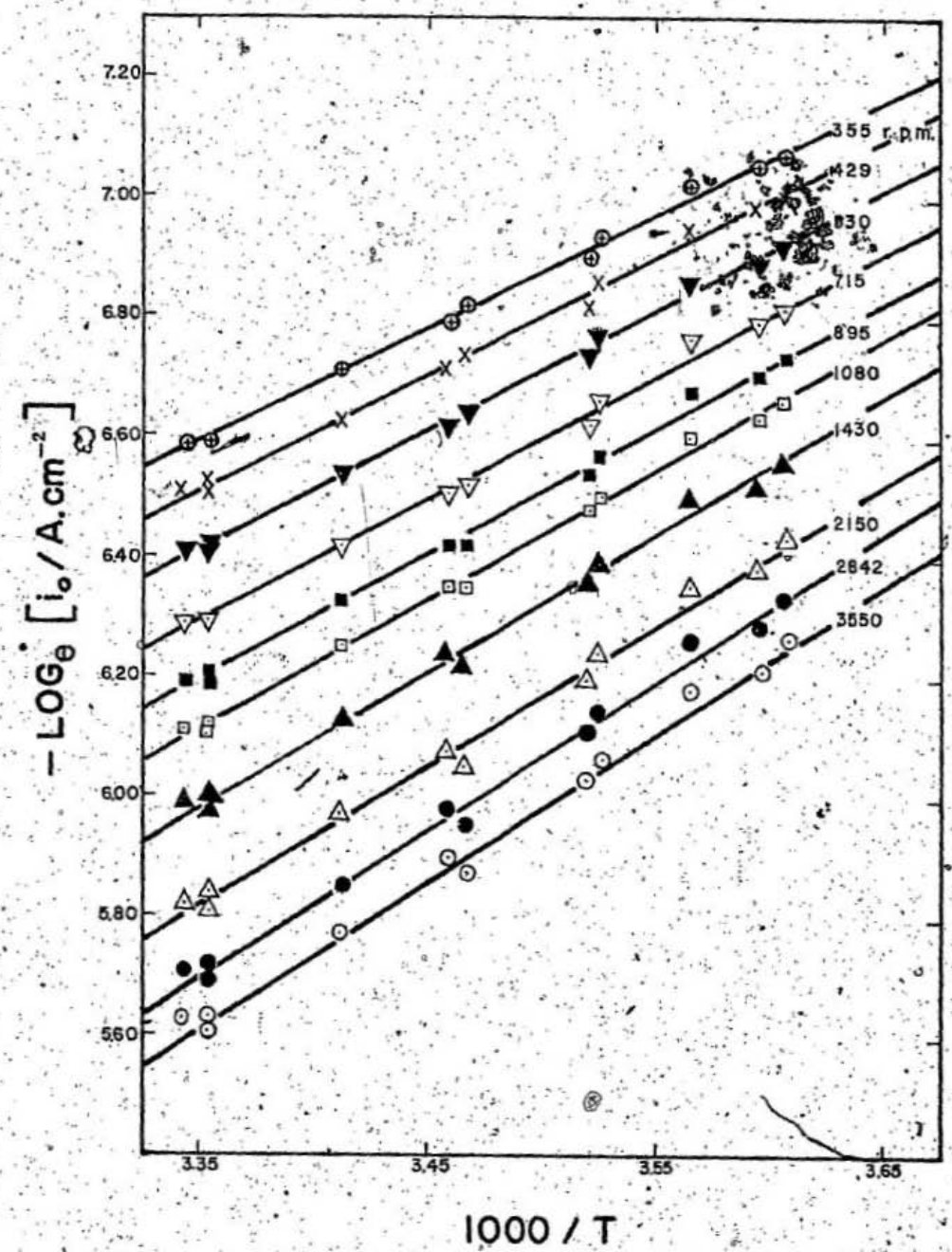

Fig. 32 Arrhenius plots performed at various rotation speeds for platinum. Data obtained from Table 6, summarized in Table 23.

Table 23 Apparent activation enthalpies as functions of rotation speed of Pt, Au, and Pd RDE's including extrapolated values.

Platinum		Gold		Palladium	
ω/rpm	$\Delta H_\omega^{\ddagger}$/kJ.mol^{-1}	ω/rpm	$\Delta H_\omega^{\ddagger}$/kJ.mol^{-1}	ω/rpm	$\Delta H_\omega^{\ddagger}$/kJ.mol^{-1}
355	15.7 ± 2.4	360	21.3 ± 5.7	362	16.2 ± 6.0
429	16.1 ± 2.0	432	22.3 ± 6.7	434	17.2 ± 5.6
530	16.5 ± 2.5	536	22.4 ± 7.2	537	17.8 ± 6.8
715	17.2 ± 1.6	720	22.7 ± 4.0	715	17.9 ± 7.4
895	17.6 ± 1.5	900	23.8 ± 4.8	900	18.4 ± 3.8
1080	18.0 ± 0.9	1080	24.1 ± 3.6	1080	18.4 ± 6.8
1430	18.7 ± 0.6	1440	24.9 ± 2.8	1440	19.2 ± 5.7
2150	19.6 ± 0.8	2160	26.0 ± 0.4	2163	19.9 ± 4.9
2842	20.2 ± 2.6	2860	26.7 ± 4.5	2860	20.1 ± 4.2
3550	20.6 ± 2.1	3560	27.3 ± 3.7	3565	20.7 ± 2.1
∞*	40.0 ± 2.4	∞*	35.1 ± 2.7	∞*	37.2 ± 0.7

*as extrapolated to infinite rotation speed.

The true $\Delta H^{\ddagger}$, obtained from a plot of $\ln(i_o)_\infty$ versus 1/T is included in this table, for comparison. The magnitudes of $\Delta H_\omega^{\ddagger}$ in Table 23 are quite similar to the enthalpies of activation reported by Bockris et al. and Trasatti et al., respectively. A simple comparison with the $\Delta H^{\ddagger}$ obtained with mass transport hindrance eliminated illustrates that the true enthalpy of activation is almost

twice as large. Therefore, any kinetic measurements made on the ferrous-ferric system under conditions similar to those used by these authors are unsatisfactory and must be rejected. As a consequence the above data analysis in terms of $\Delta H_{\omega}^{\ddagger}$ at each rotation speed serves little purpose except to show that mass transport effects can only be removed at infinite rotation speed. Upon examining Table 23 it is clear that $\Delta H_{\omega}^{\ddagger}$ increases as ω increases. Empirical plots of $\Delta H_{\omega}^{\ddagger}$ versus $\omega^{-1/2}$ appear almost linear in the practical speed range, but extrapolations of i_o to physically unattainable higher rotation speeds (e.g. 10^6 rpm) enable calculation of $\Delta H_{\omega}^{\ddagger}$ near $\omega = \infty$. Such calculations show that an empirical $\Delta H_{\omega}^{\ddagger}$ versus $\omega^{-1/2}$ plot deviates greatly from linearity as infinite rotation speed is approached. (e.g. $\Delta H^{\ddagger}$ at 10^6 rpm calculated to be 36.8 $kJ.mol^{-1}$ for the platinum data of Table 23.) Data relevant to high rotation speeds is obtainable from the extrapolated portions of inverse Levich plots ($i_o'^{-1}$ vs $\omega^{-1/2}$) between i_o's obtained at finite rotation speeds and $(i_o)_{\infty}$. To conclude, the determination of temperature dependencies of exchange current densities under partially mass transport-controlled conditions is of little value other than for the purpose for which it was used here.

Thus, we disagree with both Bockris et al. and Trasatti et al. over the magnitudes of $\Delta H^{\ddagger}$ reported by them for platinum, palladium, and gold. We feel that their methods are demonstrably inadequate, and also seriously doubt the $\Delta H^{\ddagger}$'s quoted in Table 24 for rhodium, iridium, ruthenium, and tantalum. Further experimental work along the lines illustrated here should no doubt correct these data.

The magnitudes of the activation enthalpies observed in this work are compared to the literature in Table 24.

Table 24 Activation enthalpies reported for the ferrous-ferric electrode reaction.

Medium (Metal)		$\Delta H^{\ddagger}$/kJ.mol^{-1}	Reference
1.0 mol.l^{-1} $HClO_4$	(Pt)	38 ± 7.6	Randles (17)
	(Pt)	38.6 ± 3.2	This work
	(Au)	42.9 ± 1.7	This work
	(Pd)	37.0 ± 3.0	This work
1.0 mol.l^{-1} H_2SO_4	(Pt)	21 ± 0.1*	Bockris et al.(6)
	(Pt)	23	Gallizioli, Trasatti (4)
	(Pt)	21	Agarwal (14)
	(Pd)	10 ± 0.2*	Bockris et al.(6)
	(Au)	22 ± 1.4*	Bockris et al.(6)
	(Rh)	26 ± 0.5*	Bockris et al.(6)
	(Ir)	23 ± 0.1*	Bockris et al.(6)
3.0 mol.l^{-1} H_2SO_4	(Pt)	31 ± 2.1	Su (16)
	(Pd)	38 ± 0.4	Su (16)
	(Au)	41 ± 3.3	Su (16)
1.0 mol.l^{-1} H_2SO_4	(Ru on Pt)	21	Gallizioli, Trasatti (4)
	(Ta on Pt)	23	Gallizioli, Trasatti (4)
6 mol.l^{-1} HCl	(Pt)	13 ± 3.3	Su (16)
	(Au)	11 ± 3.8	Su (16)

*These error limits are totally unrealistic.

From Table 24, the results of the present work appear to be consistent with those of Randles and Somerton[17], the only other data involving the perchlorate medium. Also, J.M. Hale[52] has theoretically calculated the free energy of activation for the ferrous-ferric system in terms of the solvent reorganization energy for formation of the transition state. He has compared this with activation free energies calculated from observed rate constants and a theoretical pre-exponential factor (10^4 $cm.s^{-1}$)[17,20]. In similar fashion, the rate constants of this work yield almost identical activation free energies (Pt, 36; Au,Pd, 38 $kJ.mol^{-1}$) with that of Hale (38 $kJ.mol^{-1}$). We then calculate small differences between activation free energy and activation enthalpy (from Table 24) for this system (i.e. $T\Delta S^{\ddagger}$ = 2.45, 4.93, -1.76 $kJ.mol^{-1}$ for Pt, Au, and Pd respectively).

In addition, the results of some homogeneous experiments may be considered, as tabulated by Reynolds and Lumry[30]. For the hexa-aquo ferrous-ferric exchange reaction a $\Delta H^{\ddagger}$ of 38.9 $kJ.mol^{-1}$ has been found by Silverman and Dodson[53] and 43.9 ± 3.6 $kJ.mol^{-1}$ by Fukushima and Reynolds[54]. These are comparable to the data for the heterogeneous system reported here. The interesting aspect of this comparison is that the Marcus[20] theory assumes that the free energy of activation for a homogeneous reaction is twice that for the corresponding heterogeneous reaction. This was the basis for extending the homogeneous theory to heterogeneous processes and was done for a model which excluded catalysis by the metal. The results of the present work disagree with this, showing $\Delta H^{\ddagger}$ to be about the same for both homogeneous and heterogeneous reactions. This seems to agree with the theory of Hush[21], which estimates only a small difference between activation free energies for the two types of reaction.

Rate Parameters and Metal Properties

Although Table 22 is suggestive of a trend in the heterogeneous rate constants, after correction for real areas, increasing from Pd to Au to Pt, such a trend may be insignificant especially in view of the results reported for $\Delta H^{\ddagger}$ and $\ln A^{\ddagger}$. The error limits of the activation enthalpies and pre-exponential factors are too great to permit one to conclude that the $\Delta H^{\ddagger}$'s and the $A^{\ddagger}$'s are distinguishable between the different metals. Attempts have been made[6,16,56,57] to correlate the observed rates of redox reactions to the electronic work function, Φ_M, of the metal on which the rates were measured. Both Bockris et al.[6] and Trasatti et al.[4,57] have identified a linear relationship between log i_o and Φ_M for a series of metals. However, both used a rate measuring technique which fails to eliminate the effect of mass transport. Bockris completely ignores this while Trasatti uses the anomalously high exchange current density of Agarwal[14] to assert the experimental soundness of the Bockris paper. In the previous section it was shown that unless the experimental conditions are free from mass transport hindrance, the resulting data yield no useful kinetic information. To further aggravate matters, both authors have used questionable values for the work functions, since the best values are obtainable using clean systems without mercury diffusion pumps.

An attempt was made to correlate data obtained in the present work with the work functions. The validity of such a correlation is strongly dependent upon having reliable values for the work functions: a quantity which we ourselves were not equipped to measure.

Eastman[58] and Rivière[59] list a series of values for the work functions of metals obtained by these authors and others. Table 25 lists preferred values for the work functions, which are to be preferred to the values in a more recent but less reliable review by Trasatti[57].

Table 25 Metal work functions and Arrhenius parameters.

Metal	Work Function Φ_M/eV	Reference	$\Delta H^{\ddagger}$/kJ.mol^{-1}	ln($A^{\ddagger}$/cm.s^{-1})
Pt	5.65	Eastman (58)	38.6 ± 3.2	10.18 ± 1.33
	5.6 to 5.8	Wilson (66)		
Pd	5.55	Eastman (58)	37.0 ± 3.0	8.54 ± 1.28
	5.5	Yu, Spicer (68)		
Au	5.1	Eastman (58)	42.9 ± 1.7	11.24 ± 0.70
	5.22	Huber (69)		

From Table 25, it is readily apparent that no correlations between metal and rate parameters have been observed in this work. However, it is necessary to recall that the dependence of rate constant, activation enthalpy, and pre-exponential factor on metal properties is not expected for a simple electron transfer. Such a correlation may still be observed if extents of chloride adsorption on the three metals were known and their effect on the kinetics could be corrected for. In this respect, only the extent of chloride adsorption on platinum has been investigated.

Table 26 summarizes the rate constants obtained in the present work and those obtained by other workers on the same and other metals and in different media.

Table 26 Rate constants for the Fe^{2+}, Fe^{3+} reaction

Medium (Metal)	$[Fe^{2+}], [Fe^{3+}]$ mol.cm^{-3}	$10^3 k_o$ / cm.s^{-1} 298.2 K	Reference
1.0 mol.l^{-1} $HClO_4$ (Pt)	10^{-4}	1.2 ± 0.1	Su (16)
"	10^{-5}	16.1 ± 0.8	Su (16)
"	10^{-5}	2.4	Jahn, Vielstich (15)
"	10^{-5}	9	Angell, Dickinson (13)
"	10^{-5}	5.8 ± 1.7	This work*
"	10^{-5}	10	Anson (11)
"	10^{-6}	14.0 ± 1.6	Su (16)
"	10^{-6}	5.2	Randles, Somerton (17)
"	10^{-6}	8.7 ± 2.6	This work*
0.1 mol.l^{-1} $HClO_4$ (Pt)	10^{-6}	11.4 ± 3.2	This work
1.0 mol.l^{-1} $HClO_4$ (Au)	10^{-5}	2.3 ± 0.6	This work
"	10^{-6}	1.6 ± 0.6	This work
1.0 mol.l^{-1} $HClO_4$ (Pd)	10^{-5}	2.0 ± 0.3	This work
"	10^{-6}	1.5 ± 0.1	This work
1.0 mol.l^{-1} H_2SO_4 (Pt)	10^{-5}	5.30	Anson (11)
"	10^{-5}	3.11	Gerischer (2)
"	10^{-5}	5.08	Wijnen, Smit (10)
"	10^{-6}	4.3	Galus, Adams (9)

Table 26 (continued)

Medium (Metal)	$[Fe^{2+}],[Fe^{3+}]$ mol.cm^{-3}	$10^3 k_o$/cm.s^{-1} 298.2 K	Reference
0.5 mol.l^{-1} H_2SO_4 (Pt)	2×10^{-6}	33	Agarwal (14)
"	10^{-5}	7	Angell, Dickinson (13)
"		10	Bockris, et al. (6)
1.92 mol.l^{-1} H_2SO_4 (Pt)	10^{-4}	0.78	Su (16)
1.92 mol.l^{-1} H_2SO_4 (Pd)	10^{-4}	0.10	Su (16)
0.91 mol.l^{-1} HSO_4^- (Pt)	10^{-4}	3.94	Barnartt (7)
0.91 mol.l^{-1} HSO_4^- (Au)	10^{-4}	31.1	Barnartt (7)
0.87 mol.l^{-1} HSO_4^- (Pt)	9.6×10^{-5}	3.86	Barnartt (12)
1.0 mol.l^{-1} Cl^- (Au)	$10^{-4}, 10^{-5}$	35	Barnartt (7)
6 mol.l^{-1} HCl (Pt)	10^{-4}	3.68	Su (16)
6 mol.l^{-1} HCl (Pd)	10^{-4}	2.80	Su (16)

*The only direct comparison between this work and the literature is for the 1.0 mol.l^{-1} $HClO_4$ (Pt) case, values reported range from $(1 - 16) \times 10^{-3}$ cm.s^{-1}. Differences occur possibly because in some cases different activation techniques were used and surface areas were not always corrected for.

An important feature of the present work was the measurement of rates on electrodes whose true surface areas were known. Roughness factors measured (3X - 6X) in this work were somewhat larger than normal, but have been seen before[13,60]. Smoother electrodes could have been obtained by using polishing powders but this would have introduced

contamination. A compromise between smoothness and cleanliness was made by machining the electrodes to a mirror finish providing a surface which was microscopically rough.

Dependence of Transfer Coefficient on Rotation Speed

In some experiments the exchange current densities calculated according to the method of Randles appeared to have some dependence upon the rotation speed. Since all the quantities used in the application of this technique were experimentally obtained, one should have confidence in their reliability. As shown in Figs. 18, 22, and 26, the reciprocal of i_{oR} obtained using the Randles approach at each rotation speed varied linearly with $\omega^{-1/2}$. In some cases the dependence is perfectly linear whereas in others, a wide range of fluctuation is observed. In these cases, a problem of how to treat the Randles data was encountered. A plot against rotation speed as performed here seemed reasonable because in the majority of cases, a definite trend with rotation speed was observable. It could be argued otherwise that such a trend was just a statistical deviation caused by random errors where a simple mean and standard deviation would have been more appropriate. Where Randles data are summarized, both numerical approaches are listed. Some of the more doubtful cases where it was felt an extrapolation was invalid have been indicated by a broken line (e.g. Figs. 18, 22, and 26). These lines were least squares predicted, having a reasonable error in the intercept but an extremely large error in the slope and low correlation coefficient. In some cases, an almost sinusoidal relationship was observed, suggesting certain possible limiting conditions at either high or low rotation speed. It appears

that a correction must be applied to Randles' expressions to render each i_{oR} independent of rotation speed. In any case, those data which did not show ideal behaviour (i.e. a plot of i^{-1} versus $\omega^{-1/2}$ has a non-zero slope) would only require a small correction to conform to Randles' theory. We can only speculate as to why this deviation occurs in some cases and not in others. The deviation did not show any systematic trend with temperature, and we can perhaps conclude that there is no kinetic basis for it. Fortunately the exchange current densities extrapolated from the empirical plots were in good agreement with those obtained by the other two methods. It is reasonable to expect that the double layer structure is dependent upon rotation speed, which may not be compensated for by the Randles approach. Thus, by applying this approach at various rotation speeds, such discrepancies could be observed. It is because of these doubts expressed in the Randles method, that these results were only used as supportive evidence of the inverse Levich plots.

The observed variation of the transfer coefficient was much more spectacular and to our knowledge has not been reported before. In this work, the same sort of increase of α with $\omega^{-1/2}$ was observed in all experiments. Unlike the exchange current density variation with ω the rate of decrease of transfer coefficient with rotation speed was temperature dependent as indicated by Figs. 19, 23, and 27 for platinum, gold, and palladium, respectively. As seen from these figures the slope was temperature dependent but the intercept at $\omega^{-1/2} = 0$ (i.e. $\omega \to \infty$) was not. The maximum variation of α with

rotation speed always occurred at the highest temperature. At the limit of extrapolation, i.e. infinite rotation speed, α had a range of 0.5 ± 0.05, but within a given experiment the range of α was much more closely defined. The fact that our results reveal a transfer coefficient of 0.5 when mass transport factors have been eliminated is not in itself surprising. The present observations lead inescapably to the conclusion that there is some hitherto unsuspected shortcoming in Randles' derivation of the equations we have used, namely equations (49), (50), (53) and (54). Table 27 summarizes experimental transfer coefficients found for the ferrous-ferric system in this work and by others.

Table 27 Transfer coefficients reported for the ferrous-ferric electrode reaction.

Medium (Metal)	Transfer Coefficient	Reference
1.0 mol.l^{-1} $HClO_4$ (Pt)	0.63	Jahn, Vielstich (15)
(Pt)	0.61	Randles, Somerton (17)
(Pt)	0.5	Angell, Dickinson (13)
(Pt, Pd, Au)	0.5 ± 0.05	This work
1.0 mol.l^{-1} H_2SO_4 (Pt)	0.46	Galus, Adams (9)
(Pt)	0.61	Wijnen, Smit (10)
(Pt)	0.42	Gerischer (2)
0.1 mol.l^{-1} H_2SO_4 (Pt)	0.40	Galus, Adams (9)
0.87 mol.l^{-1} $NaHSO_4$ (Pt)	0.5	Barnartt (12)
0.1 mol.l^{-1} $HClO_4$ (Pt)	0.78	Jordan, Javick (18)

It is interesting to see from this table that a wide range of apparent transfer coefficients both above and below 0.5 have been obtained under a variety of mass transport conditions whereas the values we report pertain to infinite rotation speed, and are valid for all temperatures in the range 273 - 298 K. As such, any of the literature values reported may be classified as "apparent" transfer coefficients, perhaps being spurious due to some experimental error or invalid assumption.

Concluding Remarks

As is sometimes the case in the course of research one uncovers more problems than originally intended to solve. This is true of this research. In this work a precision device for accurately measuring rate parameters was designed and constructed. Unfortunately, activity problems arising from the instability of the electrode surface, especially with platinum, were not eliminated and relatively high experimental errors were the case. Despite this, the ferrous-ferric kinetic system in the presence of chloride impurity in perchloric acid was characterized. Estimates of the catalytic effect of chloride impurity upon the rate constant were able to be made. As earlier proposed, an experimental method involving both radiochemical (^{36}Cl) and kinetic measurements might be useful in confirming these estimates, since in experiments of this sort, it is doubted that complete elimination of chloride ion is possible.

Undoubtedly, the superiority of the RDE as a kinetic tool has been demonstrated in overcoming mass transport-controlled polarization,

especially in the area of activation enthalpies. Thus, additional work might be performed in this area with the ferrous-ferric system in this medium on other noble metals; as well as repeating some of the studies in other media, which have been duly criticized here.

Also, to possibly overcome the effect of chloride, work might be undertaken in other non-complexing salt systems (e.g. BF_3^-, PF_6^-, etc.) which might not produce impurities.

REFERENCES

1. K.J. Vetter, Electrochemical Kinetics, p. 455, Academic Press, New York (1967).
2. H. Gerischer, Z. Elektrochem., 54, 366 (1950).
3. E. Lewartowicz, J. Chim. Phys., 49, 564, 573 (1952).
4. D. Gallizioli and S. Trasatti, J. Electroanal. Chem., 44, 367 (1973).
5. F.R. Smith and C.S. Su, J. Chem. Soc., Chem. Commun., 159 (1972).
6. J.O'M. Bockris, R.J. Mannan, and A. Damjanovic, J. Chem. Phys., 48(5), 1898 (1968).
7. S. Barnartt, Can. J. Chem., 47, 1661 (1969).
8. J.V. Petrocelli and A.A. Paulucci, J. Electrochem. Soc., 98, 291 (1951).
9. Z. Galus and R.N. Adams, J. Phys. Chem., 67, 866 (1963).
10. M.D. Wijnen and W.M. Smit, Rev. Trav. Chim. Pays-Bas, 79, 289 (1960).
11. F.C. Anson, Anal. Chem., 33, 934, 939 (1961).
12. S. Barnartt, Electrochim. Acta, 15, 1313 (1970).
13. D.H. Angell and T. Dickinson, J. Electroanal. Chem., 35, 55 (1972).
14. H.P. Agarwal, J. Electroanal. Chem., 5, 236 (1963).
15. D. Jahn and W. Vielstich, J. Electrochem. Soc., 109 (9), 849 (1962).
16. C.S. Su, Unpublished data, 1972.
17. J.E.B. Randles and K.W. Somerton, Trans. Faraday Soc., 48, 951 (1952).

18. J. Jordan and R.A. Javick, Electrochim. Acta, 6, 23 (1962).

19. D.A.J. Rand and R. Woods, J. Electroanal. Chem., 35, 209 (1972).

20. R.A. Marcus, J. Chem. Phys., 43, 679 (1965).

21. N.S. Hush, Trans. Faraday Soc., 57, 557 (1961).

22. V.G. Levich and R.R. Dogonadze, Proc. Acad. Sci. USSR, Phys. Chem. Sect., 133, 591 (1960); Collection Czech. Chem. Commun., 26, 193 (1961).

23. W.F. Libby, J. Phys. Chem., 56, 863 (1952).

24. J. Weiss, Proc. Roy. Soc. London, A222, 128 (1954).

25. K.J. Laidler, Can. J. Chem., 37, 138 (1959).

26. E. Sacher and K.J. Laidler, Trans. Faraday Soc., 59, 396 (1963).

27. N.A. Balashova and V.E. Kazarinov, Electroanalytical Chemistry, Ed. by A.J. Bard. Volume 3, Marcel Dekker, New York, 1969, pp. 135 - 197.

28. D.C. Johnson and R.W. Resnick, Anal. Chem., 49, 1918 (1977).

29. P.P. Schmidt, Electrochemistry, Specialist Periodical Reports, Chemical Society, Volume 5, 1975, p. 26.

30. W.L. Reynolds and R.W. Lumry, Mechanisms of Electron Transfer, Ronald Press, New York, 1966.

31 E. Sacher and K.J. Laidler, Modern Aspects of Electrochemistry, Volume 3, J. O'M. Bockris, editor, Butterworths, London, p. 1.

32. V.G. Levich, Advances in Electrochemistry and Electrochemical Engineering, Volume 5, P. Delahay, editor, Interscience, 1968.

33. A.J. Appleby, J.O'M. Bockris, R.K. Sen, and B.E. Conway, Electrochemistry, Volume 6, MTP International Review of Science, Butterworths, University Park Press, 1973, p. 1.

34. J.A.V. Butler, Trans. Faraday Soc., 28, 379 (1932).

35. V.G. Levich, Physicochemical Hydrodynamics, Prentice Hall, Inc., New Jersey, 1962, p. 286.

36. W.J. Albery, Electrode Kinetics, Appendix 4, Clarendon Press, Oxford, 1975.

37. J. Koryta, J. Dvorak, and V. Bohackova, Electrochemistry, Methuen and Co., London, (1970), pps 136, 336.

38. D.P. Gregory and A.C. Riddiford, J. Chem. Soc., 3756 (1956).

39. J. Newman, J. Phys. Chem., 70, 1327 (1966).

40. S. Bruckenstein, J. Electrochem. Soc., 122(2), 1215 (1975).

41. W. Nernst, Z. Physik. Chem., 47, 52 (1904).

42. E. Brunner, Z. Physik. Chem., 47, 54 (1904); 58, 1 (1907).

43. J.E.B. Randles, Can. J. Chem., 37, 238 (1959).

44. J. Wojtowicz and B.E. Conway, J. Electroanal. Chem., 13, 333 (1967).

45. A.C. Riddiford and K. Blurton, J. Electroanal. Chem., 10, 457 (1967).

46. K.J. Kretschmer, C.H. Hamann and B. Fassbender, J. Electroanal. Chem., 60, 231 (1975).

47. R. Woods, Electroanalytical Chemistry, Volume 9, A.J. Bard, editor, Marcel Dekker, Inc., New York, 1976, p. 1.

48. L. Landau, Phys. Z. Sowjetunion, 3, 664 (1933).

49. P. Delahay, Double Layer and Electrode Kinetics, Interscience (1965), p. 164.

50. A.C. Riddiford, Advances in Electrochem. and Electrochem. Eng., Volume 4, P. Delahay (editor), Interscience, 1966, p. 47.

51. Landolt-Bornstein, Physikalisch-Chemische Tabellan, Volume 2, Part 5, 1969, p. 308.

52. J.M. Hale, Reactions of Molecules at Electrodes, N.S. Hush (Editor), Wiley-Interscience, New York, 1971, p. 229.

53. J. Silverman and R.W. Dodson, J. Phys. Chem., 56, 846 (1952).

54. S. Fukushima and W.L. Reynolds, Talanta, 11, 283 (1964).

55. N.A. Balashova and V.E. Kazarinov, Elektrokhimiya, 1 (5), 512 (1965), Fig. No. 2.

56. D. Galizzioli, F. Tantardini, S. Trasatti, J. Appl. Electrochem., 5, 203 (1975).

57. S. Trasatti, Advances in Electrochem. and Electrochem. Eng., Volume 10, H. Gerischer, C.W. Tobias (editors), New York, 1977, p. 213.

58. D.E. Eastman, Physical Review, B,2(1), 1 (1970).

59. J.C. Rivière, Solid State Surface Science, M. Green (editor), Volume 1, Chap. 4, Marcel Dekker, New York, 1969.

60. A.A. Michri, A.G. Pshchenichnikov, and R. Kh. Burshtein, Elektrokhimiya, 8 (3), 364 (1972).

61. M.V. Vojnovic and D.B. Sepa, J. Chem. Phys., 51, 5344 (1969).

62. An earlier privately circulated version of reference 28.

63. K.M. Joshi, W. Mehl, and R. Parsons, Transactions of Symposium on Electrode Processes, E. Yeager (editor), Wiley, New York, 1961.

64. G. Horanyi and G. Inzelt, J. Electroanal. Chem., 86, 215 (1978).

65. G. Horanyi, J. Solt, and F. Nagy, J. Electroanal. Chem., 31, 87 (1971).

66. R.G. Wilson, J. Appl. Phys., 37, 2261 (1966).

67. L.G. Sillen and A.E. Martell, Stability Complexes of Metal-Ion Complexes, The Chemical Society, Special Publication No. 17, London, 1964, p. 318.

68. A. Y.-C. Yu and W.E. Spicer, Physical Review, 169, 497 (1968).

69. E.E. Huber, App. Phys. Letters, 8, 169 (1966).

70. J.J. Lingane, Electroanalytical Chemistry, Interscience, New York, 1958, pps. 600-602.

71. E.B. Sandell, Colorimetric Determination of Traces of Metals, Interscience - Wiley, New York, 1959.

72. J.E. Leffler and E. Grunwald, Rates and Equilibria of Organic Reactions, Wiley, New York, 1963, Chapter 9, p. 315.

73. R.R. Krug, W.G. Hunter, and R.A. Grieger, J. Phys. Chem., 80(21), 2335, 2341 (1976).